COLLAGEN METHACRYLAMIDE – A PHOTOCROSSLINKABLE, THERMOREVERSIBLE COLLAGEN-BASED BIOMATERIAL: CHARACTERIZATION AND APPLICATIONS

By

KATHRYN EMILY DRZEWIECKI

A dissertation submitted to the

Graduate School-New Brunswick

and the Graduate School of Biomedical Sciences

Rutgers, The State University of New Jersey

In partial fulfillment of the requirements

For the degree of

Doctor of Philosophy

Graduate Program in Biomedical Engineering and Quantitative Biomedicine

Written under the direction of

David Ira Shreiber

And approved by

_____

_____

_____

_____

_____

New Brunswick, New Jersey

October 2016

ABSTRACT OF THE DISSERTATION

COLLAGEN METHACRYLAMIDE – A PHOTOCROSSLINKABLE, THERMOREVERSIBLE COLLAGEN-BASED BIOMATERIAL: CHARACTERIZATION AND APPLICATIONS

By KATHRYN EMILY DRZEWIECKI

Dissertation Director: David I. Shreiber

Ideal properties of biomaterials for tissue engineering applications include biocompatibility, tissue mimicry, the ability to support cell attachment and growth, biodegradability, and control of biochemical and mechanical properties. Type-I collagen, a protein found throughout many tissues throughout the body, can be extracted from animal tissue and used to make fibrillar hydrogels or scaffolds for tissue engineering. While these collagen scaffolds have many of the optimal design parameters for biomaterials, the lack of control of scaffold properties is highly disadvantageous for its use in new tissue engineering paradigms. Previous studies have focused on developing a photoreactive collagen that could be biochemically and mechanically tuned via the application of light by functionalizing collagen with methacrylic acid to create collagen methacrylamide (CMA). This dissertation focuses on the characterization, continued development, and applications of CMA as a collagen-based biomaterial for tissue engineering.

We demonstrated that fibrillogenesis of CMA, in contrast to type-I collagen, is thermoreversible. CMA can reversibly cycle between two states: it forms fibrillar hydrogels at 37 °C, and disassembles into a liquid suspension at temperatures less than 10 °C. The CMA synthesis procedure was revisited to better understand how methacrylation caused thermoreversibility. Of two methods used for conjugation, one results in a thermoreversible collagen. Thermoreversibility was not specific to the methacrylic acid – other compounds were conjugated and found to make collagen thermoreversible.

In using circular dichroism spectroscopy to characterize the temperature-dependent protein structure of collagen, we found that collagen fibrils were displayed a unique signal; the fibril spectrum was seen as a negative peak at ~204 nm in contrast to the triple-helix signal in collagen's monomeric form that is characterized by a positive peak at ~222 nm. This signal was exclusive to the collagen fibril, and was used it as a tool to monitor collagen fibrillogenesis among other changes in collagen higher order structure

Finally, we developed a method of free-form fabrication of CMA, where hydrogels are constructed through self-assembly, photocrosslinking of specific geometries, and cold-melted to remove regions that were not exposed to light. Customized hydrogels can be fabricated with or without cells, or further processed into sponges. Hydrogels were also shown to be biocompatible in a subcutaneous implant model. In comparison to many 3D printing strategies, CMA free-form fabrication is very simple to implement and is inexpensive, prompting continued development of CMA in tissue engineering and regenerative medicine.

DEDICATION

To my amazing family, especially my fiancé, Jonathan, parents, Robert and Diana, sisters, Andrea, Danielle, and Elizabeth (and Sammi!), and grandparents, Cleonicia, John, Aurea, and Norbert. I love you.

ACKNOWLEDGEMENTS

This has been an amazing and exhausting five year journey of incredible accomplishments, fun experiences in and out of the lab, and long-lasting friendships. Rutgers Biomedical Engineering served as a constant source of frustration, mystery, and excitement for so long, and even though I am quite eager for my next adventure, it is still bittersweet. The people here at Rutgers Biomedical Engineering and my friends and family have made this journey possible, and I can't thank each of you enough for your support.

First and foremost, I would like to thank my advisor and mentor, Dr. Shreiber, for letting me have the freedom to pursue this fascinating and confusing project. I have truly developed into a better scientist and critical thinker because of you. You pushed me beyond anything I thought was possible, in work and life. I can never thank you enough for believing in me, and guiding and supporting me for these past five years.

To my committee members, Drs. Nanda, Baum, Berthiaume, and Kemnitzer: with each of your areas of expertise I was able to create a highly interdisciplinary project, which allowed me to explore materials chemistry, biochemistry, tissue engineering, and more. Thank you for your support in putting together such a unique project.

I would like to thank all of the organizations that have supported me in these past five years, which include the Department of Education, National Science Foundation, National Institutes of Health, and P.E.O. International. A

special thanks to Dr. Ijaz Ahmed, the Nanda Lab, Dr. Avanish Parmar, Derek Woloszyn, Matthew Richtmyer, Justin Sotolongo, Maria Qadri, and Juilee Malavade for your collaborative efforts.

Thank you to the Rutgers BME and QB staff, particularly Mary Ellen Presa, Mary Creteau, Larry Stromberg, Robin Yarborough, and Dr. Gail Ferstandig Arnold for always putting the students' needs first. You keep Rutgers running, and the students owe a lot to each of you for your effort every day.

I would like to thank the members of the previous Shreiber Lab cohort and my friends, Drs. Shirley Masand, Ian Gaudet, and Aaron Carlson, for their time and effort in training me and guiding me through graduate school, research, and life. The three of you showed us the true balance of "work hard, play hard" in graduate school, which I aimed to uphold after the three of you went on to bigger and better things. To the current Shreiber Lab and my students – thank you for your support through the end of my journey and the best of luck to all of you as you continue yours. I cannot wait to hear about all of your accomplishments in the future. Dr. Sagar Singh and Christopher Lowe – I am thankful to have had both of you by my side throughout my time in Shreiber Lab. We were able to share in the victories, small and large, and numerous failures that always got better. Sagar – despite the number of differences in our projects, we were always able to be there for one another, to navigate through the troubles to find the solution, and I am very grateful for that. Christopher – our lab was truly a great place to work when you joined Shreiber group, however that happened. You served as the dose of reality that I needed, and we found many ways to enjoy

life, including BBQs, science walks, and more, no matter what was going on in the lab. I am so thankful for your friendship and I hope for the day that we can work together again. To the BME girls, Maria Qadri, Laura Higgins, Kate O'Neill, and Grace Bundens: Sometimes I cannot believe how incredibly lucky we were to start at Rutgers together and form the friendships that we did. Though our crazy lives forced us to schedule time together, we always found a way. I can never thank you all enough for your love and support through the good and bad in this journey. Even though we may end up throughout the country, please don't forget the summer house plans! Lastly, many of my lifelong friends I've had growing up have constantly asked about my studies, supported me, and listened to stories of success and difficulty. You've kept me connected to my home, and I've felt like we were never apart. Thank you, all of you.

Finally, I am so thankful to have such a loving and supportive family and fiancé. My family is truly incredible, in personality and numbers, and their support and prayers mean the world to me. Visiting Buffalo to see my entire family, especially my parents, Robert and Diana Drzewiecki, my sisters, Andrea, Danielle, and Elizabeth, and my grandparents, were the breaks I needed to step away and refresh. My parents and grandparents are the most selfless people I have ever known, and have been there for me every day throughout this journey. Your faith in me motivates me to succeed, and I do not know where I would be today without that. My fiancé, Jonathan Schuster, has been at my side keeping me calm and happy through our stressful doctoral careers. He was the only person who was able to drag me away from research to take a breath of fresh air

to experience life in our travels through Buffalo, Boston, Washington D.C., and our too few vacations. He was a constant source of encouragement and love, with unwavering faith that I would always accomplish everything I set out to. Our journeys are complete, and I am so excited to start the next phase of our life together. All of you have taken care of me and helped me to succeed, and this achievement belongs to you as well. I love you all.

TABLE OF CONTENTS

TABLE OF FIGURES

TABLE OF TABLES

CHAPTER 1. INTRODUCTION

1.1 HYDROGELS IN TISSUE ENGINEERING

There is a huge demand for engineered tissues as the gap widens between patients receiving and awaiting transplants, with another patient added to the national transplant list every ten minutes [1]. In 2015, ~30,000 patients received eye, organ, and tissue transplants while ~120,000 patients awaited their own lifesaving transplant [1]. The field of tissue engineering seeks to develop replacement tissues that recapitulate the structure and function of lost organs and/or complex tissues. One such strategy for tissue repair is naturally or synthetically derived material scaffolds. In general, material scaffolds need to be biocompatible and biodegradable into tolerable byproducts [2-5]. Ideally, these scaffolds also need to mimic the target tissue structurally, mechanically, and bioactively to support the injured tissue and promote cell infiltration to direct tissue growth and regeneration [3-5].

Scaffolds may be constructed out of a variety of materials with vastly different properties. A class of scaffolds often used for soft tissue repair is hydrogels [2, 6]. Hydrogels are highly similar to soft tissue due to the 3D, water-swollen polymeric network [2, 6, 7]. Hydrogels are often classified in a number of ways, including source (synthetic, natural, or hybrid), method of network formation (chemical or physical crosslinking), degradability, and responsiveness to chemical, biochemical, or physical properties (such as pH, ligands, and temperature) [2, 7, 8].

1.2 SYNTHETIC HYDROGELS

Synthetic hydrogels are of great interest in tissue engineering for reproducibility of chemical and physical properties and control of scaffold architecture [2, 6]. However, these polymers often need to be chemically modified to have specific design parameters necessary in regenerative medicine, such as hydrogel biodegradability and cell-adhesiveness [2, 9]. In most cases, materials are amenable to modification and can be admixed to supplement material properties; however the final polymeric hydrogel or scaffold is still distinct from the native tissue structure. A few types of synthetic hydrogels with interesting properties are discussed.

Poly(N-isopropylacrylamide) (PNIPAm) is a synthetic, temperature-sensitive polymer synthesized from commercially available N-isopropylacrylamide, and forms networks through free radical copolymerization with various crosslinkers [10, 11]. These networks swell in water at temperatures below a lower critical solution temperature (LCST), usually ~32 °C, and separate at temperatures above the LCST [12]. Due to the synthetic nature of PNIPAm, it is amenable to chemical modification to change the LCST or other properties [2]. For example, PNIPAm is not naturally biodegradable, and has been engineered for partial or fully biodegradability [10, 13, 14]. PNIPAm has been researched and developed extensively in tissue engineering, particularly for its thermoresponsive property, as a nanocarrier for drug delivery or substrates for cell growth and harvest for regenerative medicine [12, 15].

The Pluronics family is a class of ABA triblock copolymers commercially available that are comprised of A = hydrophilic block poly(ethylene oxide) (PEO) and B = hydrophobic block poly(propylene oxide) (PPO) [16]. In aqueous solutions and above critical concentrations, these copolymers are capable of reversibly forming micelles based on temperature. The core of the micelle consists of hydrophobic PPO blocks, which are separated from the aqueous solution by the hydrophilic PEO chains [17]. Although Pluronic is not naturally biodegradable, it can be modified with other polymers to introduce this property [2, 18]. The properties of Pluronic copolymers can be easily tuned through varying the molar mass ratio between PPO:PEO, which may change the temperature at which micelles form or micelle diameter [19, 20]. For example, Pluronic F127 (10%) is capable of micelle formation ~22 °C, however, Pluronic F127 (15%) forms micelles ~20 °C; both revert to a liquid suspension at physiological temperature or below 15 °C [20]. Because micelle formation is reversible, this allows for a wide range of applications in drug delivery to achieve improved distribution at the tissue site and further material modifications that could allow potential targeting of diseased tissue [16]. One such admixed Pluronic formulation was examined as an excipient to promote in situ gelling for ocular drug delivery, and there are many Pluronic-containing formulations in development or clinical trials [16, 21].

Poly(ethylene) glycol (PEG) is a hydrophilic polymer that can form hydrogels through a number of mechanisms, including radiation of PEG polymers, free radical polymerization of acrylated PEGs, and other chemical

crosslinking reactions of modified PEGs, such as Michael-type addition of acrylated molecules to thiolated PEG or vice versa [22-25]. While PEG offers excellent biocompatibility, it requires modifications to fit other design properties of hydrogels, such as biodegradability and ability to support cell attachment [6, 9, 26]. Fortunately, PEG lends itself to modification of bioactive properties, and is available in a variety of structures (linear vs. branched, etc.) for control of hydrogel architecture [9, 27].

One particular modified PEG of interest is poly(ethylene) glycol diacrylate (PEGDA). PEGDA is photoreactive and forms hydrogels when exposed to free radicals generated through hydrogel exposure to light in the presence of a photoinitiator. This property offers great control over the spatial resolution of mechanical properties, or the incorporation of acrylated bioactive ligands into the hydrogel, which is necessary to support cell adhesion [9]. Recently, PEGDA has been a prominent biomaterial of interest for applications in 3D bioprinting, using layer-by-layer photocrosslinking to produce customized scaffolds, or photolithography techniques designing 3D microenvironments to guide cell behavior [28, 29].

Synthetic, biodegradable polyesters, including poly(lactic acid) (PLA), poly(glycolic acid) (PGA), and their copolymer poly(lactic-glycolic) acid (PLGA) are widely used throughout tissue engineering [2, 30]. These scaffolds have very good mechanical properties, supporting a range of applications from cartilage and bone repair, to 3D printing, to controlled release of drugs [30-35]. The backbone of the polyesters is an ester functional group that is amenable to

hydrolytic degradation, which has increased the utility of the class of polyesters and their use as a copolymer; for example PLA-PEGDA can be photocrosslinked to form a hydrogel, which will then be hydrolytically degradable [2, 24, 36, 37]. Despite the advantages of control over hydrogel mechanical and degradation properties, the acidic degradation of the polyesters promotes an immune response [38].

1.3 COLLAGEN-BASED HYDROGELS

In comparison to synthetic polymers, which have a wide range of controllable properties, natural polymers are largely biodegradable, biocompatible, and support cell adhesion and growth, but lack the ease of control and are highly variable. While there are many types of natural polymers, we focus on type-I collagen as it is one of the most widely used polymers in tissue engineering research due to its nativity to the body and tissue mimicry.

Type-I collagen is a protein found throughout the skin, bone, connective tissue, and more, comprising approximately 30% of the total protein body content [39]. For uses in tissue engineering, type-I collagen is extracted from cadavers or animal tissues, typically bovine or porcine [40]. Acid-solubilized type-I collagen is temperature and pH responsive, capable of forming fibrillar hydrogels at temperatures above 20 °C and approximately neutral pH [41-43]. These fibers in hydrogels closely mimic those found throughout the body [40]. Type-I collagen can also be chemically crosslinked using crosslinkers such as 1-ethyl-3-(3-dimethylaminopropyl) carbodiimide (EDC) and N-hydroxysulfosuccinimide (NHS),

genipin, and glutaraldehyde, or physically crosslinked using heat or irradiation [44-51]. Extensively crosslinked type-I collagen scaffolds were some of the first FDA-approved biomaterials for wound healing [52]. Unfortunately, these hydrogels or scaffolds are often mechanically weak for applications in tissue engineering without crosslinking, and are difficult to handle and fabricate [53]. Due to the ubiquity of type-I collagen throughout the body, a considerable amount of research is conducted on augmenting the properties or to improve control of collagen biomaterials for its continued use and development in tissue engineering [40, 54]. Similar to methods adopted for synthetic materials, type-I collagen has also been modified; some approaches have conjugated peptides to the collagen backbone for additional control of scaffold bioactive properties, or others have rendered type-I collagen photoreactive through the addition of methacrylate groups [55-58].

Gelatin is another natural biopolymer derived from human and animal collagen [59]. As such, the two share similar properties including bioactivity to support cell adhesion and biodegradability through natural enzymatic pathways [59-62]. In contrast to the triple-helical type-I collagen, which forms ordered, D-banded fibers in vitro at warm temperatures, gelatin randomly self-associates to form hydrogels at cold temperatures [62, 63]. Gelatin can be chemically or physically crosslinked, and biochemically modified using many of the same methods as those used to modify type-I collagen [61]. Although gelatin hydrogels lack the ordered, native tissue architecture, it is very inexpensive and is much easier to control scaffold properties for varied uses in tissue engineering [59, 62].

For example, gelatin methacrylate (GelMA) is a photoreactive gelatin that polymerizes when photocrosslinked with UV light in the presence of a photoinitiator, similar to PEGDA [64]. As such, it is highly amenable to rapid prototyping for tissue engineering in contrast to its related polymer, type-I collagen, where ordered fibrillogenesis would interfere with printing [64, 65].

1.4 COLLAGEN METHACRYLAMIDE

Many natural polymers, like gelatin, have been rendered photoreactive through the addition of methacrylate groups. These modifications allow for improved control of hydrogel properties, similar to the class of synthetic polymers. This was attempted using type-I collagen for maintenance of the natural properties and improvement of mechanical properties [66]. Brinkman reported on the methacrylation of rat tail type-I collagen through neutralization of an acid-solubilized rat tail solution, and the addition of methacrylic anhydride at varying molar ratios at 4 °C [66]. In this reaction, the methacrylates would be coupled to the lysine residues of type-I collagen. Following modification, methacrylated collagen hydrogels had an increased stiffness following photocrosslinking compared to unmodified type-I collagen hydrogels [66].

Our lab was not able to replicate this procedure and instead developed a new method for methacrylating type-I collagen similar to previous work used to conjugate peptides to type-I collagen [55]. In this method, EDC and NHS, frequently used to crosslink collagen to form scaffolds, were used. EDC is commonly used for carboxyl-to-amine crosslinking. Therefore, EDC can be used

to couple the carboxyl group on methacrylic acid to the amine group on lysine residues of type-I collagen. NHS was used in the reaction to increase reaction efficiency through stabilizing the intermediate, amine-reactive compound. The modified collagen produced had approximately 20% of the lysines methacrylated [55].

Collagen methacrylamide (CMA) was shown to be modified to contain methacrylate groups via NMR, while retaining the triple-helical structure of type-I collagen [55]. Fibers formed of type-I collagen and CMA were nearly identical in size and distribution [55]. CMA hydrogels had a storage modulus of approximately half that of type-I collagen hydrogels; however, following exposure to UV light in the presence of a photoinitiator, the storage modulus of photocrosslinked CMA hydrogels was approximately 3-to-5 fold larger than type-I collagen hydrogels [55]. The mechanical properties of CMA hydrogels could be easily tuned via the concentration of photointiator or the duration and/or intensity of light exposure. Further, the bioactive properties of CMA could be tuned via the addition of methacrylated ligands [67]. By rendering type-I collagen photoreactive, the resultant bioactive and mechanical properties of CMA hydrogels could now be spatiotemporally controlled similar to the many available synthetic and natural photoreactive polymers.

CMA was being developed in our laboratory for many applications, ranging from substrates to support and control neural stem cell differentiation to scaffolds for wound healing similar to commercially available type-I collagen scaffolds [67, 68]. These scaffolds are often produced via extensive chemical

crosslinking, followed by freezing and lyophilization [45]. In preparing CMA scaffolds for this application, we discovered that self-assembled CMA hydrogels formed liquid suspensions when cooled [67, 68]. Furthermore, hydrogels completely re-assembled when suspensions were returned to physiological temperature [67, 68]. While we had hypothesized that methacrylation derivatization would render type-I collagen photoreactive, it also may have affected molecular interactions in the collagen fibrils, potentially acting to destabilize fibers at cooler temperatures [67]. To our knowledge, CMA is the first demonstration of a rapidly thermoreversible type-I collagen, which bears further study to improve our understanding of type-I collagen fibrillogenesis and disassembly, or tissue engineering applications ranging from substrates for temporary cell culture and subsequent harvest or rapid prototyping.

1.5 THESIS SUMMARY

The long-term objectives of this research are to improve our understanding of the thermoreversibility of modified type-I collagen and to leverage the property to develop CMA for applications in tissue engineering, such as 3D printing of customized scaffolds. Type-I collagen is not often used to create customized scaffolds for regenerative medicine because its weak mechanical properties and its fibrillar structure render it difficult to 3D print. The unique combination of photoreactivity and thermoreversibility enable approaches with CMA that are not feasible with ordinary type-I collagen.

This dissertation focuses on the characterization, continued development, and applications of CMA as a collagen-based biomaterial for tissue engineering. In Chapter 2, we characterize the newly discovered, temperature-dependent properties of CMA. We show using multiple modalities that CMA rapidly and reversibly self-assembles based on temperature, forming a fibrillar hydrogel at 37 °C and a liquid suspension at 4 °C. CMA fibers and D-banding are identical in self-assembled and re-assembled states. Finally, when monitoring the temperature-dependent secondary structure of type-I collagen and CMA, we discover a unique circular dichroism (CD) spectrum that appeared in both samples at temperatures typical for fibrillogenesis.

Next, in Chapter 3, we investigate what aspects of type-I collagen modification contribute to thermoreversibility. We probe the process of CMA synthesis as well as produce other modified type-I collagens. Preparation of CMA with the appropriate photoreactive and thermoreversible properties can be achieved by varying some aspects in synthesis – such as the molar ratio of crosslinkers and methacrylic acid added. However, it is essential to utilize EDC and NHS rather than EDC alone to achieve CMA themoreversibility. Further, thermoreversibility is not unique to CMA, and we can synthesize other themoreversible collagens by coupling different moieties to type-I collagen.

In Chapter 4, we return to the unique CD spectrum that was discovered in Chapter 2. Type-I collagen and CMA have a triple-helical secondary structure, which is observed as a positive mean residue ellipticity (MRE) at 222 nm and a negative MRE at 195 nm. When monitoring the signal at 222 nm during

increasing temperature, the positive peak became strongly negative at temperatures typical of fibril formation. In this chapter, we demonstrate that this signal, newly dubbed as the collagen fibril signal, has a characteristic CD profile with a negative MRE at ~204 nm. This signal is unique to the type-I collagen fibril, appearing in physiological conditions regardless of species. Discovery of this signal now allows for monitoring multiple states of type-I collagen structure using one modality.

In Chapter 5, we develop a method for free-form fabrication of CMA. CMA thermoreversibility can be eliminated through photocrosslinking. To create customizable hydrogel and scaffold shapes, we photocrosslink self-assembled CMA through a photomask, and cold-melt the hydrogel to disassemble regions unexposed to light to obtain the photocrosslinked geometry. We evaluate the pattern fidelity of free-form fabrication, which is on the order of ~200 μm in resolution. We demonstrate the ability to construct hydrogels and scaffolds in specific geometries, and to create cell-laden, photopatterned hydrogels while preserving cell viability. We test the biocompatibility of CMA in vivo in a rat subcutaneous implant study. Both collagen and CMA derived implants evoke slight increases in cell density, collagen slightly less than CMA, at the one week post-implantation, which was likely an initial, acute inflammatory response to an implant. At six weeks, the cell density subsided, and all hydrogels were nearly degraded. Therefore, CMA is shown to be biocompatible, with no signs of cell toxicity.

Lastly, in Chapter 6, I summarize our findings and discuss future work in type-I collagen thermoreversibility, circular dichroism of type-I collagen, 3D printing technologies, and other tissue engineering applications of CMA in the context of this research.

CHAPTER 2. METHACRYLATION INDUCES RAPID, TEMPERATURE DEPENDENT, REVERSIBLE SELF-ASSEMBLY OF TYPE-I COLLAGEN

Note: Reproduced with permission from Drzewiecki KE, Parmar AS, Gaudet ID, Branch JR, Pike DH, Nanda V, and Shreiber DI. Methacrylation Induces Rapid, Temperature Dependent, Reversible Self-Assembly of Type-I Collagen. Langmuir, 2014. 30(37): p.11204-1121. DOI:10.1021/la502418s.

2.1 INTRODUCTION

Thermoreversible hydrogels are of great interest in biomedical research and allow for an extensive array of applications including cell encapsulation, release of drugs, or rapid prototyping [69, 70]. Ideally, to utilize these gel systems, a sol-gel transition occurs in a temperature range favorable for gel and cell manipulation [71]. For example, for *in vivo* utility, thermoreversible gels should form solutions at cool (< 25 °C) or hot temperatures (> 50 °C), and transition to a gel at physiological conditions upon injection [69]. Thus far, the materials used most extensively are synthetic in nature and lack the natural bioactivity of proteins often found in the extracellular matrix [2, 6]. Many synthetic polymers used in tissue engineering, such as poly(ethylene glycol) (PEG), poly(ethylene glycol)-diacrylate (PEGDA), or poly(vinyl alcohol) (PVA), are simple

cell scaffolds that often require the chemical addition of expensive growth factors or peptides prior to or following gel formation to support cell adhesion [2]. Thermoreversible gel systems composed of natural materials, such as gelatin and chitosan, are readily available, but controlling their mechanical properties has proved challenging [2]. Our group has developed a collagen-based hydrogel, collagen methacrylamide (CMA), which not only retains the natural properties of collagen, but is also photocrosslinkable and thermoreversible [55].

Type-I collagen is a natural, ubiquitous protein, comprising approximately 30% of total protein body content, and largely acts as a structural network for tissues such as skin and tendon [39, 72, 73]. Its inherent properties, including cell attachment and bioactivity, natural biodegradability, amenability to chemical modifications and/or mechanical crosslinking, and self-assembly into a fibrillar gel at physiological conditions, make collagen hydrogels advantageous for tissue engineering and regenerative medicine applications [40, 74].

The type-I collagen protein fiber is comprised of three polypeptide chains that oligomerize into an extended triple helix [75]. The constituent triplet for each chain is a Gly-X-Y sequence, where X and Y represent any amino acid, but primarily are hydroxyproline and proline, which naturally confer significant strength and rigidity to the protein as well as bioactivity [73, 75, 76]. At physiological temperature and pH, collagen molecules can further associate with other triple helical monomers to form fibrils and then fibers, where crosslinks between adjacent triple helices provide mechanical strength to the growing fiber [76].

Type-I collagen can be extracted from connective tissues, typically bovine or porcine, with relative ease, and the resulting protein maintains its ability to self-assemble into a fibrillar hydrogel at physiological pH and temperature, resulting in its widespread use for *in vitro* and *in vivo* regenerative medicine applications [40, 74]. Although collagen gels support cell adhesion and growth and are enzymatically degraded into cell-tolerated products, these scaffolds lack robust control of mechanical properties, which are emerging as important in regulating gross mechanical function and defining the microniche environment of resident cells [53, 57, 77, 78].

To address this limitation, we developed a protocol to render collagen hydrogels photocrosslinkable, which allowed spatiotemporal control of mechanical and bioactive properties. Methacrylate groups were covalently bound to the free amines on lysine groups of type-I collagen to create CMA [55]. Initial characterization showed that collagen and CMA gels maintained similar properties in secondary structure. Like collagen, CMA self-assembled into a fibrillar gel with similar fibril size and distribution [55]. Upon exposure to long wave UV light (365 nm, 100 mW/cm^2) and a photoinitiator in solution, methacrylate groups on collagen formed intermolecular crosslinks to stiffen the gel.

As a biomaterial scaffold, collagen is often frozen to generate a highly porous collagen “sponge”, and we were curious if sponges similarly prepared from CMA would retain the ability to be photocrosslinked [79, 80]. Subsequently, we discovered CMA did not freeze like collagen, prompting our interest in

studying the temperature-dependent behavior of CMA hydrogels. Herein, to our knowledge, we identify and characterize the first collagen-like protein that can repeatedly thermoreversibly self-assemble into a hydrogel at physiological conditions, as demonstrated at the molecular and supramolecular scales during cooling and reheating. Based on these newly discovered properties, CMA can be utilized as a novel model for collagen fibril formation and disassembly, as well as a collagen-like thermoreversible hydrogel for tissue engineering applications, including cell encapsulation and cell microenvironment design, drug delivery, and 3D printing.

2.2 MATERIALS AND METHODS

2.2.1 Collagen Methacrylation

The method for collagen methacrylation is described in Gaudet et al [55]. All reagents were purchased from Sigma unless otherwise stated. Briefly, type-I collagen (Elastin Products Company, C857) was modified by reacting the free amines of lysine residues with methacrylate groups to create collagen methacrylamide (CMA). The carboxyl group of methacrylic acid was activated with 1-ethyl-3-(3-dimethylaminopropyl) carbodiimide (EDC) and N-hydroxysuccinimide (NHS) in MES buffer. This mixture was added to collagen at 3.75 mg/mL in 0.02 N acetic acid to form CMA. CMA was dialyzed, lyophilized, and resuspended in 0.02 N acetic acid.

2.2.2 Rheology

Collagen or CMA was mixed in 1 mL batches containing 20 µL HEPES, 136 µL 0.15 N NaOH, 100 µL 10X PBS, 67 µL PBS (Fisher Scientific) and 677 µl type-I collagen or CMA (3.75 mg/mL) to form a 2.5 mg/mL suspension [55]. To assess the influence of temperature on the mechanical properties of the hydrogel, a sample of 200 µl was loaded into a 600 µm gap between a 20 mm top parallel plate and the bottom parallel plate of a Kinexus Ultra rotational rheometer (Malvern Instruments) at room temperature. The temperature was increased to 37 °C at a rate of 10 °C/minute with a Peltier-controlled stage and then held at 37 °C for twenty minutes to allow the sample to self-assemble. The temperature was then decreased to 4 °C and increased again to 37 °C at a rate of 2 °C/minute. During these temperature changes, the sample was continuously oscillated at 1 rad/s, 0.5% strain while measuring the resultant torque to acquire the temperature-dependent storage and loss moduli of the collagen hydrogels in shear.

To assess the extent of thermal reversibility, a 200 µl sample was prepared as previously described of either collagen or CMA and loaded onto the rheometer. The temperature was increased to 34 °C from 4°C at a rate of 10 °C/minute, held at 34 °C for 5 minutes, decreased to 4 °C at a rate of 10 °C/minute, held at 4 °C for 5 minutes, and repeated for a total of 10 cycles while the sample was oscillated and resultant storage modulus was measured as described above. The temperature was raised to 34 °C in these experiments as other work has cited some gel denaturation can occur at 37 °C [81].

2.2.3 Scanning Electron Microscopy

Multiple collagen and CMA gels were prepared as above and incubated at 37 °C on 12 mm glass coverslips for two hours. Of these, one CMA sample was disassembled by cooling the gel for 30 minutes at 4 °C, and re-assembled by re-incubating at 37 °C. Gels were then dehydrated in a series of aqueous acetone solutions (25%, 50%, 75%, and 95%) for 15 minutes each, and then placed in 100% acetone overnight. Samples were critical point dried (CPD 020, Balzers Union Limited, Balzers, Liechtenstein), sputter coated with gold/palladium (SCD 004, Balzers Union Limited, Balzers, Liechtenstein), and imaged via SEM (Amray 1830I, Amray Inc. Bedford, MA).

2.2.4 Transmission Electron Microscopy

Collagen and CMA suspensions were made as described above in microfuge tubes and placed in the incubator at 37 °C to self-assemble for 30 minutes. One sample of CMA was placed at 4 °C to disassemble for 30 minutes and then placed back in the incubator to allow for re-assembly for 30 minutes. A 10 µl sample of the supernatant of the gel was placed on a Petri dish, and an extra thick carbon 300 mesh copper grid (Electron Microscopy Sciences) was placed face-down on top of each droplet for 5 minutes. Filter paper was used to remove the sample from the TEM grid. To stain, a 10 µl droplet of 1% phosphotungstic acid (Electron Microscopy Sciences) was placed on a Petri dish and the TEM grid was placed face-down on top of the droplet for 5 minutes. Filter paper was used to remove the staining agent, and the samples were dried overnight prior to imaging. TEM studies were carried out using a JEM-100CX TEM microscope (JEOL).

2.2.5 Light Scattering

Light scattering (LS) measurements were performed on a Zetasizer Nano ZS (Malvern Instruments, UK) with a 3mW He-Ne laser at λ = 633 nm, collecting backscattered light at θ = 173°. Sample temperature during measurements was controlled to within ±0.1°C by a built-in Peltier element. Scattering intensities and autocorrelation functions were determined from the average of either three or five correlation functions, with a typical acquisition time of 60 s per correlation function. Collagen and CMA solutions were prepared either in 0.02 N acetic acid or in PBS buffer (final concentration of 0.1 mg/mL, pH 3.4 or 7 respectively). In the first set of experiments, samples were loaded into low-volume quartz batch cuvettes (ZEN2112) and equilibrated to 37 °C. Measurements were taken at 0, 5, 30, and 60 minutes. In the second set, samples of collagen and CMA at 2 mg/mL were diluted in PBS to a final concentration of 0.1 mg/mL, pH 7. Measurements were taken every 3 °C as the temperature was raised from 4 °C to 37 °C, decreased back to 4 °C, and then raised to 49 °C. The temperature was increased or decreased at a rate of 1.5 °C/minute and the temperature was equilibrated for two minutes prior to each set of measurements.

2.2.6 Circular Dichroism

Circular dichroism (CD) spectroscopy measurements were taken using an Aviv Model 400 Spectrometer (Aviv Biomedical Inc., Lakewood, N.J.). CMA and type-I collagen samples were prepared at 2 mg/mL in 0.02 N acetic acid or PBS to a final concentration of 0.1 mg/mL, pH 3.4 or 7 respectively, and then loaded into optically matched 0.1 cm path length quartz cuvettes (model 110-OS; Hellma

USA). Sample ellipticity was measured in three separate experiments (1 nm intervals, 10 s averaging). First, the ellipticity of 0.1 mg/mL samples of collagen and CMA in either 0.02 N acetic acid or in PBS was measured from 200 nm to 260 nm at 4 °C. Next, with the same samples, the ellipticity at 222 nm (the wavelength that nominally indicates triple helical content) of samples were measured as the temperature was increased from 4 °C to 60 °C at a rate of 0.33 °C/step with 2 minutes equilibration time [82]. Lastly, the ellipticity of 0.1 mg/mL samples of collagen and CMA in PBS, pH 7 was measured from 200 nm to 260 nm as the temperature was stabilized at 4 °C, raised to induce fibrillogenesis, decreased to allow for gel disassembly, re-raised to allow for re-assembly, and finally increased to 50 °C to a point of gel denaturation. In detail, samples were held at 4 °C for 5 minutes. The temperature was increased to 37 °C at a rate of 10 °C/minute, and held at 37 °C for 10 minutes to allow for self-assembly. The temperature was decreased to 4 °C at a rate of 2 °C/minute, and the sample was incubated at 4 °C for 10 minutes to allow for disassembly. Again, the temperature was increased to 37 °C at the same rate and incubation time described previously for re-assembly. Lastly, for gel denaturation, the temperature was increased to 50 °C at a rate of 2 °C/minute, and held at 50 °C for 10 minutes. All ellipticity measurements were corrected for buffer baseline.

2.3 RESULTS

2.3.1 CMA is rapidly and repeatedly thermoreversible

As previously shown in Gaudet et al, collagen and CMA self-assembled into hydrogels between 2 – 3 minutes after raising the temperature from room temperature to 37 °C [55]. The storage modulus (G') of collagen (~450 Pa) was approximately 40% greater than that of CMA (~250 Pa) (Figure 2.1). As the temperature decreased, an initial increase in the storage modulus of natural collagen was observed until ~33-34 °C, followed by a reduction. In contrast, the storage modulus of CMA decreased steadily with temperature. Whereas collagen remained a gel with a positive storage modulus throughout the temperature sweep, CMA lost the ability to store energy (G' ~ 0 Pa) as the temperature approached 4 °C. As the temperature was increased to 37 °C, CMA re-assembled into a hydrogel with a slightly higher storage modulus (G' ~ 280 Pa) than after the initial assembly.

To demonstrate the extent of CMA thermoreversibility, the storage modulus was monitored as the temperature was rapidly increased and decreased multiple times (Figure 2.2 B). The gelation of CMA rapidly occurred each time the temperature reached 34 °C. Additionally, with each cycle, as the temperature decreased to 4 °C, there was a concomitant decrease in the storage modulus. In contrast, collagen did not demonstrate this same behavior, although the storage modulus changed slightly with temperature (Figure 2.2 A). Thermoreversibility of CMA gelation is robust to multiple cycles of heating and cooling.

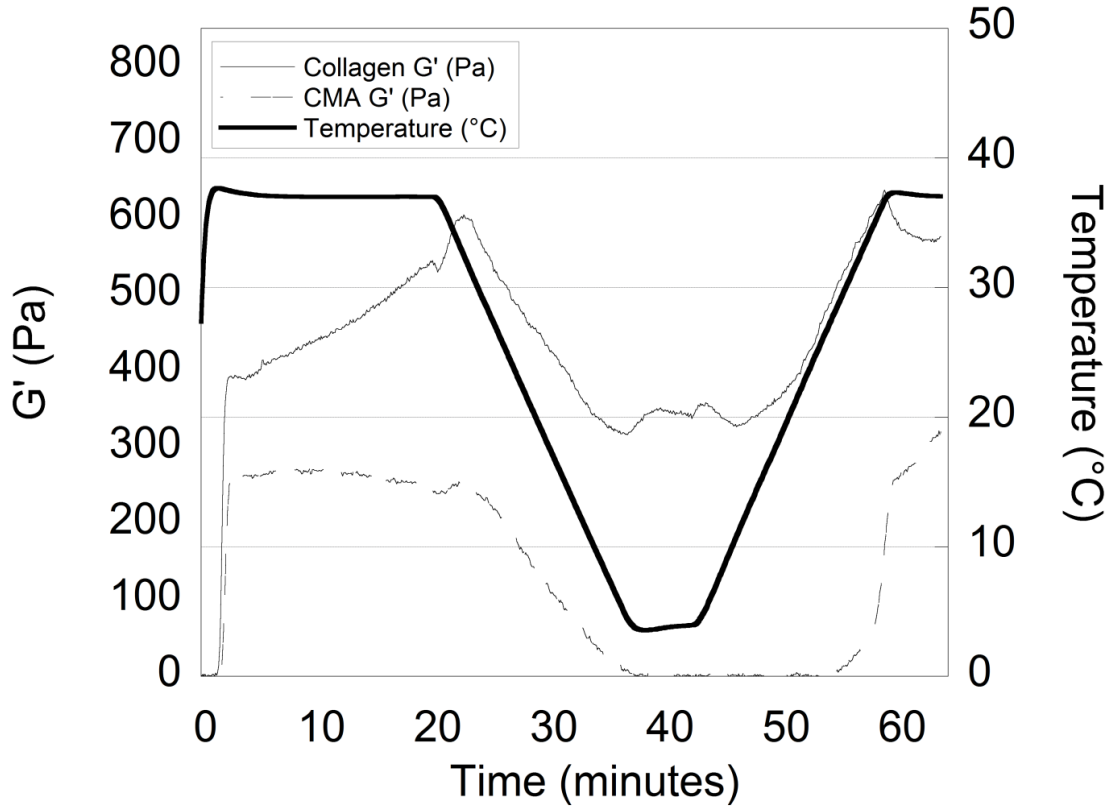

Figure 2.1 Rheology of Temperature-dependent Self-assembly and Disassembly of Collagen and CMA. Self-assembly and 'cold-melt' real-time rheological data of the storage moduli (G') of collagen (solid line) and CMA (dashed line) while the temperature (thick solid line) was increased to 37 °C, decreased to 4 °C, and increased to 37 °C at a rate of 2 °C/minute. Self-assembly of collagen and CMA gels is observed as an increase in storage modulus around t = 0 – 3 minutes. Cold-melt of CMA gels is observed as a decrease in storage modulus following t = 20 minutes.

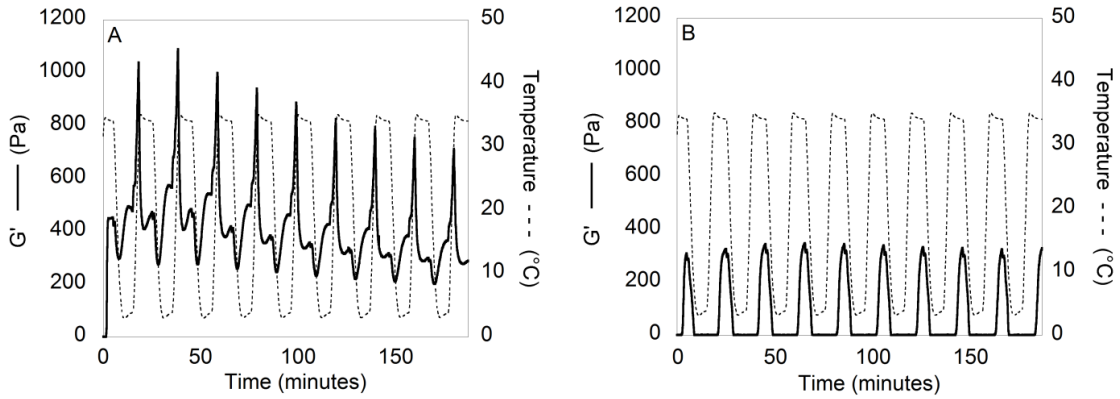

Figure 2.2 Rapid and Repeated Rheology of Temperature-dependent Self-assembly and Disassembly of Collagen and CMA. Self-assembly and 'cold-melt' rheological data of (A) collagen (G' –) and (B) CMA (G' –) with respect to temperature (- -). The temperature was cycled between 4 °C and 34 °C at a rate of 10 °C/minute with a dwell time of 5 minutes for a total of 10 cycles. CMA continues to show rapid disassembly and re-assembly as demonstrated by a decrease and increase in storage modulus, respectively, even after 10 temperature cycles. Collagen exhibits some change in storage modulus with respect to temperature, however, it remains a hydrogel throughout the temperature sweeps.

2.3.2 Collagen and CMA fibril structures are similar

Cold-melted and re-assembled CMA imaged via SEM had similar fibril formation compared to collagen or CMA gels (Figure 2.3), indicating that cold-melting and re-assembling of the hydrogel did not significantly affect fibril formation. Additionally, collagen, CMA, and cold-melted and re-assembled CMA imaged via TEM demonstrated the canonical D-periodic banding, which is a hallmark of ordered, native-like collagen assembly (Figure 2.4).

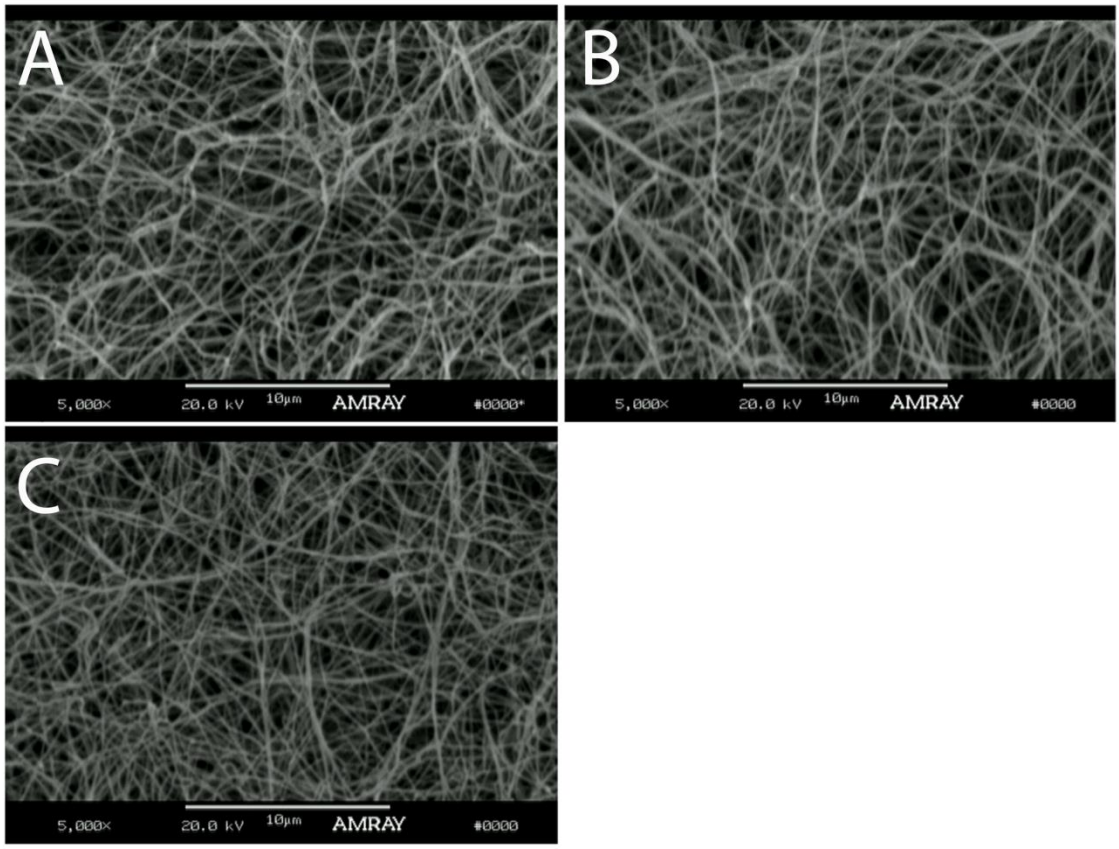

Figure 2.3 SEM of Collagen and CMA. SEM images of self-assembled collagen (A), self-assembled CMA (B), and cold-melted and re-assembled CMA gels (C) at 37 °C imaged at 5000X. Scale bar length is 10 µm. Each gel is composed of a network of fibers.

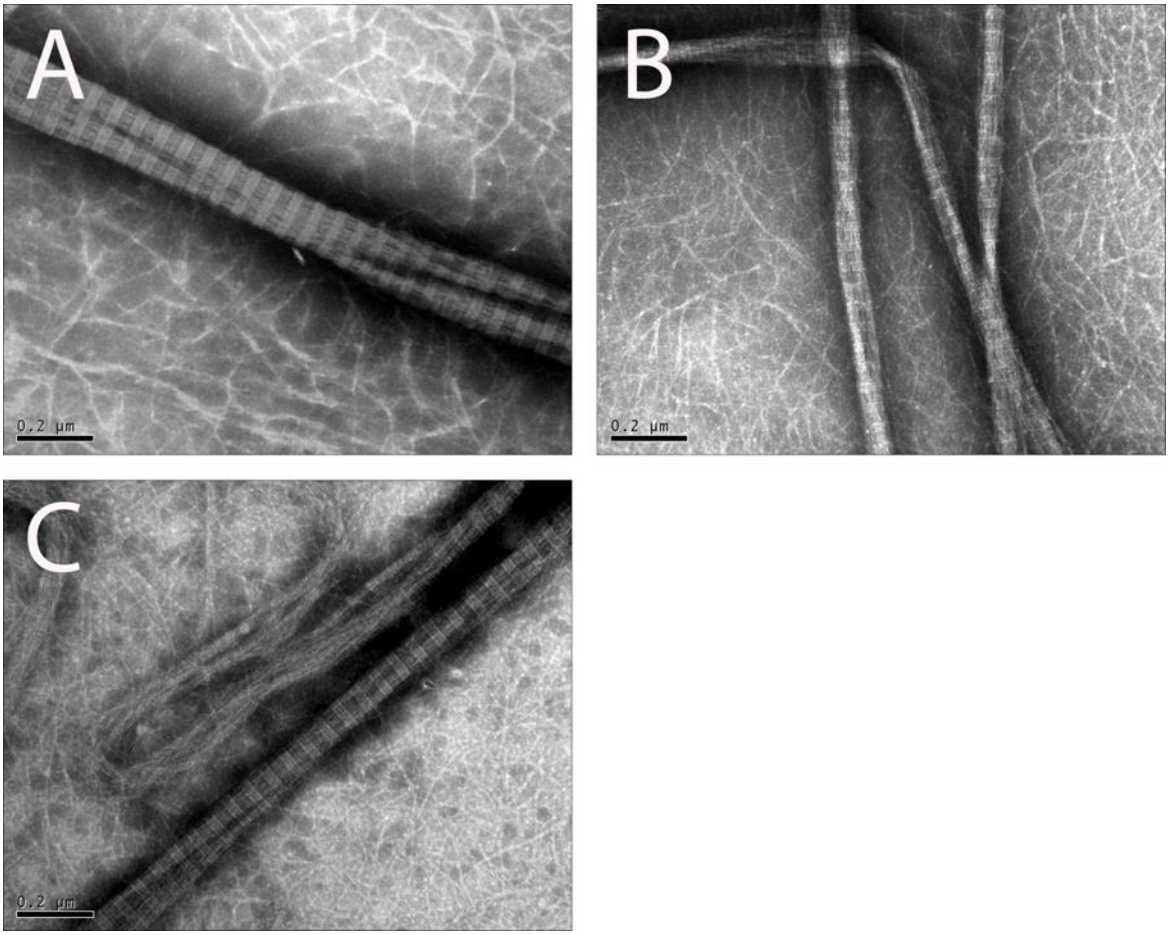

Figure 2.4 TEM of Collagen and CMA. TEM images of fibers of self-assembled collagen (A), self-assembled CMA (B), and cold-melted and reassembled CMA gels (C) at 37 °C imaged at 80000X. Scale bar length is 0.2 µm. All samples contain fibers that demonstrate approximate D-banding.

2.3.3 LS demonstrates higher order structure formation in collagen and CMA samples

Light scattering allows us to characterize particle size in solution on the orders of tens of nanometers to micrometers. However, given that the hydrodynamic properties of collagen fibers deviate significantly from the idealized behavior of spherical particles, we used the derived count rate to classify smaller and larger species based on their scattering intensity. Samples of both materials in acetic acid displayed constant and similar scattering intensities throughout the 60-minute duration of the experiment, which was consistent with the size distribution of soluble units being the same (Figure 2.5). This result demonstrates that the methacrylation process does not change the particle size of collagen compared to CMA in its soluble form. In PBS, collagen and CMA began to self-assemble immediately after samples were placed at 37 °C, as indicated by the immediate increase in light scattering and large standard deviation. Scattering intensities of collagen samples were initially larger than CMA (Figure 2.5). After 5 minutes, both samples had fully self-assembled, as shown by consistent scattering intensities (5-, 30-, and 60-minute time points). In combination with the rheological characterization, this result suggests that rapid assembly of both collagen and CMA occurs at the same time scale.

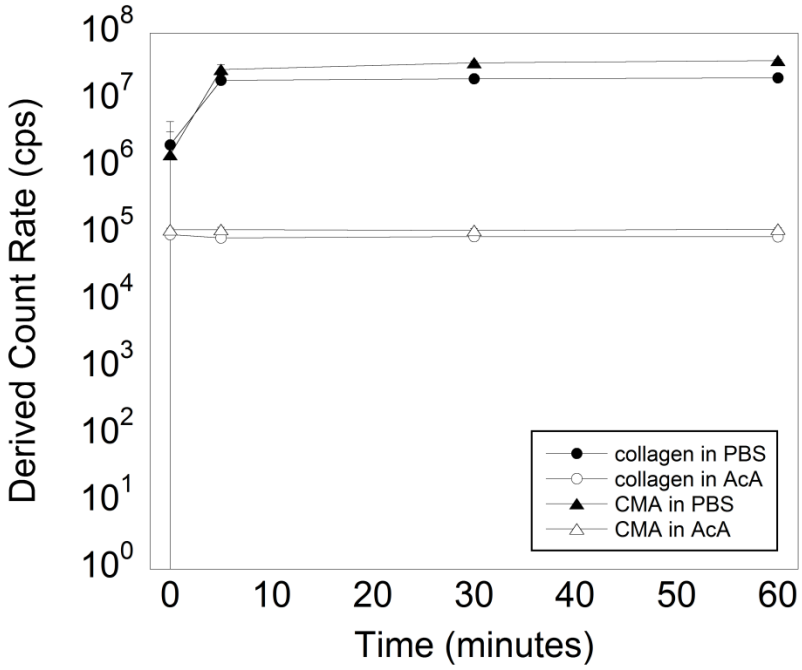

Figure 2.5 Light Scattering of Collagen and CMA. Light scattering of self-assembled collagen and CMA in acetic acid (AcA) and in PBS (open circle, filled circle, open triangle, and filled triangle, respectively) at 37 °C at 0, 5, 30, and 60 minutes. The scattering intensities were similar for collagen and CMA in each of the diluents. The scattering intensity was unchanged in acetic acid, where the low pH prevents self-assembly, but increased quickly for samples in PBS to form relatively stable structures in size by five minutes after temperature was increased. Error bars ± standard deviation.

2.3.4 CMA higher order structure reversibly disassembles and re-assembles with decreasing and increasing temperature

The size distribution of higher order structures of collagen and CMA were also characterized during cold-denaturation and re-assembly, similar to the rheology experiment. Measurements were taken every 3 °C as the temperature was raised from 4 °C to 37 °C, decreased to 4 °C, re-raised to 37 °C, and then further increased to 49 °C. Collagen and CMA in PBS had similar scattering intensities from 4 °C until the temperature for self-assembly was reached (Figure 2.6). Collagen self-assembled prior to CMA, shown again by an increase in the rate of light scattering and therefore an increase in size. As temperature was decreased back to 4 °C, CMA scattering intensity first increased, but then decreased, whereas the collagen scattering intensity remained relatively constant (Figure 2.6). This is indicative of a decrease in fibril size of CMA, whereas collagen fibril size was maintained. As the temperature was increased to 37 °C, CMA scattering intensity increased, suggestive of CMA re-assembly and an increase in fibril size.

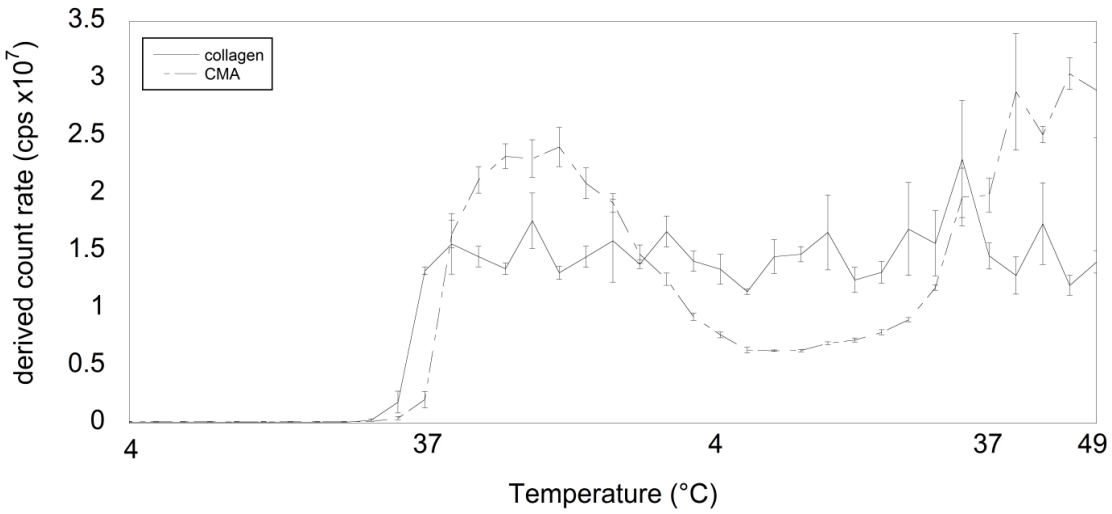

Figure 2.6 Light Scattering of Temperature-dependent Self-assembly and Disassembly of Collagen and CMA. Light scattering measurements of collagen and CMA in PBS (solid line and dashed line, respectively) were taken every 3 °C as the temperature increased from 4 °C to 37 °C, decreased back to 4 °C, and increased to 49 °C. Upon self-assembly, collagen maintained a relatively constant scattering intensity. However, the scattering intensity for CMA decreased upon cooling, and then increased again upon re-heating. Error bars ± standard deviation.

2.3.5 Collagen and CMA triple helix signal decreases coincident with self-assembly

Using circular dichroism (CD) spectroscopy, which is a measure of protein secondary structure, we observe multiple transitions in the mean residue ellipticity (MRE) at 222 nm upon heating of collagen from 4°C. The number of transitions and the temperatures at which they occur depend both on the system, CMA versus collagen, and the solution pH. Under acidic conditions, type-I collagen will form a folded triple helix that is unable to further assemble into higher-order structures [42]. Consistent with this, both collagen and CMA had a positive MRE band indicative of a triple helical supercoiled polyproline-II secondary structure at 4 °C in acetic acid (Figure 2.7 A). Both proteins denatured at 42°C, indicating that lysine methacrylation does not directly impact the stability of the triple helix itself (Figure 2.7 B).

In contrast, an additional strong negative MRE band at 222 nm was observed for both CMA and collagen when heated in PBS (Figure 2.7 B). This new transition coincided with temperature ranges (30 °C – 50 °C) that overlap with temperatures for self-assembly and denaturation observed with LS and rheology, suggesting that this negative band is diagnostic of higher-order structure.

If thermoreversibility is occurring at the level of protein structure, we would expect the positive and negative MRE bands corresponding to folded triple helix and higher order assembly to be repeatedly observed upon cycles of heating and cooling. Wavelength scans were performed on collagen and CMA samples in

PBS buffer in a temperature sweep experiment to evaluate the secondary structure at specific temperatures for self-assembly, cold-melting, and re-assembly. Heating of collagen and CMA from 4°C (Figure 2.8 A) to 37 °C (Figure 2.8 B) resulted in significant shifts in the CD spectrum from positive bands at 222 nm to strong negative bands at ~206 nm, which produced a negative ellipticity at 222 nm. After returning the samples to 4 °C to allow for cold denaturation, the collagen spectrum was unchanged indicating the preservation of the structures formed upon heating, whereas CMA regained the characteristic triple helical peak at 222 nm (Figure 2.8 C). Another round of heating drove loss of the positive MRE band for CMA at 222 nm, whereas the collagen spectrum still remained unchanged (Figure 2.8 D). Both samples fully denatured and lost all secondary structure upon a temperature increase to 50 °C (Figure 2.8 E).

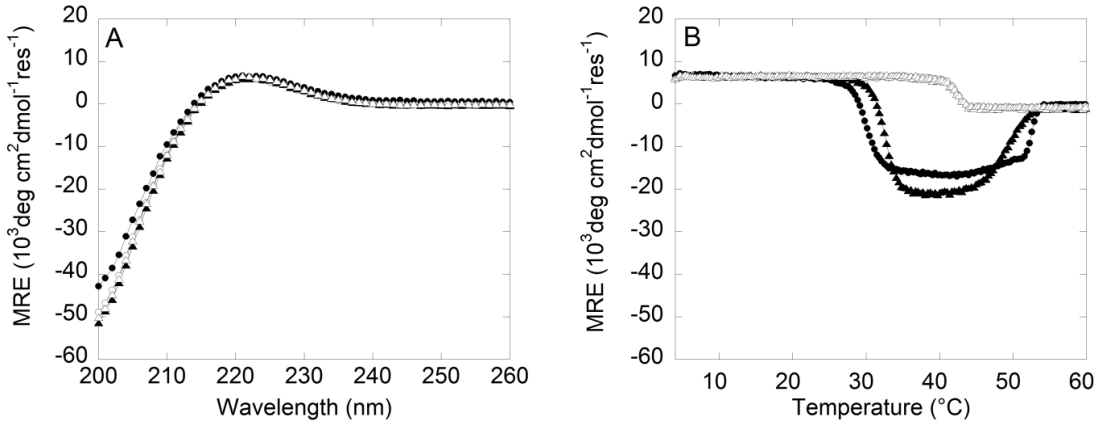

Figure 2.7 Circular Dichroism Spectroscopy of Collagen and CMA: Wavelength Scan and Temperature Melt. Circular dichroism spectroscopy wavelength scan and temperature melt of collagen and CMA samples in acetic acid (AcA) or PBS (open circle, filled circle, open triangle, filled triangle, respectively). A) All samples have a positive ellipticity peak wavelength at 222 nm. B) The ellipticity peak at 222 nm was monitored as temperature was increased from 4 °C to 60 °C. For both collagen and CMA in PBS, the positive peak at 222 nm is lost at a temperature consistent with the onset of self-assembly and is replaced by a strong negative peak until the proteins denature.

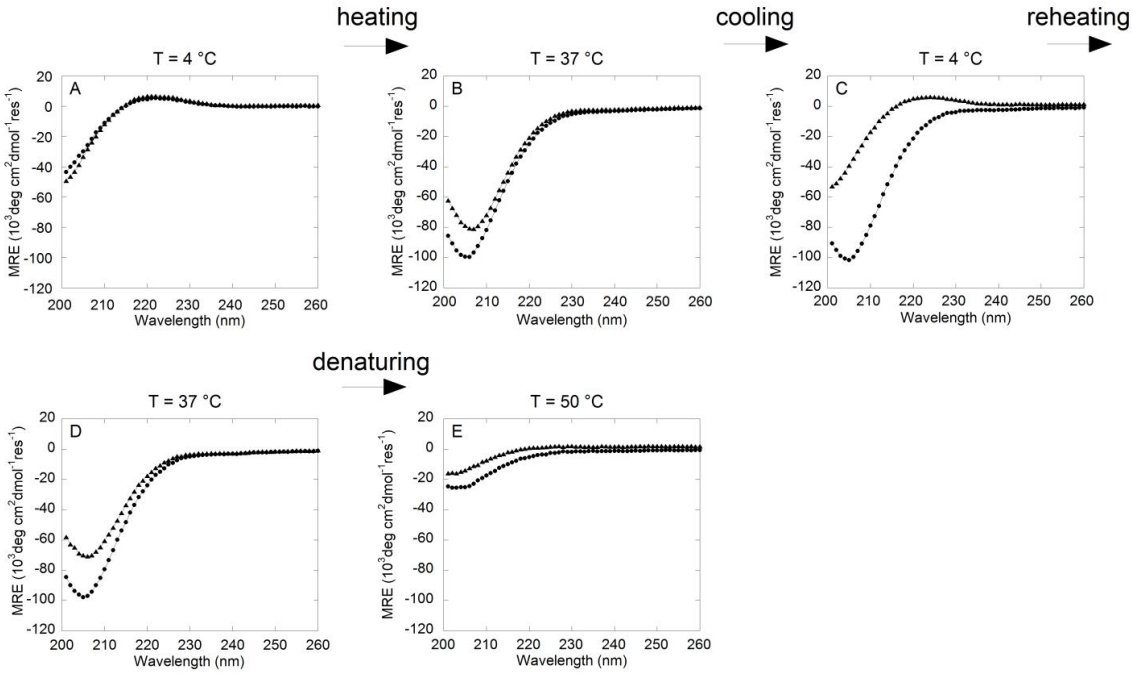

Figure 2.8 Circular Dichroism Spectroscopy of Collagen and CMA: Temperature-dependent Wavelength Scans. Circular dichroism wavelength scan from 200 nm to 260 nm of collagen (circle) and CMA (triangle) samples in PBS during cold-melt and re-assembly. The temperature was equilibrated to 4 °C, raised to 37 °C, decreased to 4 °C, increased to 37 °C, and then raised to 50 °C while wavelength scans were conducted. A) Initially, at 4 °C collagen and CMA in PBS each have positive ellipiticity peaks at 222 nm at 4 °C. B) At 37 °C, both peaks disappear. C) After returning to 4 °C, CMA regains the positive ellipticity at 222 nm, while collagen does not. D) When the temperature is returned to 37 °C, CMA loses the peak at 222 nm, and forms an identical structure to (B). Collagen remains the same. E) At 50 °C, collagen and CMA denature and lose secondary structure.

2.4 DISCUSSION

We have demonstrated and characterized the thermoreversible self-assembly of CMA caused by methacrylation of the lysine residues on type-I collagen. Previous work in our lab has used an EDC crosslinking reaction to add bioactive peptide fragments to type-I collagen gels but we have not observed the same phenomenon seen in the methacrylated collagen gels [56, 83, 84]. Type-I collagen and methacrylated collagen gels showed minimal differences in initial characterization – the sample ellipticity, fiber diameter, and count using SEM, and self-assembly properties were similar [55]. However, in characterizing and developing CMA for other applications, we found that the methacrylated collagen gels spontaneously disassembled when the temperature was decreased below 10 °C. This thermoreversible property was demonstrated in rheological measurements of the storage modulus, LS measurements of fibril size via scattering intensity, and CD measurements of the triple helix secondary structure. Cold-melted and re-assembled CMA gels formed fibrous networks and demonstrated appropriate D-banding similar to collagen or CMA hydrogels, indicating that the characteristic collagen structure is preserved. CMA exhibited a decrease in light scattering, indicative of a decrease in fibril size, a drop to zero shear modulus, and return to the hallmark triple helical CD signal following cooling, and re-assembled to a hydrogel that exhibited higher storage modulus, and a decrease of triple helix signal at physiological temperature (Figure 2.9 B). As the scattering intensity at 4 °C did not decrease to its initial value, the CMA fibrils that formed may not have completely disassembled, which could potentially

lead to larger or more fibrils and a stronger gel following re-assembly, as was observed in the cold-melt LS and rheology. Conversely, type-I collagen self-assembly was shown to be irreversible at the same time scale using these same measurements; although triple helix signal decreases in both collagen and CMA samples, collagen storage modulus remains positive, indicating a gel-like state is maintained, and light scattering intensities remain relatively constant throughout the temperature sweep (Figure 2.9 A).

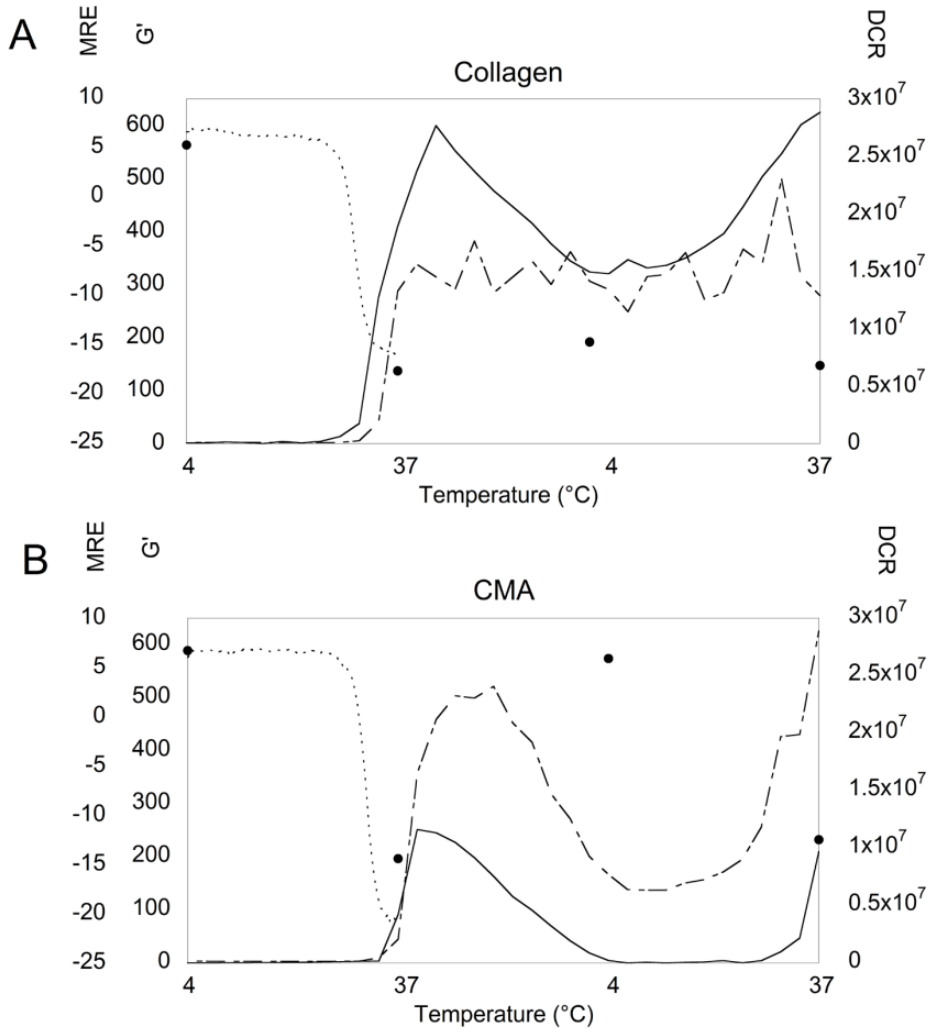

Figure 2.9 Correlation of Temperature-dependent Storage Modulus, Mean Residue Ellipticity, and Derived Count Rate of Collagen and CMA. Approximate correlations among (A) collagen and (B) CMA storage modulus (G', Pa) (solid line), derived count rate (DCR, cps) (dot-dashed line), and mean residue ellipticity (MRE, 10^3 deg cm^2 $dmol^{-1}$ res^{-1}) at 222 nm (small dashed line), derived from rheology, DLS, and temperature-melt CD spectroscopy experiments, respectively (Figs. 1, 6, and 7). Discrete MRE measurements at 222 nm obtained from wavelength scans at each temperature are also presented

(filled circle) (Figure 2.8). Initially, at 4 °C, collagen and CMA are triple helical and unassembled. At 37 °C, collagen and CMA exhibit a negative MRE, and begin to form higher order structures indicated by an increase in DCR and G'. Returning to 4 °C, CMA loses the ability to store energy, exhibiting a storage modulus of ~ 0 Pa, although DCR has not reached its initial value, while the storage modulus of collagen slightly decreases, although the DCR remains relatively constant. The MRE of CMA at 4 °C has returned to a positive value, while the MRE of collagen stays negative. Finally, at 37 °C, CMA re-assembles as seen by an increase in G' and DCR and a return to a negative MRE value, while collagen G', DCR, and MRE remain constant.

Additionally, rheology experiments demonstrate a correlation between the rate of change of the storage modulus of CMA and the cooling/heating rates compared to collagen (Figure 2.1 and Figure 2.2). Initial assembly of both collagen and CMA occurs quickly (Figure 2.1, 2 – 3 minutes). In both experiments, the rate of change of the storage modulus of CMA follows either rate, 2 °C/minute or 10 °C/minute, upon disassembly and re-assembly (Figure 2.1 and Fig 2.2 B). The lack of hysteresis upon multiple cycles is demonstrated by full sol-gel transitions occurring at the specified rate in the cooling/heating schedule in each experiment. In contrast, collagen does not exhibit complete disassembly/re-assembly and maintains a hydrogel state with positive storage modulus. However, slow disassembly and re-assembly seen with a slow cooling/heating rate (Figure 2.1) may lead to the accumulating hysteresis seen in rapid disassembly/re-assembly experiments (Figure 2.2 A).

Further, thermoreversible behavior spanned multiple concentrations, where low concentrations are required when using CD Spectroscopy and LS to prevent scattering, and high concentrations are required to discern changes in storage modulus using rheology. Interestingly, despite these differences, there was good agreement of the dynamic, temperature-dependent changes in the data across testing modalities, specifically, a lag in initial self-assembly of CMA relative to collagen (Figure 2.1), and a correlation of the loss (and re-gain) of triple helical signal in CD with assembly (and disassembly) from the other modalities.

CD spectroscopy results of self-assembled collagen and CMA exhibited trends that to our knowledge have not been shown before in the literature. Often, shorter fragments of collagen have been characterized using these methods in acidic conditions at physiological temperature. Similar to results with our collagen and CMA in acidic conditions, previous work with full length rat tail tendon collagen has shown that collagen and a glycidyl methacrylated collagen display thermal denaturing at temperatures around 40 °C and 35 °C in acidic conditions, respectively [85]. However, CD spectroscopy of our self-assembled collagen and CMA in physiological conditions lacked the positive ellipticity peak for triple helical structure. We hypothesize that collagen and CMA remain triple helical in structure, but have exhibited a change in the CD spectroscopy signal. Based on the TEM results, both self-assembled collagen and CMA exhibit D-periodic banding in the fibrils, indicating triple helical structure. This is consistent with previous studies in rat tail collagen, showing triple helical structure in aggregate fibrils using X-ray diffraction [86, 87]. Therefore, as this change in CD signal is observed in both collagen and CMA, it may be due to differences in intermolecular interactions as a result of higher order assembly, which can perturb the circular dichroism of the protein backbone. Such perturbations can be caused by aromatic amino acids, which have been shown to be involved in direct contacts between triple-helical units in the higher order assembly [88-90]. This novel observation will be studied in the future to understand the molecular determinants of the negative MRE value at 222 nm.

The characterizations presented in this paper were motivated by discovery of thermoreversible CMA self-assembly. Previous work has shown that collagen fibrillogenesis is partially dependent on the telopeptide region. The amino acid sequences of bovine type-I collagen show that the C-terminal of the telopeptide region contains a substantial number of lysines, the amino acid that the methacrylic acid is conjugated. The α1 chain contains 56 lysines while the α2 chain contains 49 lysines, of which each chain contains 17 lysines on the C-terminal telopeptide (UniProtKB/Swiss-Prot, sequences P02453.3 and P02465.2). Based on previous characterization of CMA, approximately 20% of the collagen triple helix is methacrylated [55]. The dense population of lysines in the telopeptide region may account for delays in CMA self-assembly compared to collagen, as seen in the rheology. The triple helix is intact in the methacrylated collagen, but as shown in the CD spectra, ‘assembly’ of CMA is delayed compared to collagen and denaturation occurred more rapidly, indicating that the CMA fibrils are meta-stable compared to collagen fibrils. We have previously used the same EDC crosslinking method to couple bioactive peptides to collagen but did not observe thermoreversible behavior, suggesting that the thermoreversibility is specific to the molecule added, and perhaps methacrylation uniquely. We hypothesize that the differences in intermolecular associations during self-assembly of collagen and CMA account for the thermoreversibility seen in the methacrylated collagen. As described in Kar et al., higher order assembly at physiological temperatures is predicted to occur through two steps: 1) partial unfolding of the native triple helical state to a ‘loosened’ triple helical

state, followed by 2) aggregation of ‘loosened’ triple helical molecules [91]. Of these steps, it is unlikely that there are differences in the native triple helical state of collagen and CMA based on the CD and LS results in acidic conditions. A mechanism that explains differences in aggregation may account for the thermoreversibility of CMA. The telopeptide region is particularly important in catalyzing self-assembly, and is involved in the formation of covalent crosslinks between adjacent triple helices [92, 93]. If a significant proportion of the lysines in this region are methacrylated, a perturbation of interactions between the telopeptide and triple helix may account for the formation of a less stable aggregate of CMA compared to collagen. This aggregate form may be unstable at cooler temperatures, accounting for the thermoreversibility of CMA compared to type-I collagen. Future studies will characterize where methacrylates are conjugated, and specifically, if methacrylated lysine residues in the telopeptide region of type-I collagen are the source for the protein’s thermoreversibility.

Thermoreversible biomaterials have a variety of applications in 3D cell culture, drug delivery, and tissue engineering. Based on the intrinsic properties of the biomaterial, constructs may have vastly different temperature-dependent properties, which direct the potential applications for that material. CMA self-assembly and cold-denaturing temperatures match other previously established thermoreversible biomaterials, as it loses bulk mechanical properties at temperatures less than 10 °C, and forms a soft hydrogel (~250 Pa) at physiological temperature. Current thermoreversible biomaterials are primarily synthetic hydrogels, and have been utilized for tissue engineering applications as

scaffolds for corneal wound repair, constructs for cell encapsulation, or drug delivery [94-98]. To our knowledge, CMA is the first thermoreversible, collagen-based hydrogel that has the ability to reversibly self-assemble into a fibrillar network at physiological temperature (above 20 °C), and is biodegradable through natural enzymes, biofunctional through crosslinking methods, and cytocompatible [2, 6]. Future studies will aim to utilize these unique properties of CMA for soft tissue engineering applications.

2.5 CONCLUSION

In this study, we have examined the temperature-dependent, reversible self-assembly of CMA that does not occur with type-I collagen. Collagen and CMA both demonstrate triple helical structure in soluble form, but also lose evidence of triple helical content during self-assembly in physiological conditions. When cooled, CMA gels disassemble from a fibrillar gel to a solution. Commensurate with this disassembly, light scattering decreases, indicating a decrease in fibril size, and triple helix signal is recovered. Following a temperature increase to 37 °C, CMA gels re-assemble, the rate of light scattering increases, and the triple helix secondary structure signal changes. Conversely, collagen gels maintain secondary and fibrillar structure throughout the temperature sweep, demonstrating irreversible self-assembly, at least over the time scale examined in these studies. Overall, the cause for disassembly and re-assembly of CMA gels is a result of the collagen methacrylation. CMA tertiary structure may be disrupted in the telopeptide region due to the presence of the

methacrylates, allowing for disassembly at cool temperatures. CMA may serve as a model collagen-like protein for comparison of flexibility, stability, and self-assembly to collagen, or for cold-denaturation studies. Furthermore, CMA gels have new properties as a tissue engineered scaffold; in addition to photolabile modifications of gel mechanical properties, CMA can be utilized as a thermoreversible self-assembled hydrogel. These hydrogels can be utilized in tissue engineering, cell encapsulation and microenvironment design, and as a drug delivery system.

2.6 ACKNOWLEDGMENTS

We would like to thank Dr. I John Khan for his expertise and guidance in this work. This project was supported in part by National Science Foundation Grants ARRA-CBET0846328 and DMR-0907273, the National Institutes of Health Office of the Director DP2-OD-006478-1, and fellowships from New Jersey Commission on Spinal Cord Research Fellowship 08-2937-SCR-E-0, National Science Foundation (NSF DGE 0801620, IGERT on the Integrated Science and Engineering of Stem Cells), and Rutgers-UMDNJ Biotechnology Training Program (NIH Grant Number 5T32GM008339-20).

CHAPTER 3. INVESTIGATION OF COLLAGEN MODIFICATION AND THERMOREVERSIBILITY

3.1 INTRODUCTION

The collagen family is one of the main protein families present throughout the human body, comprising approximately 30% of the total protein body content [39]. Of that, the overwhelming majority consists of type-I collagen, a protein that can form highly organized fibers that provide mechanical strength and structural support throughout the bones, skin, and connective tissue. Because of its ubiquity throughout the body, it is often used as a biomaterial for tissue engineering. It was first used in regenerative medicine over 20 years ago as a scaffold for wound healing, and continues to be explored for both soft and hard tissue engineering applications [40, 45, 54].

For use as tissue equivalents, type-I collagen is often extracted with ease from animal tissues, typically bovine or porcine, into dilute acid [40, 43]. In its isolated form, type-I collagen is usually comprised of triple-helical monomers, but sometimes is present as dimers, trimers, or larger crosslinked components [75]. Isolation of type-I collagen may also vary by telopeptide content. The telopeptide is a short nonhelical peptide region that flanks the collagen triple-helix. During isolation, this region may be removed through the use of specific enzymes such as pepsin. In either case, the collagen suspension of triple-helical monomers can self-assemble *in vitro* into a fibrillar hydrogel composed of D-banded fibers at

physiological conditions. The axial packing of the collagen molecule allows for fibril formation longer than the length of the collagen molecule (~ 300 nm) [99]. In axial packing, each molecule is staggered by ~67 nm; these length differences are the reason for a gap region, where four collagen molecules overlap, compared to the overlap region, where five collagen molecules overlap [99]. This is known as the D-period, which is approximately ~67 nm [99].

There are a variety of ways to alter the properties of the collagen fiber and fibrillar gel by changing the conditions of fibrillogenesis. For example, fibers can form at various pH and temperatures, ranging from 5 – 8 and 20 °C to 40 °C respectively, and the D-period and resulting fiber and mechanical properties change with respect to self-assembly conditions [41, 42, 100]. Fibers formed at neutral pH at 25 °C have a larger fiber diameter and form mechanically stronger hydrogels than those formed at 37 °C [41, 101]. Nikoleava et al report the most densely packed fibers and therefore smallest fiber diameter had formed at 36.5 °C due to the removal of water from the surface of collagen molecules [101].

Telopeptides can also affect fiber and gel properties. Telopeptides play an important role in catalyzing fibrillogenesis [102, 103]. Additionally, after fibrillogenesis, the collagen telopeptides stabilize fibers through crosslinks with the triple-helical regions on adjacent collagen molecules [93, 104, 105]. Treatment with enzymes such as pepsin or pronase cleaves the telopeptide region on collagen molecules. Many times, the enzymatic treatment does not result in full cleavage of the telopeptides, which merely delays, but does not prevent, collagen fibril formation [75, 106]. Depending on the extent of the

telopeptide removal, this has also been shown to affect loss of diameter uniformity, or sometimes the lack of fibril formation and instead, the formation of small non-banded fibrous aggregates [75].

In our studies, we have shown that methacrylation induces temperature-dependent reversibility of collagen fibrillogenesis [107]. Collagen methacrylamide (CMA) self-assembles into a fibrillar hydrogel at physiological conditions, and can reversibly disassemble into a liquid suspension at temperatures less than 10 °C, while telopeptide-containing type-I collagen cannot [55, 107]. While we have performed similar chemistry on type-I collagen to couple other molecules, this is the first time in which we have observed this thermoreversible behavior, suggesting that thermoreversibility may be specific to the compound added, or potentially methacrylic acid uniquely [58, 107].

Past studies in our lab have used 1-ethyl-3-(3-dimethylaminopropyl) carbodiimide (EDC) to couple bioactive ligands to type-I collagen [56, 58, 83, 108]. In water, EDC reacts with carboxylic acid groups present at the end of peptides or methacrylic acid to form an active, but unstable O-acylisourea intermediate [109]. This intermediate is displaced via nucleophilic attack from the primary amino groups (lysine residues on collagen), resulting in conjugation of the carboxyl of the bioactive ligand directly to the amine on type-I collagen [109]. To methacrylate collagen, we used EDC and N-hydroxysuccinimide (NHS), where NHS acts to stabilize the O-acrylisourea intermediate to increase conjugation efficiency [55, 109]. This reaction targets the lysines on type-I collagen and the telopeptide region contains a disproportionate number of lysines

(over 1/3 of the total lysines). Due to the importance of the telopeptides in self-assembly and fibril stabilization, it is possible that a perturbation of interactions between the telopeptide and triple helix through the addition of methacrylic acid may account for the formation of a less stable aggregate of CMA that is unstable at cooler temperatures [93, 104, 105, 107].

Herein, we aimed to interrogate the coupling chemistry used in our CMA synthesis to improve our understanding of the amount of methacrylation necessary to affect the fibril-forming properties of type-I collagen. Further, we aimed to couple other moieties to type-I collagen to discern if thermoreversible behavior could be replicated, or if it was unique to methacrylation. Interestingly, use of the NHS crosslinking agent in combination with EDC was necessary to make CMA thermoreversible; however, the amount of EDC/NHS/methacrylic acid added to collagen made no difference. Furthermore, thermoreversibility was not specific to methacrylation; other organic molecules with similar properties were conjugated to type-I collagen and were shown to induce thermoreversibility.

This work could contribute greatly to biomedical engineering, biochemistry, and medical uses for type-I collagen. First, these modified, thermoreversible collagens could serve as a model to study fibrillogenesis, which is important for collagen-based biomaterials in tissue engineering, or potentially understanding problems associated with improper assembly of collagen, which can lead to various collagen-linked disorders such as Ehlers-Danlos syndrome [110, 111]. Thermoreversible materials are also of great utility in tissue engineering for applications in drug delivery and rapid prototyping, and may also

serve as a temporary scaffold for cell encapsulation for other uses in regenerative medicine [97, 98, 112]. An improved understanding of type-I collagen methacrylation and other type-I collagen modifications will yield important insights into what contributes to thermoreversible behavior.

3.2 MATERIALS AND METHODS

3.2.1 Materials for Collagen Modification

Bovine-skin derived type-I collagen (C857) was purchased from Elastin Products Company (Owensville, MO) and prepared at 3.75 mg/mL in 0.02 M acetic acid. EDC and NHS were purchased from (03450 and 56485, respectively, Sigma-Aldrich, St. Louis, MO). MES served as the buffer for the reaction (76309, Sigma-Aldrich).

3.2.2 Collagen Methacrylation Using EDC Alone or EDC and NHS

The differences in temperature-dependent mechanical properties and grafting efficiencies were assessed following collagen methacrylation using EDC alone and using EDC and NHS, where NHS increases the efficiency of carboxyl-to-amine conjugation. CMA was prepared by methacrylating the amines of type-I collagen. The detailed reaction steps are outlined in Gaudet [67]. Batches were prepared by reacting 33.3 µg of EDC (dissolved in MES) with 33.3 µL methacrylic acid (MA) (155721, Sigma-Aldrich) or 33.3 µg EDC and 16.7 µg NHS (dissolved in MES) with 33.3 µL MA in a total volume of 667 µL of MES buffer. Reactants were vortexed and incubated at 37 °C to allow for the reaction. The mixture was

cooled for 5 minutes on ice, and then added to 10 mL of type-I collagen (3.75 mg/mL in 0.02 M acetic acid). The CMA mixture reacted for 24 hours on a rotator at 4 °C. The CMA mixture was dialyzed using SnakeSkin Dialysis Tubing (68100, Thermo Fisher Scientific, Waltham, MA) with a molecular weight cut off of 10,000 against 1.5 L of 0.02 M acetic acid for 4, 12, and 24 hours. The product was frozen at -20 °C and -80 °C for four hours each, and then lyophilized for 72 hours. Freeze dried CMA was weighed and resuspended at 3.75 mg/mL in 0.02 M acetic acid by mixing overnight at 4 °C using the rotator. At all points during the reaction and use of CMA, solutions or samples were kept on ice and shielded from light. Grafting estimation and rheology measurements were performed on collagen and CMA samples as outlined below.

3.2.3 Collagen Methacrylation in Varying Volumetric Ratios

CMA was produced keeping the molar ratio of EDC/NHS/MA (reaction mixture) constant, but varying the volumetric ratio of the reaction mixture to collagen. In our standard protocol to prepare, CMA, 667 µL of mixture is added to 10 mL of type-I collagen. For the purposes of this study, the ratio of reaction mixture to collagen will be referred to as 1:1 or 100:100 as the standard volumetric ratio, and the ratio was further decreased. We produced that sample (100:100) as a positive control, and also produced CMA with ratios of reaction mixture to collagen as follows: 75:100, 50:100, 25:100, and 5:100. These CMA samples are hereby named 100%, 75%, 50%, 25%, and 5% CMA, respectively. The remainder of the synthesis was performed as outlined previously. Again,

freeze dried CMA was weighed and resuspended at 3.75 mg/mL in 0.02 M acetic acid, and grafting estimation and rheology measurements were performed.

3.2.4 Methacrylation of Atelocollagen

Atelocollagen was purchased from Elastin Products Company (PC278) and resolubilized at 3.75 mg/mL in 0.02 acetic acid. Atelocollagen was methacrylated using the standard protocol with EDC/NHS as described in 3.2.2. Freeze-dried atelo-CMA was weighed and resuspended at 3.75 mg/mL in 0.02 M acetic acid and was further examined for the percent methacrylated in comparison to atelocollagen. The mechanical properties of both atelocollagen and atelo-CMA were also compared.

3.2.5 Collagen Modification Using Alternate Moieties

Collagen was modified using 12 unique organic compounds in addition to methacrylic acid, with molecular weights ranging from ~40 Da to ~350 Da and pKa ranging from ~2.5 to ~6.5. Collagen was reacted with the same molar ratio of EDC/NHS/MA for each organic compound, with volumetric ratios of the reaction mixture and collagen ranging between 5:100 and 100:100 (referred to as 5% - 100%). This was due to solubility issues with a subset of the organic compounds. Further details regarding the exact organic compound coupled or reaction methods cannot be disclosed at this time. All other steps in the synthesis process remained the same, and freeze dried samples were reconstituted in 0.02 M acetic acid at 3.75 mg/mL for further grafting efficiency and rheology testing.

3.2.6 Grafting Efficiency Estimation

Fluorescamine (F9015, Sigma-Aldrich) is a non-fluorescent compound that becomes fluorescent when reacted with a protein that contains free amines on lysines and N-terminal amines. This can be used to measure the amount of lysines that are consumed through methacrylation or coupling of other moieties. Type-I collagen at 3.75 mg/mL, 3 mg/mL, 2.25 mg/mL, 1.5 mg/mL, 0.75 mg/mL, and 0 mg/mL in 0.02 M acetic acid is used to create a standard curve. The modified collagen sample was used at 3.75 mg/mL. All samples (500 µL each) were incubated at 60 °C to denature the proteins. Samples were plated (75 µL/well) in a 96 well plate. Fluorescamine was dissolved at 3 mg/mL in neat acetone, and 25 µL of the dissolved fluorescamine was added to each well. The plate was incubated for 10 minutes under aluminum foil at room temperature. The well plate was read for fluorescence emission from the bottom of the plate using an Infinite M200 Pro (Tecan, Männedorf, Switzerland) by exciting at 400 nm, emitting at 460 nm, at multiple reads per well with an area of 750 μm^2 with 4x4, circles and gain 100. The average fluorescence intensity for each collagen concentration (n = 5) was plotted and fit to a linear curve, from which the "predicted concentration" of the modified sample could be determined. The percent grafting efficiency was calculated by dividing the actual concentration of modified collagen (3.75 mg/mL) by the "predicted concentration" and multiplying by 100%. Unless otherwise stated, variations in CMA or other grafted collagens have only been synthesized once, and therefore, grafting efficiency may in fact vary.

3.2.7 Rheology

Collagen (C857 or PC 278) was mixed in 500 µL batches containing 10 µL 1M HEPES (H3537, Sigma-Aldrich), 63 or 65 µL 0.15N NaOH (S2770, Sigma-Aldrich), 50 µL 10X PBS (P5493, Sigma-Aldrich), 38.5 or 36.5 µL1X PBS (860454, Thermo Fisher Scientific) and 338.5 µL type-I collagen in 0.02 N acetic acid. The variations in 0.15N NaOH and 1X PBS varied based on the lot of collagen used. CMA or other photoreactive collagens were mixed in 500 µL batches containing 10 µL HEPES, 67 or 68 µL 0.15N NaOH, 50 µL 10X PBS, 29.5 or 28.5 µL1X PBS, 5 µL of 10% Irgacure (I2959, a gift from Ciba Specialty Chemicals) in neat methanol, and 338.5 µL CMA or other photoreactive collagens in 0.02 N acetic acid. Irgacure was not included with modified collagens synthesized that were not photoreactive. Instead, these preparations were supplemented with 5 µL additional 1X PBS to reach 500 µL.

Rheological measurements were performed with two protocols for each formulation. To assess the temperature-dependent mechanical properties of the collagen-based hydrogels, a sample of 200 µl was loaded between a 20 mm top parallel plate and the bottom parallel plate of a Kinexus Ultra rotational rheometer (Malvern Instruments, Malvern, UK). The temperature was increased from 25 °C to 37 °C at a rate of 10 °C/minute with a Peltier-controlled stage. Depending on the modified collagen tested, the temperature was held at 37 °C for at least 20 minutes, with a maximum time of one hour. To assess potential thermoreversibility, the temperature was then decreased to 4 °C and increased again to 37 °C at a rate of 2 °C/minute, and given an additional 10 minutes to 1

hour at 37 °C for re-assembly, again depending on the batch of modified collagen tested.

To assess the photocrosslinkability, similar measurements were performed, but a quartz bottom plate was used to allow for UV photocrosslinking during rheology. Photoreactive hydrogels were self-assembled at 37 °C for 10 minutes to 30 minutes depending on the modified collagen. Hydrogels were photocrosslinked after fully self-assembled for two minutes using UV light (365 nm, 50 mW/cm^2).

Throughout all rheology measurements, the sample was oscillated at 1 rad/s, 0.5% strain while measuring the resultant torque to acquire the storage and loss moduli of the hydrogels.

The mechanical properties were obtained for three separately prepared samples via rheology, and the resultant curve is the average of that data. In some cases, a representative rheology curve is shown for each sample for clarity. Additionally, for discrete storage moduli values, the modulus shown is the average of 5 minutes of measurements for the averaged real-time storage modulus data. The storage modulus was verified to be constant at this time.

3.2.8 Machine Learning

The dataset consisted of the experimentally-derived physical properties of the organic compounds, including molecular weight, partition coefficient (logP), and pKa. Molecular weight ranged from ~ 40 Da to ~350 Da, logP ranged from ~-3 to ~2.5, and pKa ranged from ~2.5 to ~6.5. Some predicted values were added

to the dataset due to the lack of experimental data; of 13 unique organic compounds, the logP of two compounds and the logP and pKa of one compound were predicted. Values were obtained from Sigma-Aldrich product information, PubChem, the Human Metabolome Database, and the Biological Magnetic Resonance Bank [113-117]. The dataset also consisted of properties of the collagen modified with the respective organic compound. These properties including grafting efficiency (%), the storage modulus of prepared hydrogels after 15 minutes at 37 °C (Pa), and the thermoreversibility (binary), determined experimentally as outlined above.

WEKA (Waikato Environment for Knowledge Analysis) is an open source JAVA software package (University of Waikato, New Zealand) issued under the GNU General Public License. WEKA was utilized for data classification, regression, and clustering. A comma separated value file containing data for each modified collagen was loaded into WEKA software. All attributes were numeric, with the exception of thermoreversibility, which was converted to binary in WEKA. All algorithms ran with WEKA default settings unless otherwise specified.

The J48 tree (C4.5 algorithm in WEKA) was used with 10-fold cross validation and reduced error pruning. The splitting criterion for the J48 classifier is normalized information gain, which is employed recursively on progressively smaller sublists for the decision tree [118]. This classifier was implemented due to its simple algorithm, ease of construction, and strong learning ability [118, 119]. In cross validation, data is partitioned into two groups where one portion of

the data is used as a training set while the rest of the dataset is used as a validation set; this process was repeated 10 times in our classification [120]. We also employed reduced error pruning with 10-fold cross validation to create the simplest tree without reducing the accuracy of the decision tree [121]. Data was classified in this method two ways, and was varied based on the number of instances at a particular identified node. In the first classification scheme, the minimum number of instances at a node was 2, whereas in the second classification scheme, the number of instances was increased to 10. The latter classification scheme allowed for the design of the 'simplest tree.' The confidence in the decision trees were measured using the kappa statistic, a quantitative measurement of agreement of variation in the 10-fold cross validation runs [122]. A kappa statistic of 1 indicates perfect agreement, where a value of 0 indicates agreement by chance [122].

Lastly, multiple or simple linear regression with 10-fold cross validation was performed on the dataset to model the potential relationship of all variables to either grafting efficiency or storage modulus. The correlation coefficient was used to evaluate regression.

3.3 RESULTS

3.3.1 Crosslinkers EDC and NHS used in combination produce a thermoreversible collagen

Different combinations of EDC and EDC/NHS were used in the past to generate a photocrosslinkable collagen. Previously, this protocol was optimized for the maximum storage modulus following photocrosslinking for the highest control over CMA hydrogel mechanical properties [67]. In this study, we investigated the temperature-dependent mechanical properties and grafting efficiency of CMA prepared with EDC or EDC/NHS. Grafting efficiencies for batches of CMA: EDC/NHS range from ~25% – ~60%, while those for CMA: EDC range from ~10 – ~26% (Figure 3.1). While these ranges for estimated methacrylation overlap, there are discernable differences in the mechanical properties of the resultant batches of CMA (Figure 3.2). In contrast to CMA prepared with EDC/NHS, which is fully thermoreversible at cool temperatures, CMA prepared with EDC is not; the storage modulus decreases steadily as the temperature decreases, but never reaches ~0 Pa (Figure 3.2 A). Additionally, CMA prepared with EDC has lower mechanical properties once photocrosslinked, reaching less than half of the storage modulus of fully photocrosslinked CMA prepared with EDC/NHS (Figure 3.2 B and C).

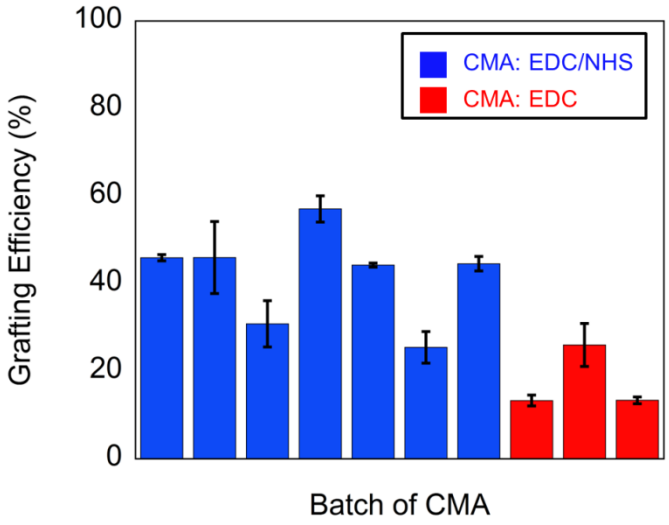

Figure 3.1 Grafting Efficiency of CMA Prepared with EDC or EDC/NHS. CMA synthesized using crosslinkers EDC/NHS was typically more methacrylated than CMA synthesized using EDC. The amount of methcrylation ranged from ~25% – ~60% in batches prepared with EDC/NHS compared to ~10% – ~26% in batches prepared with EDC.

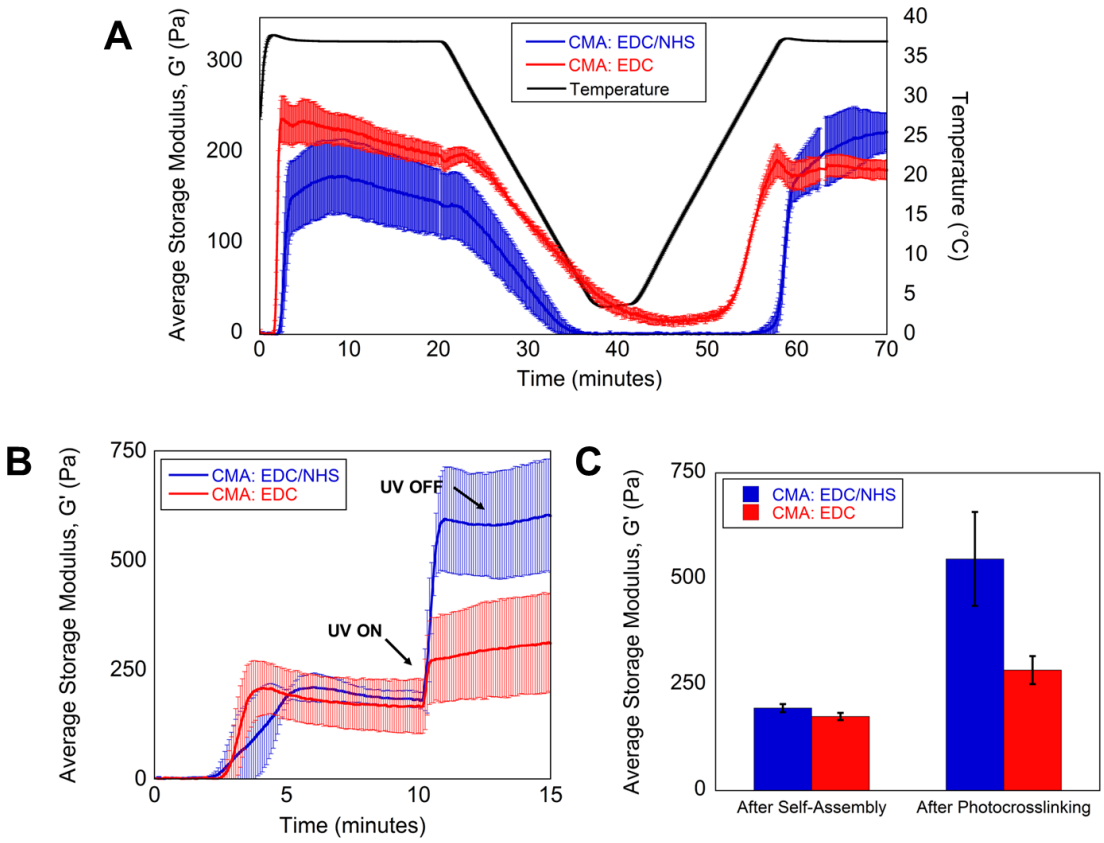

Figure 3.2 Temperature-dependent Rheology of CMA Prepared with EDC or EDC/NHS. A) Self-assembly of CMA prepared with EDC/NHS was thermoreversible, whereas self-assembly of CMA prepared with EDC was not fully reversible. While hydrogels of CMA prepared with EDC did not fully disassemble, the storage modulus (G') of these hydrogels decreased significantly at cool temperatures. **B) and C)** The mechanical properties of CMA prepared with EDC/NHS and CMA prepared with EDC were quite similar following initial self-assembly. After UV exposure, G' of photocrosslinked CMA hydrogels prepared with EDC/NHS had an approximate 3-fold increase compared to the

initial G', in contrast to G' of photocrosslinked CMA hydrogels prepared with EDC that merely doubled after photocrosslinking.

3.3.2 Low methacrylation still results in a thermoreversible collagen, but is less photoreactive

The molar amount of EDC/NHS/MA is in excess compared to the number of lysines on type-I collagen. Therefore, in typical batches of CMA, we believe we are at maximal coupling under the conditions of which the reaction is performed. The volumetric ratio of EDC/NHS/MA to collagen was varied to investigate if it was possible to synthesize a thermoreversible, methacrylated collagen with less functionalization. Four batches of CMA were prepared in which the volumetric ratio ranged from 5 – 75:100 (EDC/NHS/MA:collagen) compared to the standard 100:100 ratio. These ratios are referred to hereafter as 5% through 100% for 5:100 through 100:100, respectively. The grafting efficiency of CMA produced with 5% of the standard volume had the lowest methacrylation, with ~15% of the lysines modified (Figure 3.3). The grafting efficiencies of other prepared batches, 25% and 75%, were similar to the standard batch, whereas the 50% batch was slightly less modified. Despite the differences in the amount of methcrylation, all prepared batches of CMA were fully thermoreversible, and had similar kinetics of self-assembly (Figure 3.4). In examining the photocrosslinkable properties of these batches, CMA produced with 5% of the standard volume had the lowest modulus after photocrosslinking (Figure 3.4 B and C). This is not surprising since the amount of methacrylation in this batch was the lowest. The remaining batches had similar mechanical properties following self-assembly and photocrosslinking despite differences in the volumetric ratio (Figure 3.4 B and C).

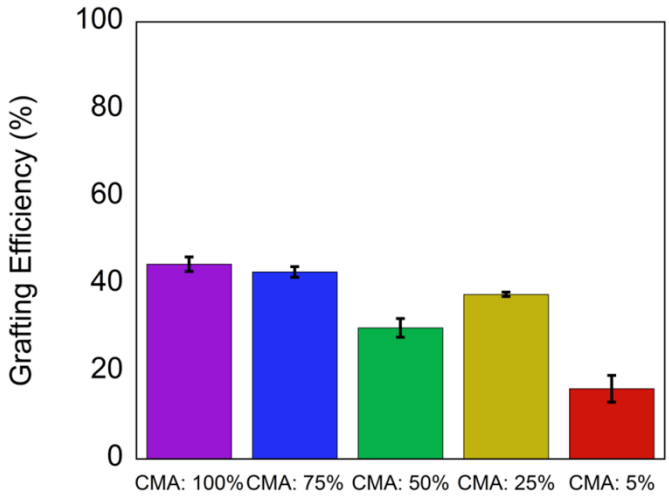

Figure 3.3 Grafting Efficiency of CMA Prepared with Varied Volumetric Ratios of EDC/NHS/Methacrylic Acid to Collagen. Grafting efficiency of CMA prepared with different volumetric ratios of reactants: collagen were similar, except for the 5%. The grafting efficiency of CMA 5% was the lowest at ~16%. The grafting efficiency of the remaining batches of CMA ranged from ~30% – ~40%.

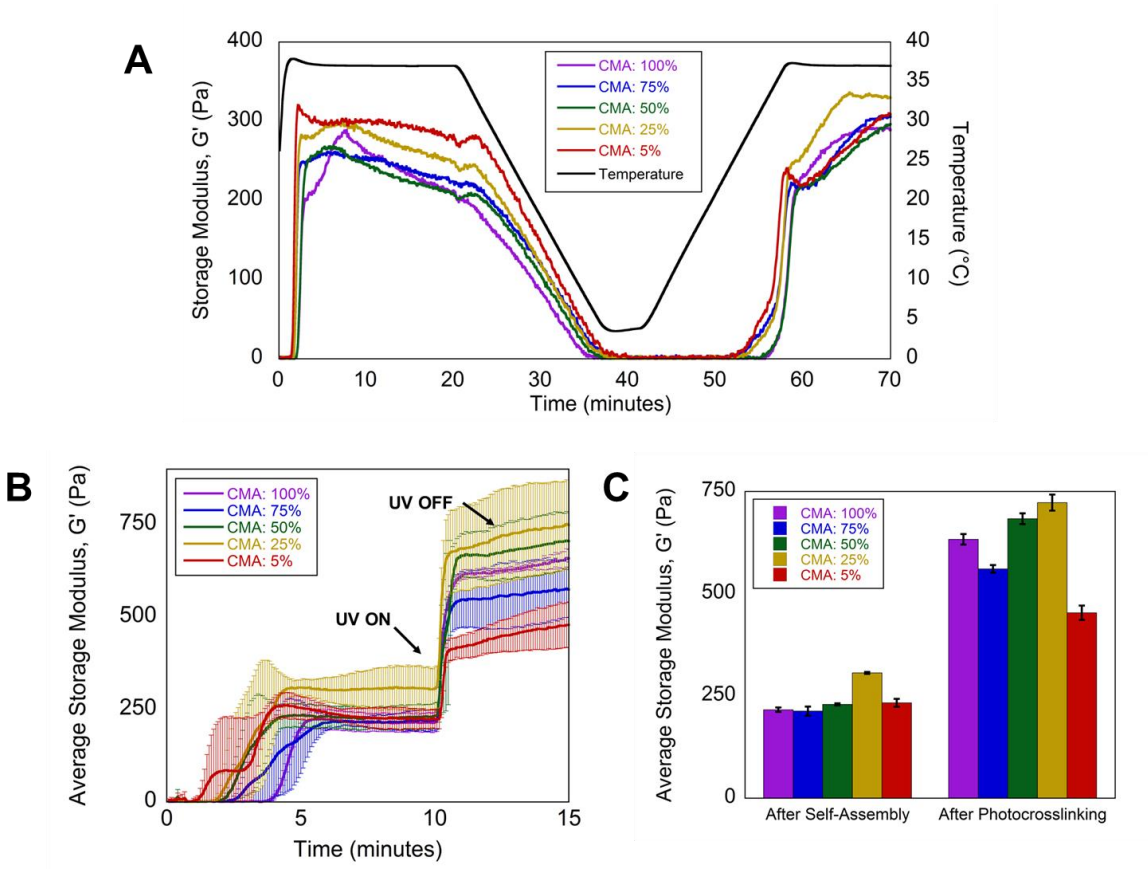

Figure 3.4 Temperature-dependent Rheology of CMA Prepared with Varied Volumetric Ratios of EDC/NHS/Methacrylic Acid to Collagen. A) CMA functionalized with methacrylic acid to varying degrees was rapidly thermoreversible, with similar time scales for self-assembly, disassembly, and reassembly. **B) and C)** All samples self-assembled at similar rates. The initial modulus following self-assembly was similar between all batches of CMA, except CMA 25%, which was slightly higher. Following photocrosslinking, the storage modulus (G') of CMA 5% doubled, in contrast to the remaining batches, whose G' nearly tripled.

3.3.3 Atelocollagen and Atelo-CMA are both thermoreversible

To further investigate the role of the telopeptides in CMA thermoreversibility, atelocollagen was methacrylated and probed for self-assembly and disassembly kinetics. Atelo-CMA was measured to be ~60% methacrylated, which is on the same order of methacrylation compared to CMA synthesized from telocollagen. In temperature-dependent rheology, both atelocollagen and atelo-CMA were thermoreversible on the time-scales observed (Figure 3.5 B). This is interesting given that telocollagen is not thermoreversible, however, CMA is (Figure 3.5 A). Because telopeptides are known to stabilize fibers, it is not surprising that atelocollagen is thermoreversible, and has been shown in the literature [123, 124]. However, it is possible that fibers could be stabilized over longer self-assembly times [93, 104, 105]. Atelocollagen and atelo-CMA were still thermoreversible even if hydrogels were self-assembled for four hours in comparison to one hour (Figure 3.5 A). Atelo-CMA samples were also self-assembled and assayed for the mechanical properties following photocrosslinking. Following self-assembly, in comparing telocollagen, CMA, atelocollagen, and atelo-CMA, CMA had the highest storage modulus and atelocollagen had the lowest (Figure 3.6). In previous work, telocollagen has typically had a higher storage modulus than CMA and is highly susceptible to lot-to-lot collagen variability [55]. Atelo-CMA was photocrosslinked, and approximately tripled in storage modulus, which is consistent with increase in mechanical properties exhibited in CMA synthesized from telocollagen.

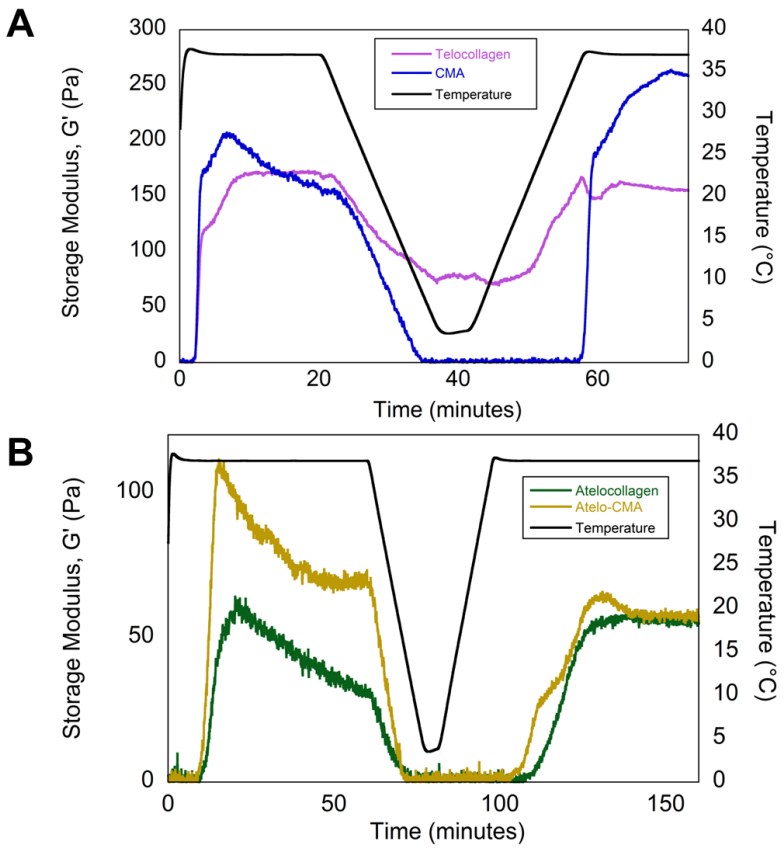

Figure 3.5 Cold-Melt Rheology of Telocollagen, CMA, Atelocollagen, Atelo-CMA. A) CMA demonstrated rapid, reversible self-assembly at cool temperatures, in contrast to telocollagen, which is not fully reversible. The storage modulus (G') of collagen decreased and increased concamitant with the temperature changes; CMA rapidly disassembled at cool temperatures and reached G' ~ 0 Pa, and quickly reassembled upon the temperature increase to 37 °C. **B)** Atelocollagen and Atelo-CMA demonstrated similar trends to CMA, but on much longer time scales. Atelocollagen samples had slower self-assembly kinetics, but stabilized after one hour at 37 °C. Both rapidly disassembled due to cooling, and re-assembled after stabilizing at 37 °C.

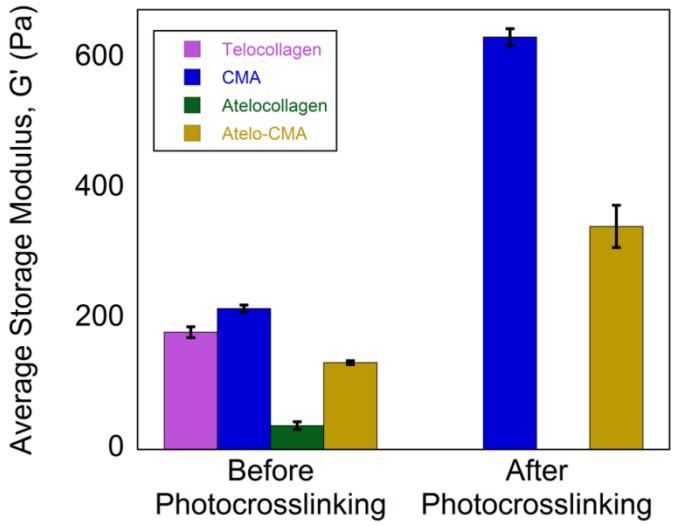

Figure 3.6 Temperature-dependent Rheology of Telocollagen, CMA, Atelocollagen, Atelo-CMA Before and After Photocrosslinking. The storage modulus (G') of telo-containing collagens upon self-assembly was higher than that of the atelocollagen samples. After photocrosslinking, G' of CMA approximately tripled, which was consistent with previous observations. G' of atelo-CMA also approximately tripled after photocrosslinking, despite the difference between starting collagen sources.

3.3.4 Collagen thermoreversibility is not unique to methacrylation

To determine if thermoreversibility was unique to methacrylation, 12 different organic compounds were coupled to type-I collagen using an approach similar to the standard CMA synthesis protocol. These organic compounds all had at least one carboxylic acid for coupling to the lysines on type-I collagen. Of the batches synthesized, 3 of the organic compounds were found to make type-I collagen fully thermoreversible in addition to methacrylic acid (Figure 3.7). While the mechanical properties and thermoreversibility of the specific organic compounds grafted to type-I collagen were found to be similar to CMA, it was also seen that one such modification significantly slowed the kinetics of fibril formation in comparison to the others. Grafting efficiencies of the modification were found to be very similar to those obtained for methacrylation of type-I collagen (Figure 3.8). The lowest grafting efficiency obtained for one of the fully thermoreversible, modified collagens was ~19%. The grafting efficiencies of the other modified collagens were also within this range, demonstrating that type-I collagen was successfully modified. Further, these results demonstrated the amount of modification did not dictate thermoreversibility, and therefore, the thermal behavior of type-I collagen must be partially determined by the properties of the moiety grafted.

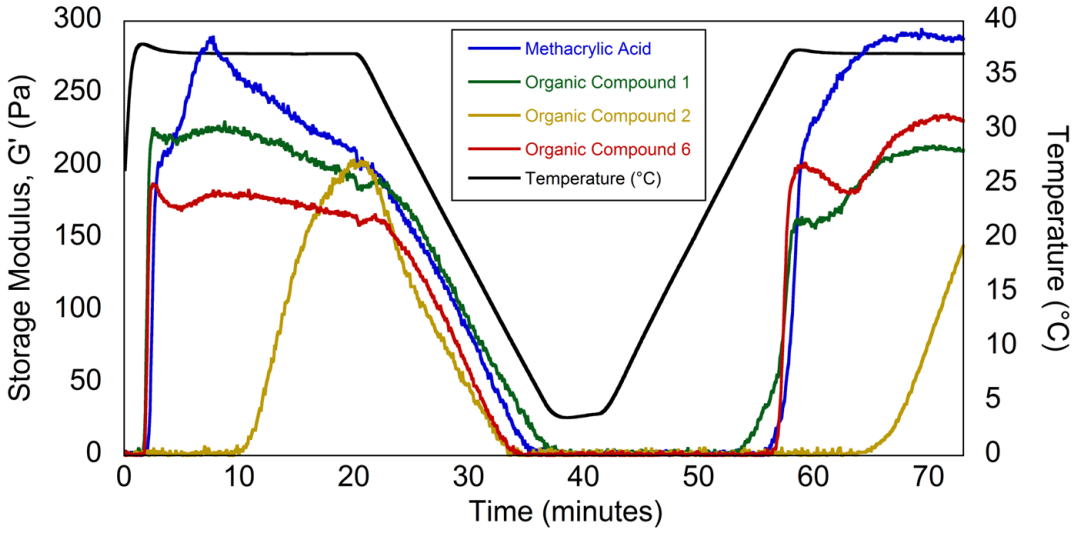

Figure 3.7 Cold-Melt Rheology of Modified Collagens. Of the 12 unique organic compounds coupled to type-I collagen, three of them resulted in modifying collagen thermoreversibility. The kinetics of self-assembly compared to CMA were quite similar amongst the molecules except for Organic Compound #2. All samples fully disassembled at similar rates at cool temperatures, and re-assembled upon reaching 37 °C. Again, collagen modified with Organic Compound #2 re-assembled at a slower rate compared to the other modified collagens.

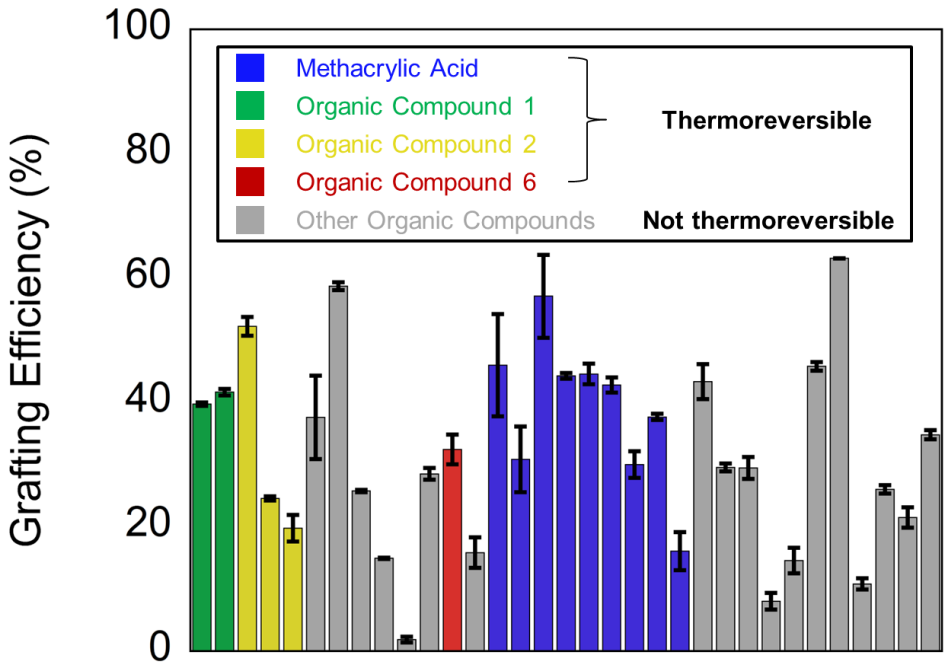

Figure 3.8 Grafting Efficiency of Modified Collagens. All modified collagens were successfully modified, with grafting efficiencies ranging between ~2% and ~60%. Only a subset of these modifications resulted in modifying the thermoreversible properties of collagen.

3.3.5 Modified collagens can be correctly classified for thermoreversible properties using moiety molecular weight and pKa

To further investigate thermoreversible collagens for models of collagen self-assembly and disassembly or uses in regenerative medicine, the data collected regarding these samples was further characterized using machine learning strategies. A plot matrix shown demonstrates clear delineations between 1) thermoreversibility and molecular weight and 2) thermoreversibility and pKa (orange circles) (Figure 3.9). Further, thermoreversible collagens with similar molecular weight and pKa cluster when categorized amongst the remaining variables in the dataset (red points within yellow highlighted regions). Interestingly, grafting efficiency alone does not help to predict thermoreversibility (green highlighted region).

A decision tree was used to classify modified collagens based on thermoreversibility using the properties of the molecules grafted and properties of the modified collagens as the dataset. The data was successfully sorted into thermoreversible and non-reversible classes based on molecular weight and logP, correctly classifying ~90.9% of the data through cross-validation (Figure 3.10 A). Many of the non-reversible collagens were successfully classified by molecular weight. The majority of the molecules with low molecular weight (< 116.16 Da) resulted in grafted collagens that were thermoreversible, however two were not; these grafted-collagens could be sorted as non-reversible using logP. The kappa statistic for this classification was ~0.82, meaning that the data had almost perfect agreement between validation runs.

Molecular weight was excluded from classification to determine the next likely set of variables to dictate classification. In this case, the decision tree classified thermoreversible and non-reversible grafted collagens based on pKa, where $4.2 < pKa \leq 4.88$, were thermoreversible (Figure 3.10 B). This decision tree classified ~93.9% of the data correctly in cross validation, and the kappa statistic was ~0.88, demonstrating a slight improvement compared to the first classification scheme.

As stated in the methods, some predicted values for data were used in this analysis. When the classification schemes above were run without grafted collagens with predicted data points, the same decision trees were obtained, although with reduced positive classification and confidence due to fewer data points.

The data was also classified to create the ‘simplest tree,’ essentially classifying based on a variable if more than 10 instances appeared in a node (Figure 3.11). Datasets could be successfully classified using molecular weight or pKa (when molecular weight was excluded), with ~87.8% of the data correctly classified in both cases. Due to further pruning in the decision tree, the kappa statistic decreased to ~0.76 for both classification schemes. This is still classified as substantial agreement, but has an advantage over previous classification schemes as it requires less data.

Multiple or simple linear regression was used to determine if a relationship existed between grafting efficiency and/or storage modulus and the remaining

variables. However, correlation coefficients in regression equations were too low to consider the equations to be significant. Correlation coefficients were less than ~0.3.

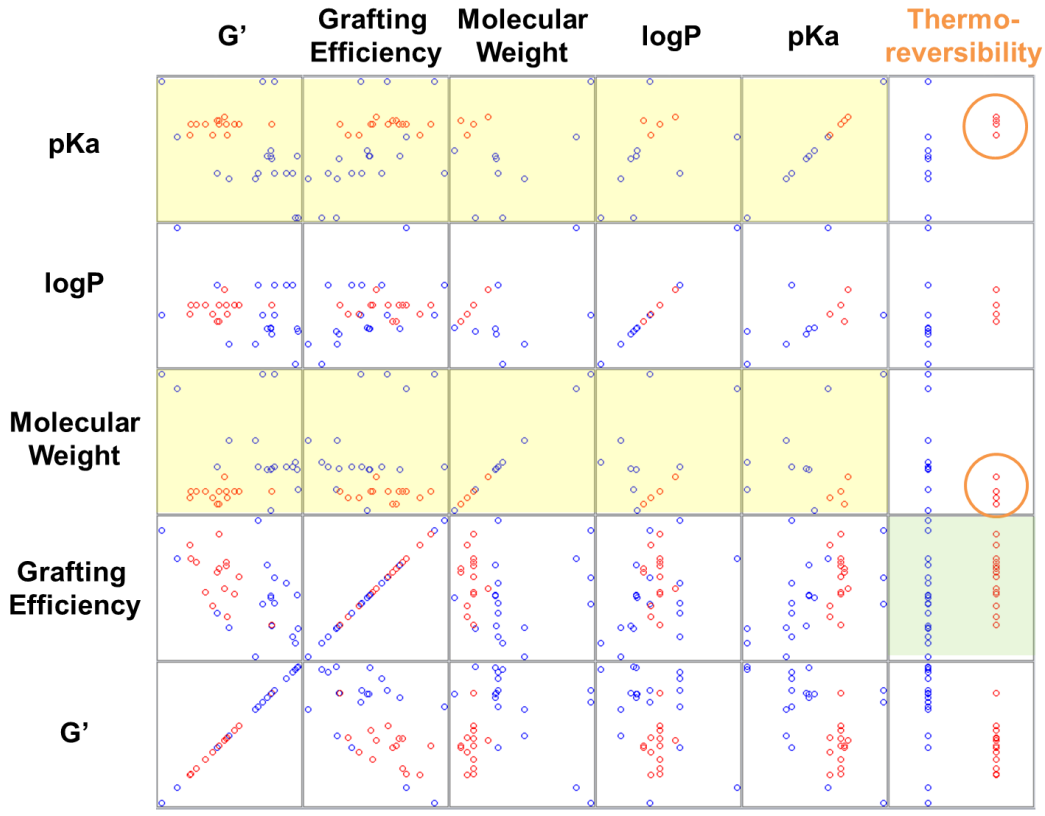

Figure 3.9 Plot Matrix of Properties of Modified Collagens. Plot matrix of the properties of the molecules (pKa, logP, and molecular weight) and the properties of the grafted collagens (grafting efficiency, storage modulus (G'), and thermoreversibility). Thermoreversible samples are shown as red points, whereas non-reversible samples are shown as blue points. Thermoreversibility was delineated quite well by specific properties of the molecules, namely molecular weight or pKa, and clustered well (orange circles). Further, thermoreversible collagens clustered well when molecular weight or pKa were compared to other properties of the molecules or resultant grafted collagens (yellow regions). The amount of modification alone did not dictate thermoreversibility (green region).

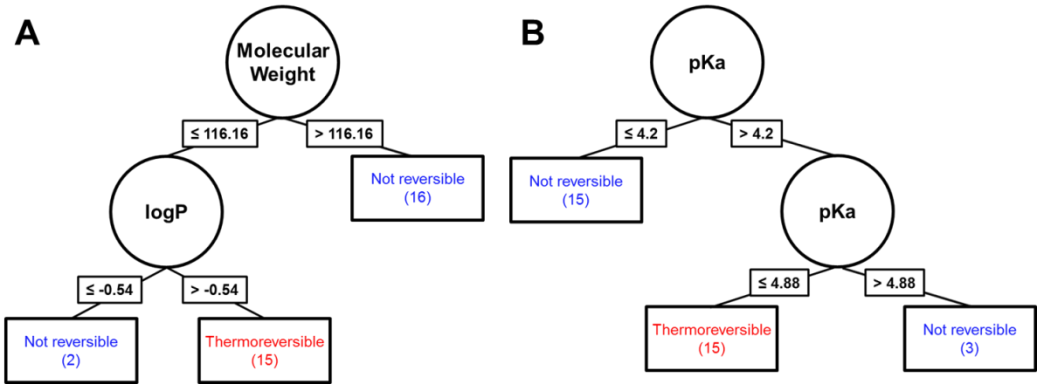

Figure 3.10 Decision Tree for Collagen Thermoreversibility. A) Decision tree successfully classified ~90.9% of the data through cross validation. Data was classified initially by molecular weight, where most molecules with molecular weight greater than 116.16 Da were successfully classified as not reversible. Molecules with low molecular weight that were not thermoreversible were correctly classified using logP. Thermoreversible collagens were ultimately classified by molecular weight ≤ 116.16 Da and logP > - 0.54. **B)** When molecular weight was excluded from the dataset, pKa successfully classified ~93.9% of the data through cross validation. Data was classified as thermoreversible if 4.2 < pKa ≤ 4.88.

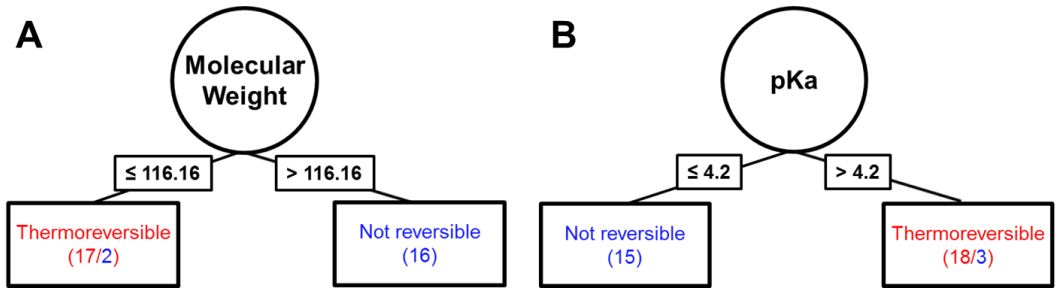

Figure 3.11 Simplest Decision Tree for Collagen Thermoreversibility. Data was classified to create the 'simplest tree,' removing nodes that contained less than 10 instances for a simple classification scheme. Datasets were classified by either molecular weight or pKa, where ~87.8% of the dataset was classified correctly using either metric. **A)** Two samples were incorrectly classified to be thermoreversible, and **B)** Three samples were incorrectly classified to be thermoreversible.

3.4 DISCUSSION

Many factors have been shown to dictate properties of type-I collagen self-assembly, including the presence of telopeptides, buffer, pH, and temperature [41, 42, 100, 101, 106]. These properties include fibril diameter dictated by differences in fibril packing, or differences in mechanical properties of fibrillar hydrogels [41, 101]. In our previous work, we have further modified the bioactive properties of type-I collagen through the crosslinking of peptides to lysine residues, which has slightly changed the mechanical properties of the modified collagen [58]. To our knowledge, CMA, a methacrylated type-I collagen, was the first modified, full length collagen that could reversibly self-assemble based on temperature [107]. No other modifications of collagen have caused similar changes in the thermoreversible behavior of type-I collagen.

In synthesizing peptide-grafted collagens, the crosslinker EDC was utilized; this was in contrast to the established protocol for CMA, where EDC and NHS were used in combination to couple methacrylic acid to type-I collagen. Previously, EDC was used alone to synthesize CMA, but the resultant hydrogel mechanical properties following photocrosslinking were quite weak [67]. This result was duplicated in our study, where CMA prepared solely with EDC less than doubled in storage modulus following photocrosslinking compared to CMA prepared with EDC/NHS, which more than tripled. On the whole, grafting efficiency of CMA prepared with EDC compared to CMA prepared with EDC and NHS was lower. Despite successful grafting of methacrylic acid to collagen, CMA prepared with EDC was not thermoreversible. It may indicate that a threshold of

methacrylation is necessary to make collagen reversible; however, even batches that were ~16% methacrylated when prepared with EDC/NHS were reversible. Further, methacrylation is not the sole modification that produces thermorversible collagens – other organic compounds – particularly those with low molecular weight, are also thermoreversible.

The machine learning analyses overwhelmingly showed clear separation between thermoreversible and non-reversible collagens based on molecular weight and pKa; molecules with low molecular weight, and log P > -0.57 were theremoreversible. The pKa of molecules grafted that resulted in making collagen thermoreversible were very close to the pH at which the reaction takes place. Molecules where $4.2 < pKa \leq 4.88$ resulted in modifying the thermal properties of type-I collagen. The pH of the MES buffer, which is what EDC/NHS/molecule is solubilized in for carboxyl activation, has a pH of approximately 2.5 – 4.0. However, when added to collagen, the pH increases to approximately 4.5, which is the pKa of the molecules that result in thermoreversible collagens. This also suggests that grafting efficiency plays a role in thermoreversibility, because the pKa of the molecule grafted may dictate where the collagen is modified specifically rather than the amount of modification.

An original theory related to thermoreversibility was that because the telopeptide region contains a disproportionate number of lysine residues compared to the entire collagen molecule, it is possible that a significant amount of lysines in this region were modified, which may have contributed to fibril destabilization at cool temperatures [107]. In methacrylating atelocollagen, we

found that both atelocollagen and atelo-CMA were thermoreversible. This informed us that thermoreversibility may in fact be partially dictated by how the telopeptide regions are modified, or even in the absence of the telopeptides. However, atelocollagen was still successfully methacrylated without the telopeptides present; atelo-CMA was found to be ~60% methacrylated, and was as photoreactive as CMA. Because the amount of methacrylation was high in atelo-CMA, it is likely that many modifications occur throughout the triple-helical region in addition to the telopeptides.

Overall, thermoreversibility is likely dictated by a number of factors, and there is much to be studied about the conditions of synthesis that are used to make collagen thermoreversible. In our experiments, we have not produced a thermoreversible collagen solely using EDC. It is possible that the use of EDC and NHS in combination plays a role in the location of functionalization on the collagen molecule. Additionally, because NHS stabilizes the molecular intermediate, these molecules may be present for longer periods of time and more able to couple to specific lysines on collagen, which then may interfere with fibril stabilization. Lastly, EDC/NHS together are extensively used to crosslink the collagen directly, potentially interfering with proper fibril formation and/or disallowing natural crosslinking to occur that may stabilize collagen fibrils; this scenario is unlikely, because the molecule that is activated is in molar excess of the EDC/NHS, and this activation occurs prior to adding to the collagen solution.

The most likely explanation is that the biochemical properties of molecules, in combination with the specific crosslinkers used, allow for grafting to

specific sites throughout the collagen molecule. These specific modifications likely interfere with proper fibrillogenesis, and destabilize fibers in a temperature-dependent manner. Future studies using mass spectrometry would aid significantly in studying where specific modifications occur in the functionalized collagens to better determine how such modifications contribute to thermoreversibility. Preliminary studies of mass spectrometry on type-I collagen have shown that some of the collagen sequences were methacrylated; however, issues with solubility and enzymatic digestion in sample preparation resulted in low protein concentrations for testing. There are a variety of protocols that we can utilize for enzymatic digestion that may improve these outcomes [125-127].

While these studies do not offer a complete explanation for collagen thermoreversibility, it provides a significant starting point for the generation of a database of reversible collagens. The decision trees generated from the experimental datasets are quite accurate in using properties of the molecules grafted to predict thermoreversibility of grafted collagens. This tool may prove quite useful as a preliminary screen for new molecules to couple to collagen in further computational or experimental studies. This dataset can be used as a training set for building computational models to predict collagen thermoreversibility with alternate molecules. For example, coarse grain models of collagen fibers with a percentage of lysines modified could be stabilized at body temperature and then subject to dynamic temperature changes while measuring variations in structural stability surrounding the modification. These studies may be used to improve models of collagen self-assembly and disassembly for

studies of collagen mutations in diseases in disorders with improper fibril formation. It may also aid biochemistry studies for those synthesizing collagen-based peptides, where short collagen peptides are able to assemble into triple-helices, but do not typically form ordered D-banded fibrils [128]. In the lab, thermoreversible collagens may serve as a temporary substrate for cells for growth or differentiation prior to transplantation [97, 129]. From a materials perspective, a thermoreversible collagen has a variety of uses, particularly in drug delivery or rapid prototyping [98, 112]. An understanding of how such modifications contribute to thermoreversibility may allow for specific control over the temperature-dependent properties, for example, disassembly at 25 °C instead of 4 °C. A deeper knowledge of what dictates collagen thermoreversibility and the ability to control its properties would contribute to significant future developments in biochemistry of collagen structure and self-assembly, biomaterial inventions, and medicine overall.

3.5 CONCLUSION

Type-I collagen has the ability to form D-banded fibers at physiological conditions, and this phenomenon is not reversible. In our development of collagen-based materials, we discovered that methacrylation of the lysines made collagen thermoreversible; fibrillar collagen methacrylamide (CMA) hydrogels that formed at 37 °C could reversibly disassemble into a liquid suspension at 4 °C. In this study, the phenomenon was further investigated by interrogating aspects of CMA synthesis; variations of the crosslinkers (EDC or EDC/NHS), the

volumes of reactants to collagen, and the molecules used to graft to collagen were varied. Additionally, the thermoreversibility of telocollagen and atelocollagen were assessed in comparison to methacrylation of the two collagen sources. Interestingly, only EDC/NHS can be utilized to synthesize thermoreversible collagens, in our experience. Further, varying the volumetric ratio of the reactants to collagen resulted in making collagen thermoreversible, although lower volumetric ratios did lower the percent of collagen modified. Methacrylation was not the unique cause of thermoreversibility; other molecules can be used to make collagen reversible. Grafted collagens were successfully classified based on thermoreversibility using properties of the molecules grafted, including molecular weight and pKa. The exact phenomenon of how this process makes collagen thermoreversible is unknown; further research will focus on where the collagen molecules are modified will contribute significantly in understanding collagen themoreversibility. Modified, thermoreversible collagens are very important for future understanding of collagen self-assembly and disassembly, particularly in biochemistry studies of collagen-based peptides or causes of collagen-based diseases, and the development of new collagen-based materials in tissue engineering and regenerative medicine.

CHAPTER 4. MONITORING COLLAGEN FIBRILLOGENESIS USING CIRCULAR DICHROISM SPECTROSCOPY: A NEW USE FOR AN OLD TECHNIQUE

4.1 INTRODUCTION

Type-I collagen is widely studied for many biomedical applications: it is a major component of scaffolds in tissue engineering and *in vitro* cell substrates for studying cell adhesion, migration, and differentiation [40, 54, 60, 77, 130]. Many implantable materials are collagen-based and are commonly used for treatment of burns and scars [131, 132]. Cosmetic companies produce a variety of collagen creams and injections as anti-aging treatments [133]. In addition to its widespread use and continued development as a biomaterial throughout the biotechnology and cosmetics sectors, collagen is also studied to better understand how mutations in structure or synthesis lead to diseases such as Ehlers–Danlos syndrome or Osteogenesis imperfecta [110, 111]. Due to its extensive presence throughout the body, roles in various pathologies, and potential therapeutic uses, it is necessary to study collagen structure, functions, and interactions.

The 29 members of the collagen family in animals comprise approximately 30% of the total protein body content [39]. Among these, type-I collagen is predominant, and is herein referred to as collagen unless otherwise stated [40]. Collagen comprises two α1 and one α2 left-handed poly-proline II helices, which

oligomerize into a right-handed triple-helix [39]. The fibrillar segments are composed of repeating triplet sequences Gly-X-Y, where X and Y can be any amino acid, but are primarily proline and hydroxyproline [75].

The process of collagen fibrillogenesis produces highly organized fibrils with an evident D-periodic banding every 67 nm along the axis (Figure 4.1 A). This periodic banding is the result of two repeating patterns in the fibril: the overlap region, where there are 5 collagen segments, and the gap region where there are four [99]. This packing allows for the formation of collagen fibers that are longer than the collagen monomer (~300 nm), and the specific arrangement of these fibers results in tissues with varied mechanical properties throughout the body [99, 134].

Although *in vivo* assembly of collagen is tightly regulated by the cell, much of the structural and functional features of assembled fibrils can also be recreated *in vitro* under appropriate conditions [40, 75, 135, 136]. To study fibril formation *in vitro*, collagen can be extracted from a variety of source animal tissues into neutral salt or buffers, or more frequently, into dilute acidic solutions [40]. The process of fibrillogenesis can be controlled by varying pH, temperature, and buffer conditions [41, 42, 100, 101, 107, 137-139]. Under acidic conditions, collagen exists primarily as a soluble triple-helix below its melting transition around 42 °C [42, 107]. At neutral pH, collagen readily forms fibrils above 20 °C [42]. Thus, by manipulating solution conditions, the various stages of collagen assembly can be isolated and studied independently.

The soluble triple-helix and fibril stages of collagen self-assembly have been studied using different experimental methods. The unique supercoiled poly-proline II type secondary structure of the peptide chain in the soluble helix allows for characterization by circular dichroism (CD) spectroscopy [75]. CD spectroscopy measures the difference in the absorption of left-handed and right-handed circularly polarized light by the ensemble of peptide bond chromophores in a protein [140]. In the case of the triple-helix, the protein backbone exhibits unique CD transitions including a positive band at 222 nm and a negative band at 195 nm [140]. CD has been a powerful tool for studying the folding of collagen and other model triple-helical peptide systems [141].

Fibril formation during self-assembly can be studied using a number of scattering and mechanical methods. A low temperature collagen solution in the triple-helical state can be induced to form fibrils by changing solution conditions to physiological pH and temperature [75]. Typical fibrillogenesis proceeds through an initial lag phase, rapid growth of collagen fibrils, and a plateau phase when collagen fibrils mature and stabilize [142, 143]. Depending on the technique utilized, some or all of these phases may be captured. Following the growth phase, transmission electron microscopy or atomic force microscopy can image collagen fibril structure, notably the characteristic D-banding of fibrils based on the stagger between collagen segments (Figure 4.1 A) [99]. At high collagen concentrations, rheological properties can be monitored as collagen self-assembles into a fibrillar hydrogel to capture changes in the storage modulus that coincide with the transition from a liquid suspension to a semi-solid hydrogel

(Figure 4.1 B). Measurements such as this are widely used to measure the amount of energy a material stores in response to a stress, which is particularly important for load-bearing scaffolds. Optical measurements can also be used to study fibrillogenesis and structure. Light scattering, often called turbidity, is utilized to monitor fibrillogenesis, typically in low concentration collagen samples. In this case, collagen self-assembly is measured as the optical density of the solution during the lag, growth, and plateau phases [144]. In another technique, the structure of fibrils can be clearly observed using second-harmonic generation light microscopy, a specialized and well-established optical method that is particularly sensitive to the collagen structure [145-147].

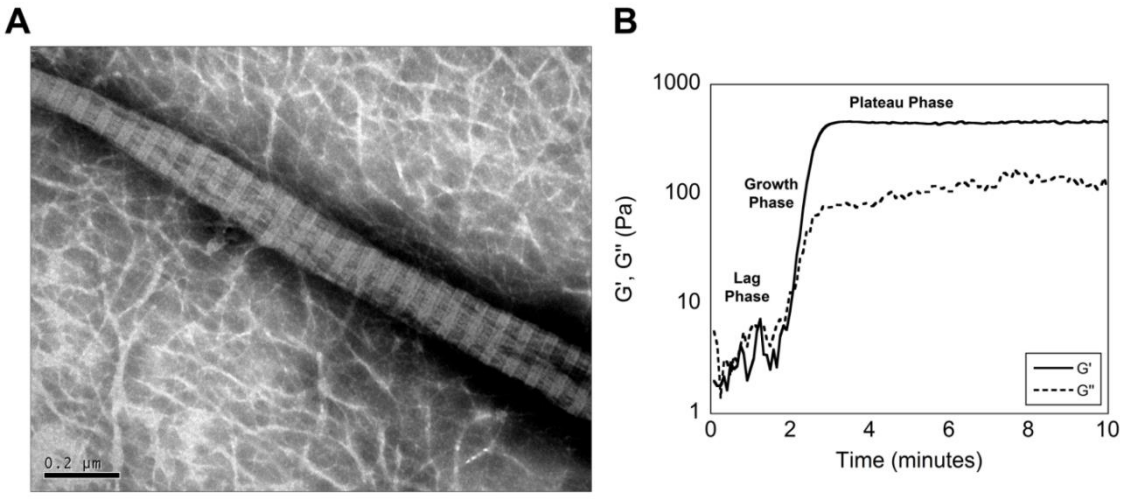

Figure 4.1 Example of Methods to Monitor Fibril Formation A) For transmission electron microscopy, collagen samples were prepared and imaged as described previously [107]. Transmission electron microscopy allows for visualization of ordered D-banding in collagen fibrils. B) Samples for rheological testing were prepared and loaded on the rheometer as described. The temperature was immediately raised to 37 °C, and the sample was continually oscillated to 0.5% strain at 1 rad/s for ten minutes while measuring the resultant torque to obtain the temperature-dependent sample storage and loss moduli (G' and G'', respectively). Rheology allows for characterization of the mechanical properties of type-I collagen hydrogels; the process of collagen fibrillogenesis manifests as a lag phase, where the storage modulus and loss modulus (G' and G", respectively) are essentially 0 Pa, a growth phase of fibril formation, exhibited as an increase in both G' and G", and a plateau phase indicative of fibril stabilization, where G' and G" are constant.

Although powerful methods exist to study either the triple-helix or the fibril state of collagen, few approaches allow concurrent observation of folding and higher-order assembly. Such studies generally rely on methods such as X-ray scattering to observe species over a wide range of size scales [148]. Here, we describe the observation of fibrillogenesis using CD spectroscopy under conditions in which both triple-helix and fibril can be simultaneously observed. In a study of temperature induced self-assembly of a chemically modified collagen derivative, a unique spectrum was observed coincident with fibrillogenesis that was distinct from that of a triple-helix [107]. Here, we establish the shape of this component and show its utility in studying hierarchic assembly. Because collagen solutions are most often analyzed under conditions where fibrillogenesis is inhibited, this signal has not been extensively described or studied [81, 138, 149-156]. However, given the wide accessibility of CD spectroscopy, the identification of a collagen fibril-associated spectrum presents opportunities to study collagen fibrillogenesis and associated structural transitions in solution.

4.2 MATERIALS AND METHODS

4.2.1 Materials

Experiments were performed with collagen from a number of different sources and vendors. Type-I collagen extracted from bovine skin (C857, Telo-EPC) was obtained from Elastin Products Company (Owensville, MO). Separate solutions of bovine skin derived type-I collagen with and without telopeptides (TeloCol #5026-D, Telo-ABM and PureCol #5005-B, Atelo-ABM) were obtained from Advanced Biomatrix (Carlsbad, CA). Rat tail type-I collagen (CB354249, RT) was obtained from Thermo Fisher Scientific (Waltham, MA). Human type-III collagen (#5021, Type-III) was purchased from Advanced Biomatrix. Gelatin (G-9391) was purchased from Sigma-Aldrich (St. Louis, MO). All other materials were purchased from Sigma-Aldrich unless otherwise stated.

4.2.2 Circular Dichroism

CD spectra were obtained using an Aviv Model 400 Spectrometer (Aviv Biomedical Inc., Lakewood, NJ). All samples were prepared to a final concentration of 0.1 mg/mL unless otherwise stated. Table 4.1 provides details for sample preparation and nomenclature. Samples (300 µL) were loaded into optically matched 0.1 cm path length quartz cuvettes (Model 110-OS, Hellma USA, Plainview, NY). All ellipticity measurements were performed using the same cell for baselines and samples. Ellipticity measurements were corrected for buffer baseline, and when possible, ellipticity was converted to mean residue ellipticity (MRE) using sequence lengths for type-I and type-III collagen as identified in UniProtKB (Table 4.1) and molecular weight provided by the

manufacturers. Ellipticity values were excluded if the dynode voltage exceeded 600 V. Error bars are not shown for CD measurements for clarity; however, the maximum machine percent error obtained was an error of 8%, while the average machine percent error was ~2.5% in the peak wavelength regions (220 nm – 225 nm or 198 nm – 210 nm).

CD experiments were performed while varying wavelength and temperature. Experiments are described in brief, and additional experimental parameters for CD are outlined in Table 4.2. Triple-helical content of all samples was confirmed via wavelength scans at 4 °C (Table 4.2, experiment 1). Folding and assembly of samples was monitored as the ellipticity at 222 nm – where a positive band coincides with triple-helix structure. Structural changes were measured as the temperature was raised from 4 °C to 60 °C using a slow rate of 0.1 °C/minute to minimize kinetic effects, as described in Persikov et al [157]. Separately, the total secondary structure change in response to increasing temperature was captured by measuring wavelength spectra from 4 °C to 60 °C (Table 4.2, experiment 2).

Digestion kinetics were observed by following changes in the CD spectrum of collagen upon addition of type-I collagenase (Table 4.2, experiment 3). Ellipticity was monitored at 4 °C and 37 °C to confirm triple-helical and fibril content, respectively. Then, type-I collagenase or buffer was added to each cuvette and wavelength scans were performed over the course of the digest.

Sample Name	Type	Source	Buffer	pH	UniProtKB Sequence	Manufacturer
Telo-EPC	Type-I collagen	Bovine	0.02 M acetic acid (AcA)	4	P02453, P02465	Elastin Products Company
			PBS	7		
			PBS and 1M glycerol	7		
Telo-ABM	Type-I collagen	Bovine	0.01 M hydrochloric acid (HCl)	2	P02453, P02465	Advanced Biomatrix
			PBS	7		
Atelo-ABM	Type-I collagen (no telopeptides)	Bovine	0.01 M hydrochloric acid (HCl)	2	P02453, P02465 (no telopeptides)	Advanced Biomatrix
			PBS	7		
RT	Type-I collagen	Rat	0.02 M acetic acid (AcA)	4	P02454, P02466	Thermo Fisher Scientific
			PBS	7		
Type-III	Type-III collagen	Human	0.01 M hydrochloric acid (HCl)	2	P02461	Advanced Biomatrix
			PBS	7		
Gelatin	Denatured collagen	Bovine	PBS	7	N/A	Sigma-Aldrich

Table 4.1 Collagen Sample Preparations. Description of collagens, manufacturers, types, sources, buffers, sample pH for experiments, and UniProtKB references for mean residue ellipticity approximations.

Experiment Number	Samples	Wavelength (nm)	Temperature (°C)	Averaging Time (s)	Wavelength Increment (nm)	Temperature Step (°C)	Equilibration Time (min)	Notes
1	Telo-EPC, Telo-ABM, Atelo-ABM, RT, Type-III,	260-195	4	10	1	N/A	2	• All samples at 0.1 mg/mL except Telo-EPC at 0.1, 0.05, 0.025, and 0.01 mg/mL
	Gelatin	222	4-60	10	N/A	0.33	2	• All samples at 0.1 mg/mL except Telo-EPC at 0.1, 0.05, 0.025, and 0.01 mg/mL • Performed from 4 °C to 60 °C and returned to 4 °C
2	Telo-EPC	260-200	4-60	3	2	0.33	6	• N/A
3	Telo-EPC with and without type-I collagenase	240-198	4	3	2	N/A	2	• Telo-EPC prepared at 0.05 mg/mL in PBS • Sample volumes of 250 µL
		240-198	37	3	2	N/A	2	• Samples from above given 1 hour for self-assembly
		240-200	37	3	2	N/A	2	• 50 µL of either 0.04 mM $CaCl_2$ (Fisher) in PBS (Fisher) or 3 mg/mL type-I collagenase (C1030, Sigma) in 0.04 mM $CaCl_2$ in PBS was added to each cuvette prior to measurement

Table 4.2 Parameters of CD Spectroscopy experiments. Outlined for each set of collagen samples with additional notes to clarify procedures.

4.2.3 Rheology

The mechanical properties of collagen hydrogels were characterized for a subset of the previously described samples. Telo-EPC was mixed in 500 µL batches containing 10 µL 1M HEPES, 65 µL 0.15M NaOH, 50 µL 10X PBS, 36.5 µL 1X PBS (Thermo Fisher Scientific), and 338.5 µL Telo-EPC (3.75 mg/mL, solubilized in 0.02N acetic acid) to create a 2.5 mg/mL collagen suspension. In separate samples of Telo-EPC, the 1X PBS was replaced with 36.5 µL of 13.7 M glycerol, which prevented self-assembly for a final concentration of 1 M glycerol in the buffered collagen sample [81]. Telo-ABM and Atelo-ABM batches were prepared according to protocols from Advanced Biomatrix [158, 159]. Briefly, 400 µL of Telo-ABM (3.1 mg/mL) was mixed with 50 µL of 10X PBS and 61 µL of 0.1 M NaOH, and 400 µL of Atelo-ABM (3.1 mg/mL) was mixed with 50 µL of 10X PBS and 62 µL of 0.1 M NaOH to create 2.4 mg/mL suspensions. RT samples were diluted from 10 mg/mL to 3.75 mg/mL in 0.02 N acetic acid, and were buffered according to the formula for Telo-EPC to prepare a collagen suspension at a final concentration of 2.5 mg/mL. Acid-buffered samples were also tested for their inability to self-assemble by diluting the samples in acid (acetic acid or hydrochloric acid, see Table 1) to the final concentrations as outlined above. A representative sample is shown for each collagen formulation.

Gelatin samples were assayed for hydrogel formation. Samples were prepared at 25 mg/mL in PBS, and were fully solubilized through heating at 37 °C. Rheology measurements were performed differently for gelatin compared to type-I collagen, which forms a hydrogel at low temperatures (~ 4 °C) rather than

physiological temperature (37 °C). In these measurements, samples were plated at 25 °C; the temperature was increased to 37 °C to ensure the gelatin was fully fluid, decreased to 4 °C at a rate of 2 °C/minute, and held at 4 °C for 15 minutes to assay for hydrogel formation. Measurements of three separately prepared samples were taken and averaged.

The temperature-dependent mechanical properties were assessed using a Kinexus Ultra rotational rheometer (Malvern Instruments, Malvern, UK). A 200 µl sample was loaded into a 600 µm gap between parallel plates separated by 20 mm. The bottom plate was connected to a Peltier temperature-controlled stage. To acquire the fibrillogenesis profile, the temperature was raised from 4 °C to 60 °C at a rate of 1 °C/minute. The sample was continually oscillated to 0.5% strain at 1 rad/s while measuring the resultant torque to obtain the temperature-dependent sample storage modulus (G').

4.2.4 Light Scattering

Light scattering measurements were performed on a Zetasizer Nano ZS (Malvern Instruments, Malvern, UK) with a 3mW He-Ne laser at λ = 633 nm, collecting backscattered light at θ = 173°. A built-in Peltier element controlled sample temperature during measurements to within ±0.1°C. Scattering intensities and autocorrelation functions were determined from the average of either three or five correlation functions, with a typical acquisition time of 60 s per correlation function. Type-I (Telo-EPC) and type-III solutions were prepared in PBS buffer (final concentration of 0.1 mg/mL). Samples were loaded into low-volume quartz batch cuvettes (ZEN2112) and equilibrated to 37 °C. Measurements of three

separately prepared samples of each type were taken every minute for 30 minutes and averaged.

4.2.5 Independent Component Analysis

The circular dichroism spectral component associated with the collagen fibril was determined from a data set of 60 experimental CD spectra for 0.1 mg/mL Telo-EPC (Table 2, experiment 2). Reconstruction of all 60 spectra was attempted using a mixture of constrained triple-helix and random-coil spectra plus a third unconstrained component associated with the assembled fibril. The fast independent component analysis (fastICA) algorithm was used to determine the unconstrained component and the weights of the three components as a function of temperature [160-162]. Chi-square analysis indicated that three components were sufficient to determine the series of experimental spectra. Considering each CD spectrum as a linear combination of component spectra, the component spectra were fit to equation 1 using error weighted multiple regression to determine the fractional population of each component with changing temperature:

$$X_T = f_H(T)H + f_F(T)F + f_M(T)M \qquad \text{(Eq. 1)}$$

where X_T is the measured spectrum at temperature T; *H*, *F*, and *M* correspond to the fitted component spectra corresponding to triple-helix, fibril, and random-coil (heat denatured collagen), respectively. $f_H(T)$, $f_F(T)$, and $f_M(T)$ are the fraction of the signal corresponding to these spectral components at temperature *T.*

To observe the presence of the independent components as collagen was degraded by collagenase, the components were fit using the same approach as above on a set of 66 experimental CD spectra taken over several hours for the same collagen sample treated with type-I collagenase at a constant temperature of 37 °C (Table 2, experiment 3). Three-variable regression with all components was applied across the entire data set.

4.3 RESULTS

4.3.1 Type-I collagen exhibits a decrease in triple-helix signal coincident with fibrillogenesis

The first indication of a fibril-like species observable by CD came from the coincidence of temperature-induced spectral changes with mechanical changes that signify collagen fibrillogenesis. At 4 °C, Telo-EPC collagen samples in PBS exhibited triple-helical structure (positive MRE at 222 nm) in CD spectroscopy, while collagen hydrogels had not yet formed (G' ~ 0) (Figure 4.2 and Figure 4.3 A). An increase in the negative amplitude of the band at 222 nm emerged in CD coincident with the temperature of Telo-EPC fibrillogenesis observed in rheology (Figure 4.3 A). During further heating, both measurement modalities confirmed sample denaturation, as the MRE and G' approached 0. Ellipticity and fibrillogenesis of Telo-EPC collagen samples were also monitored under acidic conditions, which prevented self-assembly. At 4°C, samples were triple-helical and manifested as a liquid suspension with no appreciable change in shear modulus (G' ~ 0) (Figure 4.2 and Figure 4.3 A). As the temperature was

increased, Telo-EPC in acidic conditions denatured after 42 °C in CD, and the collagen sample did not self-assemble (Figure 4.3 A).

The emergence of this negative signal at 222 nm occurred at temperatures and conditions consistent with collagen fibrillogenesis. The strong, negative MRE indicates the formation of an alternate higher order structure rather than denaturation or random-coil, which would exhibit no signal. It is important to note that the dynode voltage, which increases with increasing sample optical density, did not significantly change during the length of the experiment; this indicates that the negative signal was not a result of scattering, which would otherwise prevent an accurate measurement of ellipticity (Figure 4.4). It is unknown if the collagen fibril mass is completely optically active and therefore if the observed signal is truly in mean per-residue ellipticity; however, the signal clearly represents a structural change as a result of collagen fibrillogenesis. Importantly, this distinct transition at 222 nm from a positive-to-negative MRE occurred at physiological temperature and pH conditions capable of hydrogel formation in rheology measurements, despite slight differences in experimental parameters.

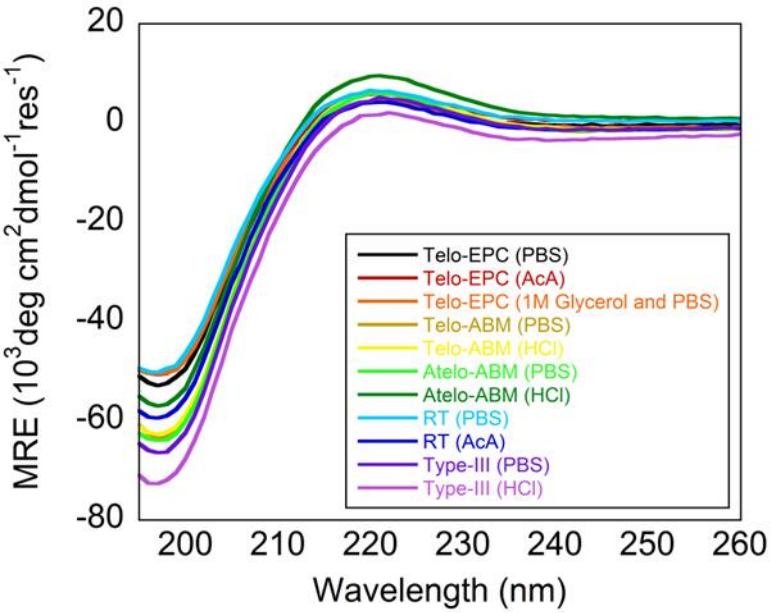

Figure 4.2 Triple-helix Signal of All Collagen Samples. MRE of collagen samples was measured from 260 nm – 195 nm at 4 ºC. All collagens, regardless of buffer, demonstrated triple-helical content via CD measurements as a positive peak at 222 nm and a negative peak near 195 nm.

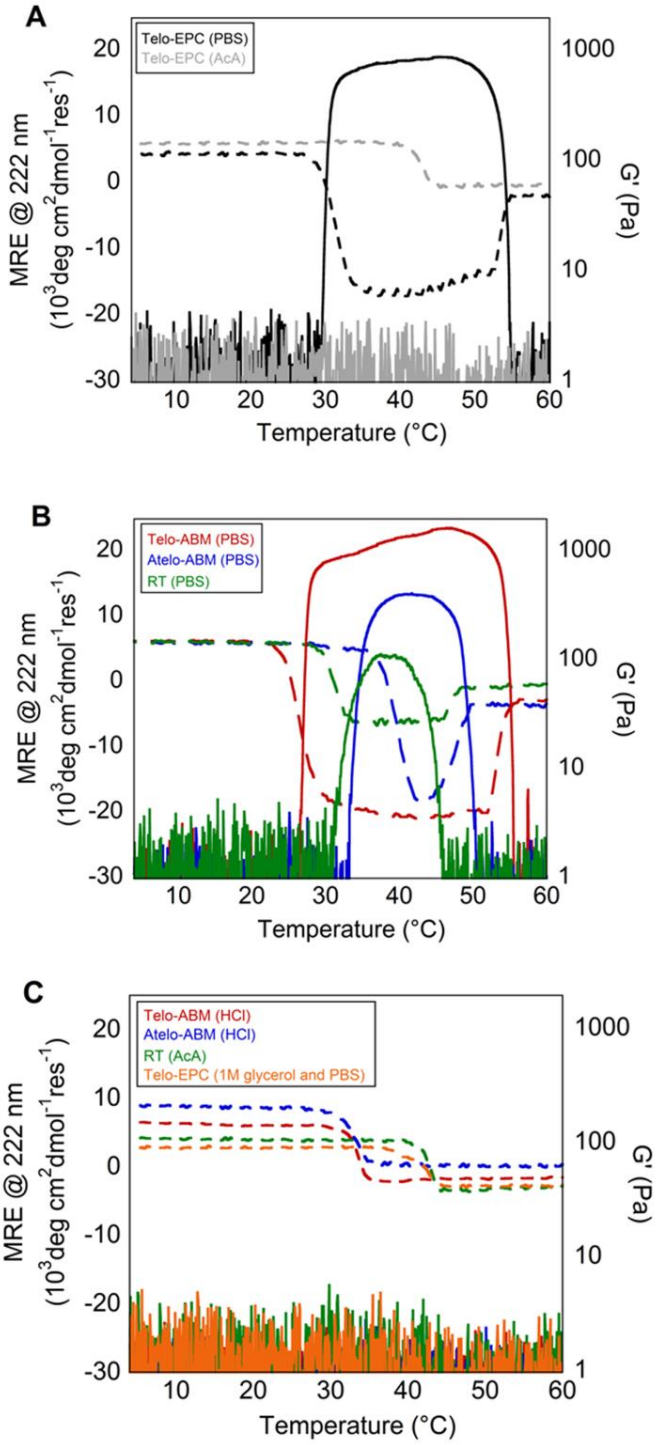
A
Telo-EPC (PBS)
Telo-EPC (AcA)
MRE @ 222 nm
(10^3deg cm^2dmol^-1res^-1)
G' (Pa)
Temperature (°C)
B
Telo-ABM (PBS)
Atelo-ABM (PBS)
RT (PBS)
MRE @ 222 nm
(10^3deg cm^2dmol^-1res^-1)
G' (Pa)
Temperature (°C)
C
Telo-ABM (HCl)
Atelo-ABM (HCl)
RT (AcA)
Telo-EPC (1M glycerol and PBS)
MRE @ 222 nm
(10^3deg cm^2dmol^-1res^-1)
G' (Pa)
Temperature (°C)

Figure 4.3 CD Spectroscopy and Rheology of Collagen. MRE at 222 nm (dashed lines) and the storage modulus (G') (solid lines) was measured from 4 ºC to 60 ºC. A) Measuring the ellipticity at 222 nm, Telo-EPC in acidic conditions exhibited one transition at approximately 42 ºC, in contrast to Telo-EPC in PBS, which exhibited two transitions in ellipticity: one at approximately 30 ºC and one after 50 ºC. These transitions were strongly coincident with fibrillogensis and denaturation measured via rheology: Telo-EPC exhibited an increase in G' at the same temperature as the decrease in MRE at 222 nm. Both signals transitioned to 0 as the fibrils degraded at high temperatures. No such correlation existed for Telo-EPC in acidic buffer when collagen is incapable of self-assembly. B) Similar CD signatures displayed for other collagens capable of self-assembly: Telo-ABM, Atelo-ABM, and RT collagens in PBS exhibited two ellipticity transitions that correlated with collagen hydrogel formation and heat denaturation via rheology. C) Telo-ABM, Atelo-ABM, RT collagen in acidic conditions, and Telo-EPC in 1M glycerol and PBS were incapable of self-assembly via rheology, and demonstrated only one ellipticity transition from triple-helix to a disordered state.

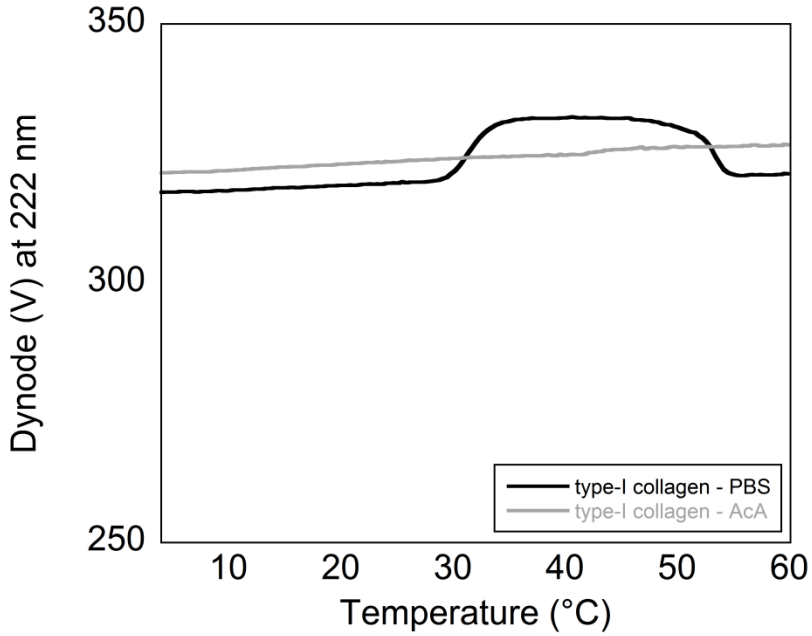

Figure 4.4 Representative Dynode Voltage Change in Temperature Melt. Representative example of the change in dynode voltage at 222 nm throughout a temperature melt experiment (Figure 4.3 A) with Telo-EPC in acidic and physiological buffers. The dynode voltage did not exceed 600V, which indicated that the change in ellipticity was due to structural changes in the protein sample and not the result of light scattering.

4.3.2 Alternate collagens exhibit the emergence of the negative band and are capable of self-assembly at physiologic conditions

Spectroscopic signals can be highly sensitive to impurities or variations in preparations by different vendors or laboratories. To address this, we monitored undigested and pepsin-digested bovine collagen (Telo-ABM and Atelo-ABM, respectively) to determine if the unique CD signal was a result of specific molecular interactions occurring within the non-triple-helical telopeptide region. Further, to test if the emergence of the negative signal was bovine species-specific, we also performed CD spectroscopy measurements using rat tail type-I collagen (RT).

At 4 °C, Telo-ABM, Atelo-ABM, and RT samples in physiological buffer were triple-helical and remained liquid suspensions (Figure 4.2 and Figure 4.3 B). At physiological pH, the negative MRE signal emerged in CD at temperatures where samples had undergone fibrillogenesis in parallel rheology measurements (Figure 4.3 B). The profile of the band for Telo-ABM was similar to Telo-EPC, which suggests that impurities and differences in extraction and purification were not responsible for the negative band (Figure 4.3 A and Figure 4.3 B). The decrease in MRE and increase in G' for the pepsin-digested Atelo-ABM samples occurred at higher temperatures and returned to zero at lower temperatures compared to the undigested bovine telocollagens (Figure 4.3 B). RT samples also exhibited a delay in fibrillogenesis and denatured at lower temperatures than bovine telocollagens. Overall, the collagen samples exhibited characteristic self-

assembly in rheology at temperatures and buffer conditions that matched the emergence of a negative CD band.

4.3.3 The negative band is not observed if self-assembly is inhibited

To evaluate if self-assembly was necessary to produce this unique CD signature, the ellipticity and fibrillogenesis profiles of Telo-ABM, Atelo-ABM, and RT in acidic conditions was monitored during temperature sweeps that allow for self-assembly at neutral pH. In separate Telo-EPC samples, glycerol was used prevent self-assembly while maintaining neutral pH [81]. Triple-helical structure was evident for each of these conditions at 4 ºC (Figure 4.2). When the temperature was increased from 4 °C to 60 °C, samples did not present the negative band prior to denaturing between 35 °C and 42 °C (Figure 4.3 C). Failure to self-assemble was confirmed with rotational rheometry.

4.3.4 Type-III collagen does not display distinct negative MRE transition during temperature-dependent CD spectroscopy

Type-I and type-III collagen are in the fibril-forming family of collagens [39]. Both are found throughout the body, but type-III collagen is frequently found on the periphery of type-I fibers in the skin and elsewhere [163]. To determine if the negative MRE signal is specifically diagnostic of interactions in type-I collagen fibrils, the MRE of type-III collagen in acidic and physiological buffer was monitored from 4 °C to 60 °C. Type-III, like Telo-EPC and Telo-ABM, was triple-helical at 4 °C (Figure 4.2). However, type-III in physiological buffer denatured without presenting the negative MRE signal (Figure 4.5). Type-III at acidic pH denatured at lower temperatures and at a higher rate than samples at neutral pH.

The concentration of type-III collagen necessary for self-assembly rheologically was prohibitive, so self-assembly measurements were performed via light scattering [107]. The derived count rate of type-III samples at neutral pH was on average slightly lower than type-I samples (Figure 4.6). Because type-III can rarely be isolated from type-I, ‘self-assembly’ seen via light scattering may be the result of fibrillogenesis of either solely type-III collagen or type-III and contaminating type-I fibrils. Regardless, the emergence of the negative signal at 222 nm is not generalized to all fibril-forming members of collagen.

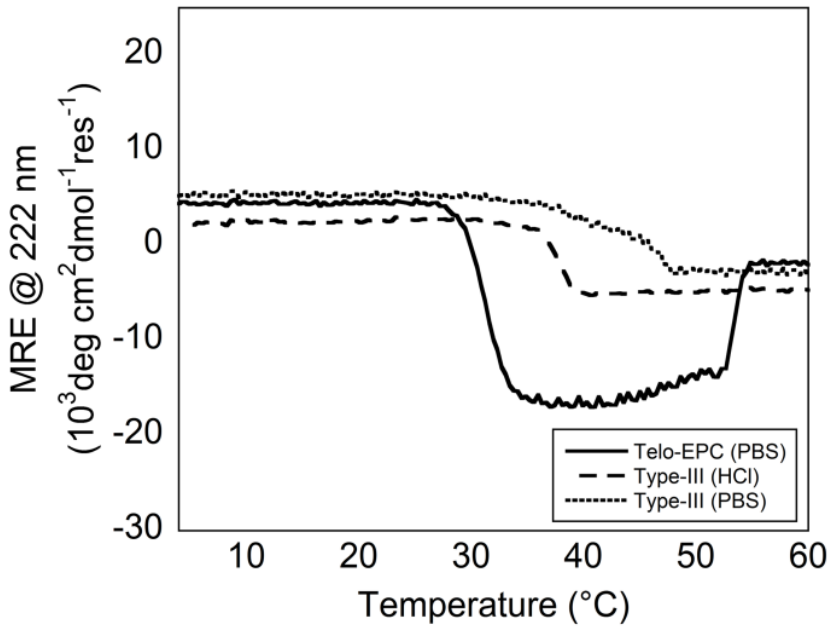

Figure 4.5 CD Spectroscopy of Type-I and Type-III Collagen. MRE at 222 nm of type-I and type-III collagen was measured from 4 ºC to 60 ºC. Telo-EPC samples in physiological buffer exhibited the two transitions in ellipticity at 222 nm as previously described in Figure 4.3 A. Type-III samples in both acidic and physiological buffers exhibited one transition as the ellipticity at 222 nm was monitored during heating. Samples in acidic buffer degraded more rapidly than those in physiological buffer.

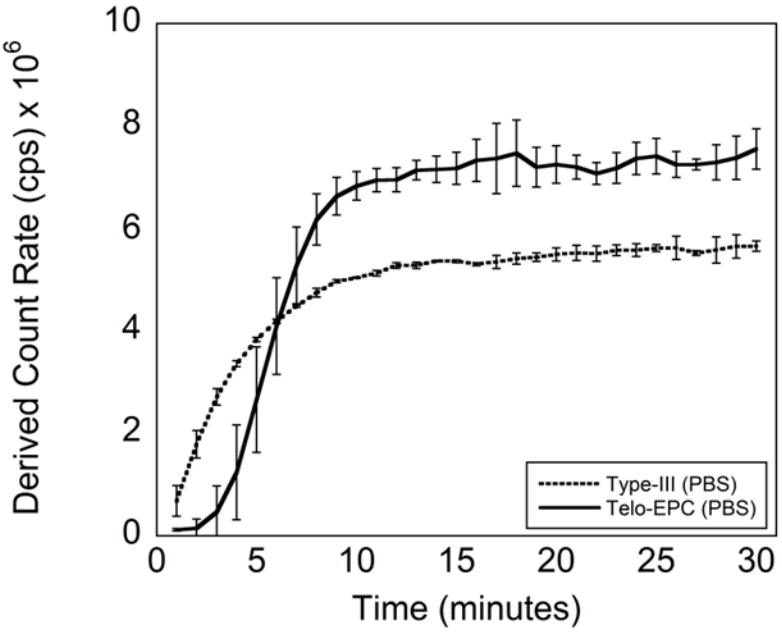

Figure 4.6 Light Scattering of Type-I and Type-III Collagen. The derived count rate of type-I (Telo-EPC) and type-III collagen samples was monitored at 37 ºC as samples formed fibrils. Telo-EPC and type-III samples were both capable of self-assembly, demonstrated as an increase in derived count rate during heating presumably due to fibril formation. Type-I and type-III collagen are very difficult to isolate from one another, therefore, it is not possible to determine if the increase in scattering as seen in these results is due to fibrillogenesis of solely type-III or type-I and type-III fibrils.

4.3.5 Gelatin does not exhibit spectral transitions associated with fibrillogenesis

Collagen denaturation into gelatin is essentially irreversible, allowing us to determine if the negative ellipticity is specific to the type-I collagen sequence or to specific interactions and structures as a result of ordered collagen fibrillogenesis. Interestingly, both samples are capable of higher order structure formation: whereas type-I collagen is known to self-assemble into D-banded fibrils at warm temperatures (~ 37 ºC), gelatin is known to partially refold into a triple-helix and even form networks (albeit at much higher concentrations) at low temperatures (4 ºC) (Figure 4.7). Therefore, forward (4 °C to 60 °C) and reverse (60 ºC to 4 ºC) temperature melts were performed on type-I collagen and gelatin to allow for self-assembly in both conditions, if possible. Both samples maintained triple-helix signal at low temperatures (4 °C to 20 °C), although the magnitude of triple-helix signal was lower in gelatin samples compared to collagen. Gelatin samples denatured at temperatures above 20 ºC, whereas collagen demonstrated the emergence of the negative MRE signal at temperatures coincident for self-assembly (Figure 4.8). Collagen samples denatured at temperatures above 50 °C. During the reverse melt, denatured collagen and gelatin samples displayed nearly identical CD spectra equivalent to an MRE signal of 0. Some partial-refolding into triple-helices was observed at low temperatures (below 20 °C). These results demonstrate that the ability to form structured collagen fibrils is necessary to generate the negative MRE signal.

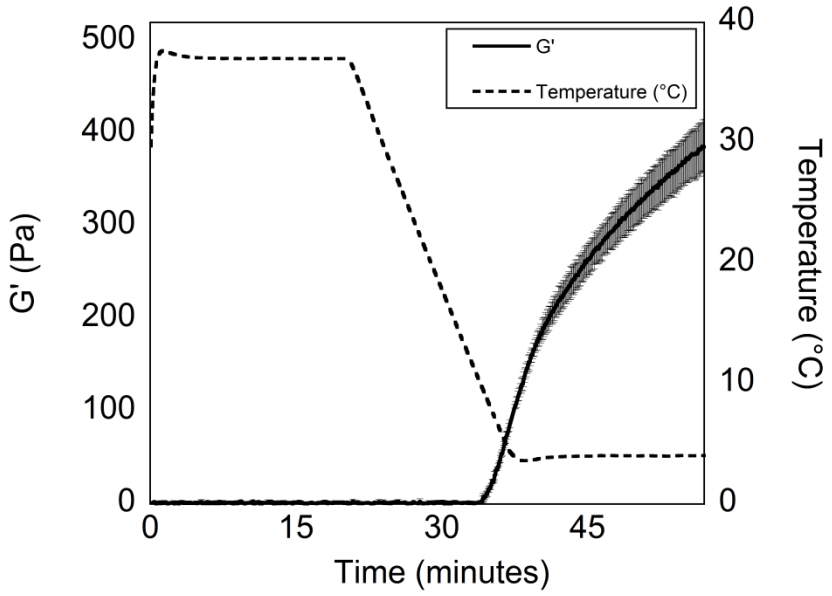

Figure 4.7 Rheology of Gelatin. The increase in storage modulus at temperatures below 10 °C indicated that gelatin was capable of forming a hydrogel at relatively high concentrations and low temperatures.

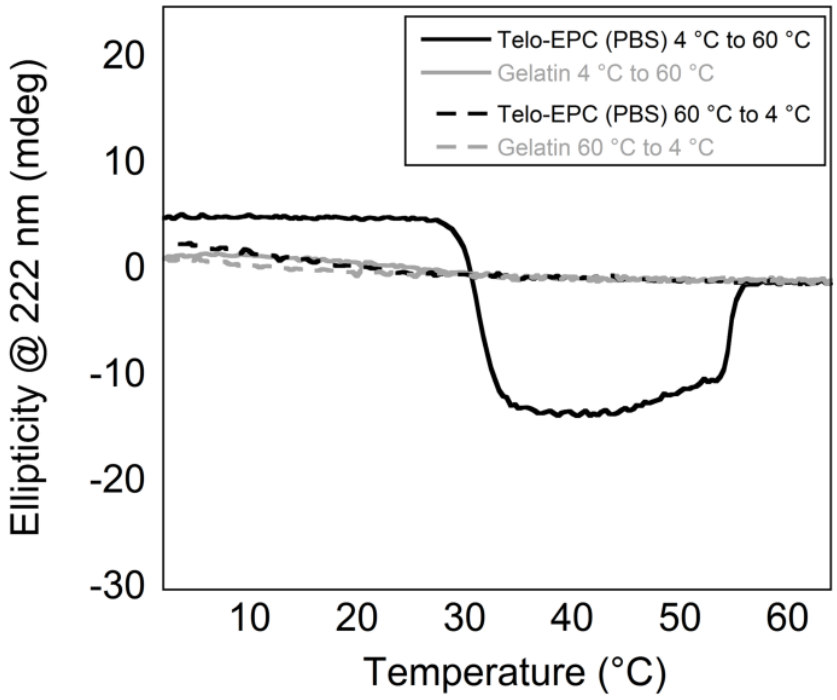

Figure 4.8 CD Spectroscopy of Type-I Collagen and Gelatin. The ellipticity at 222 nm of Telo-EPC and gelatin samples was examined from 4 ºC to 60 ºC to 4 ºC. Forward melt: the Telo-EPC sample exhibited the two transitions as shown previously. Gelatin was slightly triple-helical, but less than Telo-EPC, and slowly degraded after 20 ºC. Reverse melt: After heat denaturation, Telo-EPC and gelatin exhibited minimal changes in ellipticity until temperatures below 20 ºC when some triple-helix refolding occurred.

4.3.6 CD spectroscopy can monitor collagen fibrillogenesis at low concentrations

One potential advantage of CD versus other methods for studying assembly is the ability to work at relatively low sample volumes and concentrations. Lowering collagen concentration was expected to impair fibrillogenesis. To explore the sensitivity of this assay, the ellipticity at 222 nm was monitored as a function of temperature for collagen concentrations from 0.01 mg/mL – 0.1 mg/mL. At 4 ºC, samples at 0.1 mg/mL and 0.05 mg/mL demonstrated the positive peak at 222 nm (Figure 4.9 A). Samples at lower concentrations (0.025 mg/mL and 0.01 mg/mL) were not capable of generating a detectable triple-helix signal. When the signal was monitored from 4 ºC to 60 ºC, type-I collagen samples at concentrations of 0.025 mg/ml and above demonstrated the emergence of a negative signal at 222 nm (Figure 4.9 B). The temperature at which this negative signal emerged was concentration-dependent; at concentrations of 0.1 mg/mL, the temperature to catalyze self-assembly was lower than the temperature required for samples at 0.05 mg/mL and 0.025 mg/mL. This is consistent with the expected nucleation-growth mechanism of fibrillogenesis where increasing concentration would reduce the activation energy for nucleating assembly [164]. The signal of the 0.01 mg/mL sample changed slightly over the course of the measurement, conveying minimal information regarding fibril formation. Overall, this assay is sensitive to collagen fibrillogenesis at concentrations as low as 0.025 mg/mL.

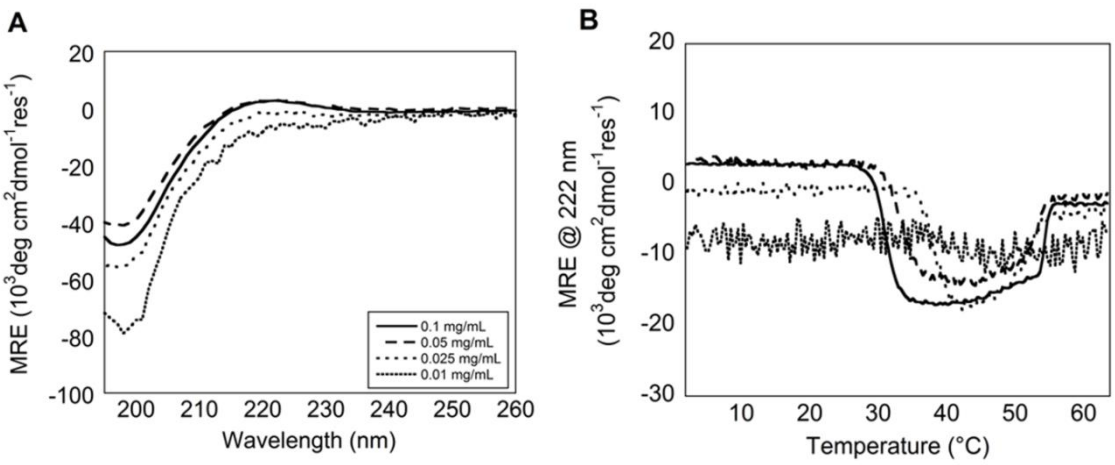

Figure 4.9 Concentration-dependent Evaluation of the CD Spectroscopy of Type-I Collagen. A) Wavelength spectra were captured from Telo-EPC samples of decreasing concentrations at 4 ºC. Sample concentrations of Telo-EPC at 0.1 mg/mL and 0.05 mg/mL exhibited the characteristic positive peak at 222 nm and negative peak at 195 nm indicative of triple-helical content. Sample concentrations of Telo-EPC at 0.025 mg/mL and 0.01 mg/mL did not exhibit the positive peak at 222 nm, but did exhibit the negative peak at 195 nm. B) Sample MRE at 222 nm was monitored as the temperature was increased from 4 ºC to 60 ºC of Telo-EPC samples of decreasing concentrations. Telo-EPC samples at concentrations of 0.025 mg/mL and higher exhibited the emergence of a negative signal at 222 nm at temperatures for self-assembly, and a second transition of the MRE to 0 as the samples denatured. Telo-EPC at 0.01 mg/mL did not exhibit clear transitions in MRE compared to the other samples.

4.3.7 A strong negative signal emerges at lower wavelengths to decrease the MRE at 222 nm

The CD experiments were primarily carried out by monitoring MRE at 222 nm; however, the collagen fibril was potentially a distinct component with its own spectral signature. Accordingly, the ellipticity from 200 nm – 260 nm was captured as a function of temperature from 4 ºC to 60 ºC in 1 °C increments. Telo-EPC exhibited significant changes in the spectral shape as a function of temperature with characteristic triple-helical and random-coil spectra at the beginning and end of the melt respectively (Figure 4.10 A). At fibrillogenesis temperatures, the spectra lacked the positive band at 222 nm and had a pronounced negative band around 204 nm – 210 nm. These spectra could not be reconstructed by a superposition of triple-helical and denatured spectra, which indicated the presence of another component. The temperature dependence of ellipiticity over a series of wavelengths showed two major transitions, one near 30 ºC and the other around 50 ºC coinciding with fibrillogenesis and denaturation respectively (Figure 4.10 B).

The CD signal at a given temperature is presumably a mixture of spectral components corresponding to triple-helix, random-coil, and one or several other species. The signal processing algorithm of fast independent component analysis (fastICA) was employed to reconstruct the observed spectra as a linear combination of such components. It was determined that three components were sufficient to reconstruct spectra from 4 ºC to 60 ºC (Figure 4.11 A). If the components determined by fastICA were unconstrained, none of the spectral

shapes corresponded to known species such as that of a canonical triple-helix or random-coil. Therefore, we chose to constrain two of the three components to have triple-helix and random-coil shapes respectively, and solved for the third component – the expected fibril spectrum. From this experiment, the fibril spectrum had a strong negative band around 204 nm – 210 nm – a new shape that does not match known secondary structure spectra (Figure 4.11 B). The emergence of this component coinciding with fibrillogenesis was responsible for the observed change in ellipticity at 222 nm in the previous experiments.

With this analysis, it is possible to track the relative abundance of helix, fibril, and coil species with increasing temperature. Weights of the three components required to reconstruct the experimental spectra as a function of temperature were extracted from the fastICA analysis (Figure 4.11 C). Fitting fractional populations to a set of Hill-type parameters provide insight into the nature of structural transitions from triple-helix to fibril and from fibril to denatured collagen (random-coil) (Figure 4.12). The first transition was characterized by the change from triple-helix to fibril components at 25 °C. This transition occurred over a short temperature range, consistent with rapid fibril assembly upon nucleation observed by other methods. The loss of the fibril component and emergence of the denatured coil component coincided at ~45 °C.

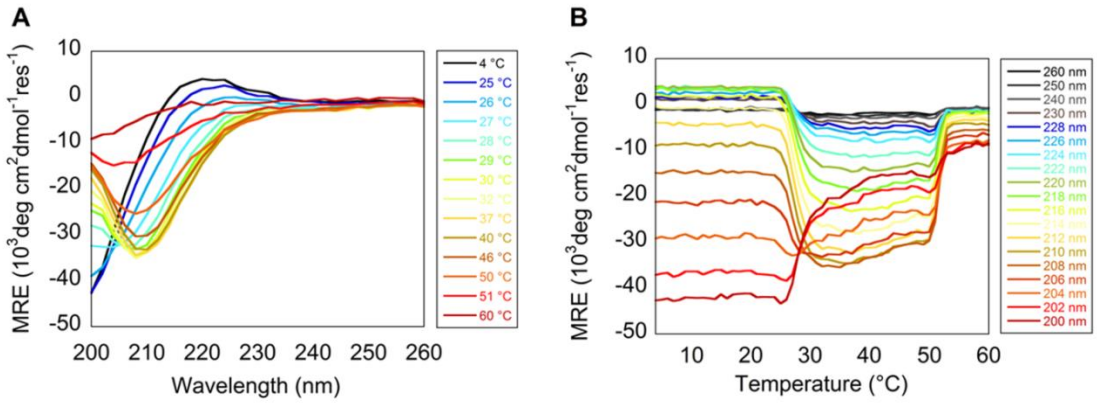

Figure 4.10 Temperature-dependent Wavelength Scan of Collagen Fibrillogenesis. The MRE as a function of wavelength and temperature was captured to monitor self-assembly and denaturation for a Telo-EPC sample. A) Wavelength spectra were captured every degree from 4 ºC to 60 ºC. Only spectra where changes took place are shown for clarity. Samples remained triple-helical until 25 ºC when the positive peak at 222 nm began to decrease. At 28 ºC, a negative signal at ~210 nm appeared, the positive signal at 222 nm continued to decrease, and the signal at 200 nm increased. By 32 ºC, the negative peak at ~210 nm was evident, the peak at 222 nm disappeared, and the signal at 200 nm has increased. At 46 ºC, samples exhibited early signs of denaturation as the negative peak at ~210 nm increased. At 51 ºC, the sample was denatured. B) Samples exhibited the most change in signal during temperatures coincident for self-assembly at 210 nm and 200 nm, where the negative peak at 210 nm emerged, and the negative signal at 200 nm increased.

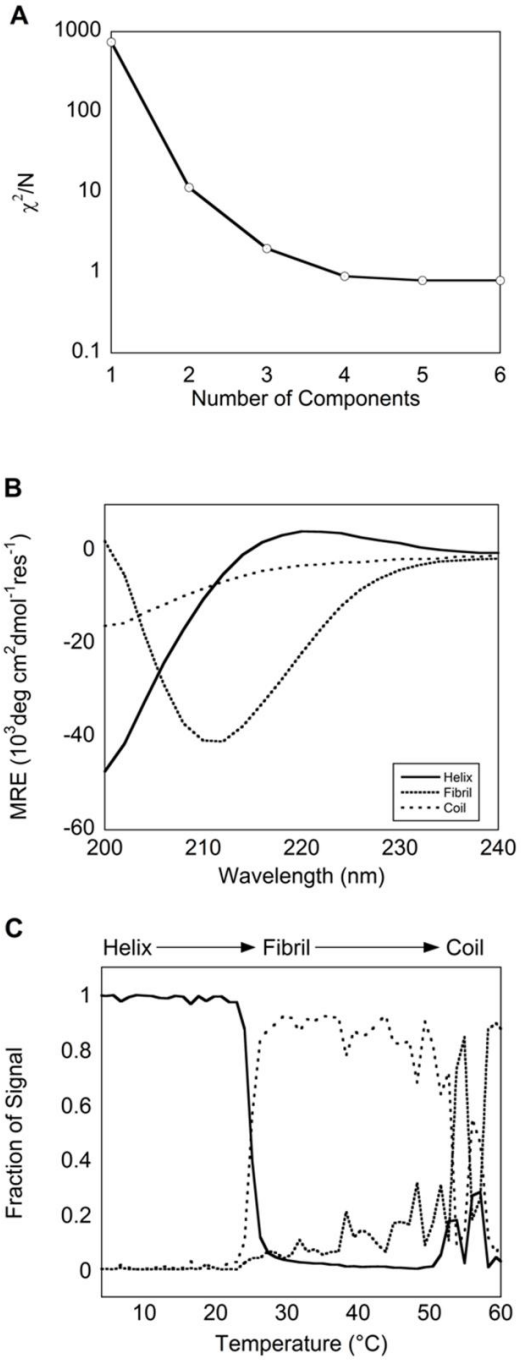

Figure 4.11 Reproduction of Collagen Circular Dichroism Using Independent Component Analysis. A) In identifying a fibril spectral component in the temperature-dependent fibrillogenesis of Telo-EPC, analysis indicated

three components were sufficient to recover experimental spectra at all temperatures (χ^2/N = 2.0 for N=3). B) In addition to constrained helix and coil components, a fibril spectral component was identified with a negative band at 210 nm for this experiment. C) The fraction of signal of the three species as a function of temperature reveal two transitions, from helix to fibril and from fibril to coil, as previously identified in the Telo-EPC temperature melt data (Figure 4.3 A).

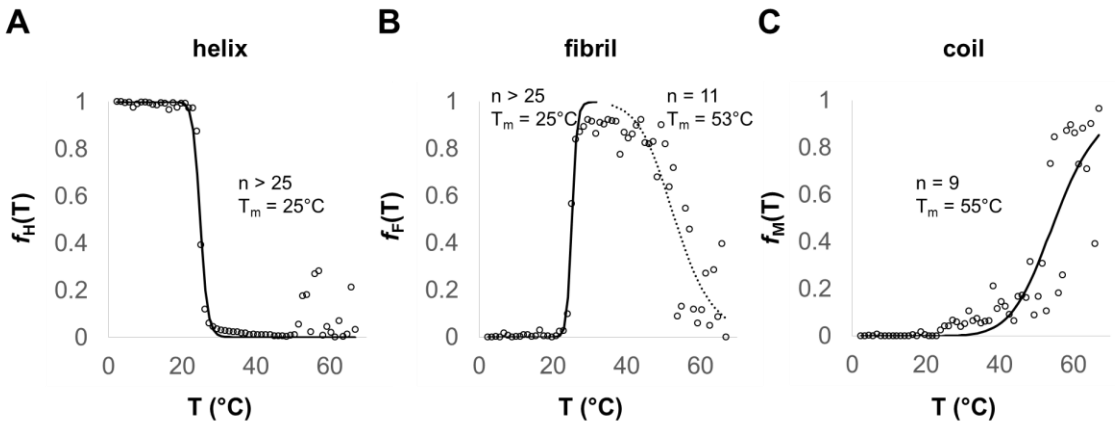

Figure 4.12 Fractional Populations of Helix, Fibril, and Coil. $f_H(T)$, $f_F(T)$ and $f_M(T)$ corresponding to fractional helix (A), fibril (B), and coil (C) species from deconvolution of the Telo-EPC melt (Figure 4.10 and Figure 4.11). Fractional populations were fit to a Hill-plot type of function: $f = T^n / (T^n + T_m{}^n)$, with *n* as the steepness of the transition at temperature T_m. Helix and coil (A and C) fractional populations were each fit to one transition. Fibril (B) fractional populations were fit to two transitions corresponding to the emergence (solid line) and loss (dotted line) of this species.

4.3.8 The collagen fibril signal is sensitive to enzymatic digestion

The ability to discriminate helix, fibril, and coil populations in a single sample can facilitate real-time observation of structural changes in collagen during biological processes. Collagen degradation by bacterial collagenases cleaves collagen relatively non-specifically, unlike matrix metalloproteases which often target a specific site on collagen [165]. Given the challenges associated with simultaneously monitoring the multiple structural forms of collagen, little is known about how collagenase degradation proceeds. Atomic force microscopy imaging under solution conditions has provided some insight into real-time structural changes during degradation [166]. The ability to monitor the fibril state of collagen by CD should give us dynamic information about this process.

We monitored the enzymatic digestion of type-I collagen fibrils using the transition of the collagen fibril signal to random-coil to indicate fibril digestion type-I collagenase recognizes and cleaves between the Y-Gly bonds in the '…Gly-X-Y-Gly-X-Y…' sequence [167]. Collagen samples were measured for triple-helical signal at 4 ºC and then for fibril signal after 30 minutes incubation at 37 ºC prior to adding type-I collagenase to one of the samples (Figure 4.13 A). Both samples demonstrated triple-helical signal at 4 ºC and the fibril signal at 37 ºC. An increase in the signal at 204 nm occurred after introduction of type-I collagenase or buffer to the cuvettes, potentially due to the slight dilution of the samples (Figure 4.13 A and B). Throughout the measurement, type-I collagen with added buffer exhibited minor changes in the ellipticity profile (Figure 4.13 B). In contrast, when type-I collagen was treated with type-I collagenase, a lag

phase of approximately 30 minutes was observed in the enzymatic activity, followed by a slow increase in the negative peak at 204 nm. The signal transitioned to random-coil quite rapidly after approximately 3 hours (Fig 4.13 C). Review of the raw data showed that the collagenase signal did reappear after the digestion, presumably with some type-I collagen fragments remaining (Figure 4.14). Changes in the CD signature during this digestion suggest a slow decrease in fibril population, until the enzymatic activity promotes complete digestion to random-coil, with a similar signal to the heat-denatured state.

Fitting of the obtained CD spectra to helix, fibril, and coil components suggested that this process proceeds from a helix-fibril mixture to triple-helix to coil, with a short-term existence of long-lived triple-helical intermediates prior to complete digestion (Figure 4.13 D). The prediction of a helix-fibril intermediate in this computational analysis is likely because the measured fibril signal may not be truly mean per-residue ellipticity, as previously discussed. Overall, the experimental and reconstructed spectra corroborate with other experimental data suggestive of collagenase digestion as slow thinning of fibrils over time [166]. Combining CD with other structural characterization methods on similarly prepared samples could provide insight into collagen remodeling processes such as this at multiple levels of structural detail.

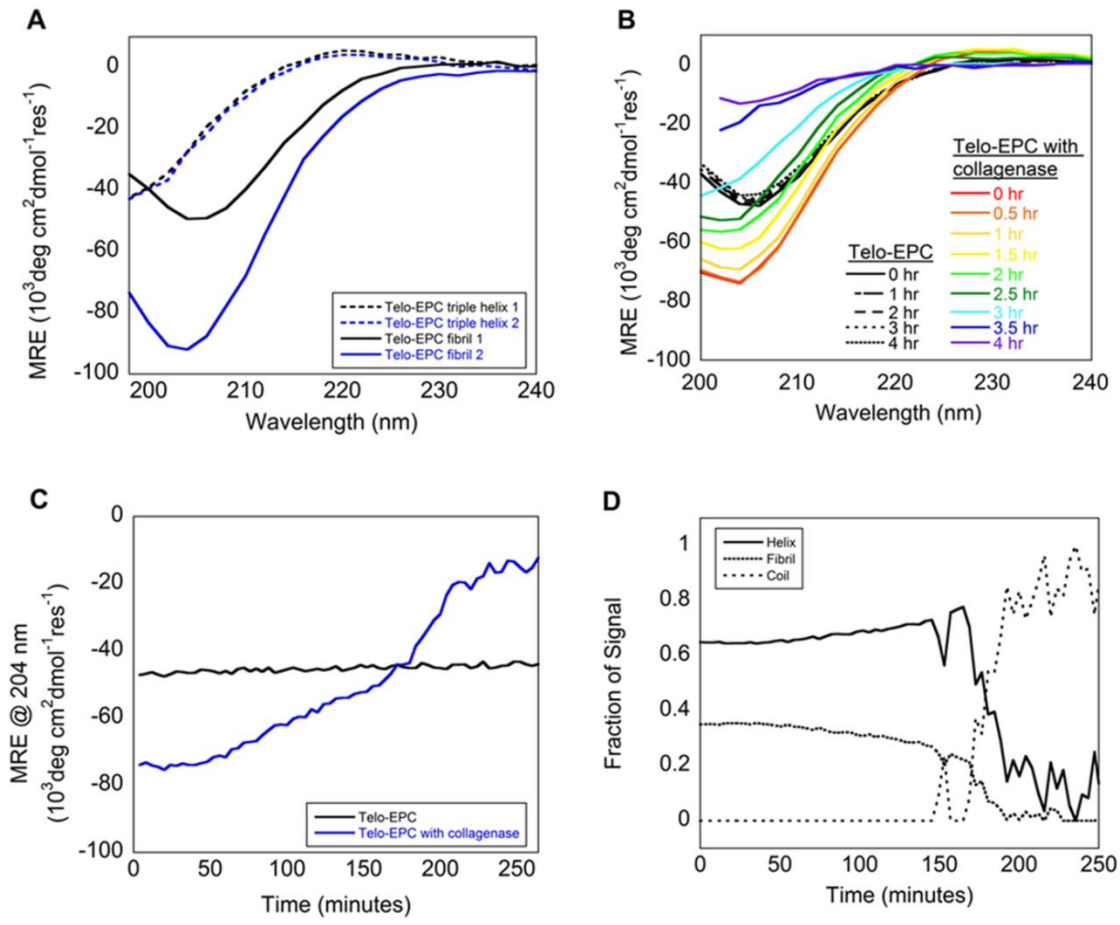

Figure 4.13 Experimental and Computational Analysis of Enzymatic Digestion of Type-I Collagen. A) Telo-EPC samples were measured for triple-helical content and fibril content as the ellipticity was measured from 240 nm – 198 nm. Samples 1 and 2 were prepared identically, where sample 2 was ultimately treated with collagenase. Samples had identical triple-helical content with a positive peak at 222 nm. Both fibrils had negative peaks at 204 nm, with the magnitude at ~204 nm greater in one than the other. B) Wavelength spectra were obtained over the course of four hours as collagenase was added to one cuvette. Data is omitted at the later timepoints after the dynode voltage exceeded

600V. The CD signature of the Telo-EPC sample with buffer added did not change over the course of four hours. In contrast, the sample with added collagenase exhibited an increase in MRE at 204 nm starting after one hour, and was fully degraded by four hours, as indicated by a random coil signal. C) Sample MRE at 204 nm was plotted as a function of time. The MRE at 204 nm of the Telo-EPC sample with collagenase added slowly increased over time in contrast to the Telo-EPC sample with buffer added, which remained constant over time. D) The previously identified components were fit to the collagenase data, and demonstrated a substantial helix (~62%) and fibril (~38%) component prior to degradation. When substantial digestion began to occur (Figure 4.13 C, T = 3 hr) the helix component increased and the fibril component decreased, demonstrating fibril digestion into smaller triple-helical components before full digestion. The helix component subsequently decreased as the coil component increased.

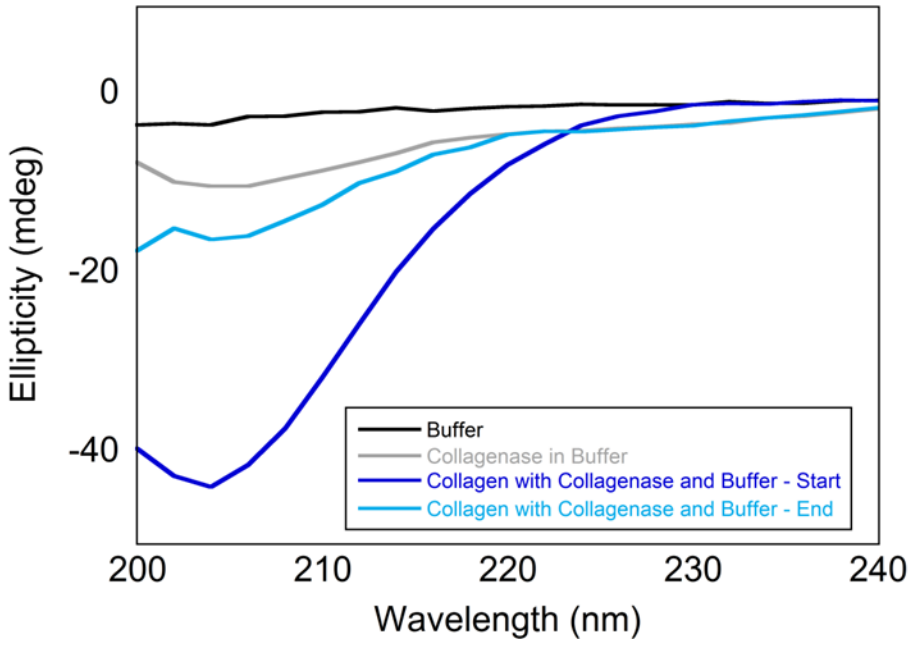

Figure 4.14. Wavelength Scan of Collagenase Before and After Digestion. Raw wavelength spectra of buffer, type-I collagenase in buffer, and the starting and ending spectra of type-I collagen with collagenase from 240 – 200 nm. There is no buffer/enzyme subtraction or MRE correction in this figure. The collagenase signal is slightly more negative in the lower wavelength regions compared to the buffer signal. When collagen and collagenase are in the cuvette at the beginning of the measurement, the measurement is primarily our fibrillar collagen with the negative peak at ~204 nm. When the collagen is digested we see a similar spectra compared to the original collagenase signal, presumably with some fragments of type-I collagen remaining.

4.4. DISCUSSION

There is strong evidence that a unique CD spectral component can be associated with the presence of assembled collagen fibrils. Our identified collagen fibril spectrum is distinct from collagen in acidic triple-helix form. It is similar in spectral shape to the poly-proline II structure (Figure 4.15), however, the signals are tremendously different in magnitude [168, 169]. This signal is strongly correlated with other measurements of fibrillogenesis such as rheology, and is evident for a number of type-I collagens from diverse source tissues and species. Solution conditions that inhibit fibril formation prevent this spectral component from being observed, indicating that a contaminating signal from another protein is unlikely. Interestingly, type-III collagen, although triple-helical and considered a fibril-forming collagen, did not display the collagen fibril spectrum even though light scattering measurements may have eluded to some type of self-assembly. This may have occurred because type-I and type-III collagens can rarely be isolated from each other, and contaminating type-I collagen may have contributed to higher order self-assembly.

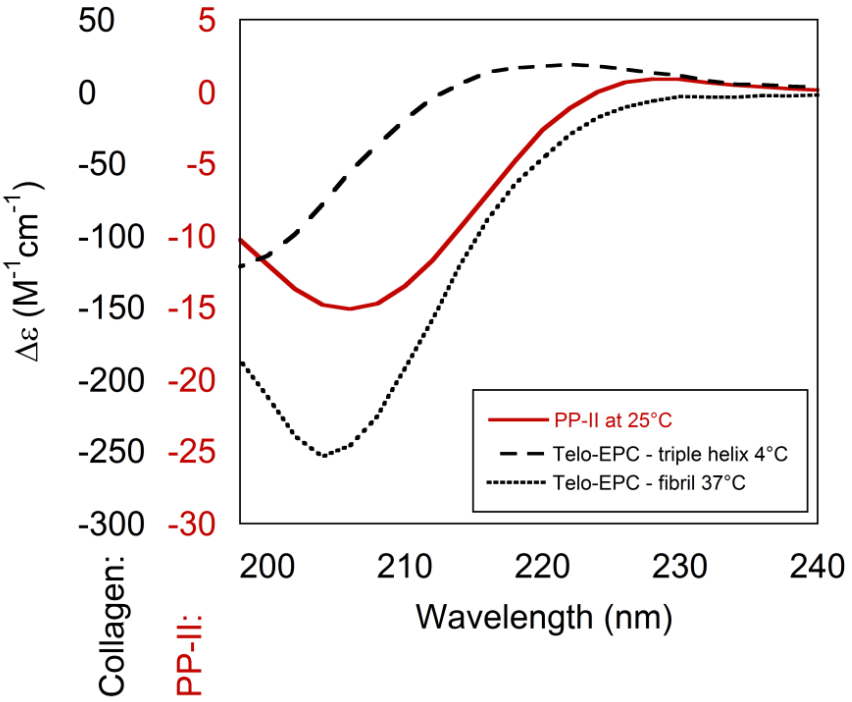

Figure 4.15 Comparison of Circular Dichroism of Type-I Collagen Triple-helix and Fibril to Poly-proline II. Wavelength spectra of Telo-EPC in triple-helical (4 °C) and fibril states (37 °C) (from Figure 4.5 A) were compared to the poly-proline II (PP-II) signal obtained by Lopes et al [168]. To ensure the units were the same, MRE of our collagen signals was converted to Δε [170-172]. Note that the collagen signals are an order of magnitude greater than the PP-II signal. Signal information for PP-II was downloaded from the Protein Circular Dichroism Data Bank [173]. The PP-II from Lopes et al was purchased from Sigma-Aldrich, and had a molecular weight of 1,000 Da – 10,000 Da in comparison to the collagen triple-helix, which is ~350,000 Da [168]. The Telo-EPC triple-helix signal and PP-II signal are clearly distinct, particularly when comparing the positive peak at 222 nm and the lack of a negative peak at 204 nm. The CD signature of

Telo-EPC fibril signal and PP-II are similar in spectral shape, but the amplitude of the peaks differ by over an order of magnitude.

CD spectroscopy was performed at much slower temperature rates in comparison to rheology where faster temperature rates were required to confidently avoid sample dehydration. Despite differences in experimental conditions between CD spectroscopy and rheology, and in collagen concentrations, the emergence of a negative signal occurred at approximately the same temperature as fibrillogenesis. Rheology and CD spectroscopy captured differences in the kinetics of self-assembly: when comparing telo and atelocollagens it was evident that the presence of the telopeptides catalyzed fibril formation, which is a well-characterized phenomenon in the literature [102, 103, 106]. Additionally, rheology and CD demonstrated that the transition to gelatin occurred at lower temperatures for rat tail collagen than bovine skin collagen, implying a difference in fibril stability between species of type-I collagen. The unique, temperature-dependent profiles of the negative MRE signal suggest that the collagen fibril spectrum provides information about the kinetics of fibrillogenesis and potentially speaks to the structural changes occurring as a result of fibril formation.

The molecular structure that causes this spectroscopic signal appears to be specific to type-I collagen fibrillogenesis. Other forms of aggregation, such as amyloid aggregation, occur after protein unfolding and result in an increase in dynode voltage due to scattering, which was not observed in our measurements (Figure 4.4) [174]. When the evolution of this signal was captured as a function of temperature, it was clear that the emergence of a strong negative signal in regions between 204 nm – 210 nm was the dominant signal change at

temperatures for self-assembly, decreasing the MRE at 222 nm. Given the magnitude of this effect, we are likely observing structural changes of the peptide bond. We have postulated two mechanisms that may contribute to the CD signal: 1) supercoiling in the microfibril, or 2) change in solvent dielectric due to partial water exclusion and ordering inside the fibril. This would change the chromophore site energies, causing shifts in the CD spectrum [175].

Although the structural and photophysical origins of the collagen fibril spectrum are yet to be determined, this signature is useful for studying assay for collagen fibrillogenesis and measures of fibril stability. This is particularly advantageous for studies of mutated collagens and/or collagen mimetic peptides, when sample availability is problematic. This method and unique spectroscopic signal may provide further insight into the method for collagen fibrillogenesis and/or the specific molecular interactions that promote or inhibit fibril formation.

Other processes that greatly affect our understanding of the collagen fibril, such as mechanisms of metalloproteinase digestion of fibers and molecular crosslinking, may be studied using this diagnostic tool. In real-time atomic force microscopy (AFM) studies of collagenase degradation of collagen, thinning and shortening of mature D-periodic banded fibrils was observed over the course of an hour, whereas our digestion proceeded over the course of 3 hours [166]. Differences between the digestions may be the result of dissimilar sample preparation of collagen or collagenase, and/or experimental conditions. Similar to the mechanism outlined by Paige et al, we demonstrated that digestion proceeded gradually as collagenase cleaved the collagen fibrils randomly until

the fibrils disaggregated into a denatured state [166]. Interestingly, fastICA of our collagenase degradation data suggested digestion of the collagen helix-fibril population into triple-helical components briefly before full protein denaturation. To add to the mechanism, CD spectroscopy revealed that the collagenase digestion may proceed as follows: 1) collagen thinning over the course of the first three hours (identified by our study and Paige et al), followed by 2) cooperative degradation of the ‘thinned’ collagen molecules to a random-coil state. The latter described structural change could not be observed using AFM, but was observable via CD spectroscopy, a significant benefit to using CD to understand such mechanisms [166].

CD spectroscopy may also be useful in materials science research to understand structural changes associated with collagen modifications through chemical or UV crosslinking or molecular coupling of chemical moieties. Herein, we have demonstrated how the utility of CD spectroscopy can be expanded to include secondary structure estimation of type-I collagen monomers and fibrils, and the evolution of the collagen fibril signal, which are of importance in medical research in studies of collagen structure and fibrillogenesis.

CHAPTER 5. USING A THERMOREVERSIBLE, PHOTOCROSSLINKABLE COLLAGEN FOR FREE-FORM FABRICATION OF SCAFFOLDS FOR REGENERATIVE MEDICINE

5.1 INTRODUCTION

Solid free-form fabrication and 3D printing have vastly improved the ease and speed in customizing and producing patient-specific scaffolds in medicine at relatively low cost [3, 176-180]. While 3D printing platforms and speed in printing have progressed, there is a significant lack in diversity of printable biomaterials [3, 180, 181]. Additionally, much of the advancement in 3D printing tissue constructs has been in bone and cartilage engineering due to the ease in printing and handling scaffolds [3]. There is a great need to print scaffolds for all tissue types of biomaterials with desirable properties, which include biocompatibility, timely biodegradability, and mechanical and bioactive tissue mimicry [3, 182, 183].

Type-I collagen, the major protein constituent of soft tissue, is a natural choice of base material for 3D printing applications as it supports cell adhesion, and is native to many tissues throughout the body [39]. In one of its first uses in tissue engineering, collagen was formulated as an extensively crosslinked freeze-dried sponge for covering and healing deep wounds resulting from burn injury [45]. Collagen sponge wound coverings prevent foreign substances from entering the wound site, and promote cellular infiltration at the injury site to

facilitate new tissue growth and remodeling [45, 184]. While the applications of collagen sponges in tissue engineering are extensive, its uses in solid free-form fabrication or 3D printing applications to create hydrogels or sponges in defined geometries is limited. Type-I collagen has relatively weak mechanical properties, unless extensively crosslinked, and is difficult to handle or fabricate compared to competing synthetic or modified polymers [53]. It also forms highly ordered D-banded fibers at physiological conditions and requires high concentrations or crosslinking to match properties of tissues; all of which significantly disrupt 3D printing, especially forms of nozzle-based 3D printing [4, 40, 185, 186]. Type-I collagen is used in solid free-form fabrication techniques with ease, however, requires the use of a negative mold to construct the tissue of interest [187]. Unfortunately, this may delay treatment for the patient due to increased processing times for scaffold customization [177, 178].

Despite these difficulties, there have been many attempts of varying degrees of success in creating collagen-containing scaffolds for regenerative medicine through 3D printing or solid free-form fabrication. Some of these techniques include multiphoton crosslinking, extrusion, and inkjet bioprinting [188-193]. Many of these methods utilize alternate polymers for “printing,” but research has progressed to developing rapid prototyping techniques that can handle collagen gel-like slurries. In Díaz Nocera et al, 3D printed collagen constructs were created using rehydrated lyophilized collagen sponges as the ‘ink,’ filling the attached bioprinter syringes with the collagen sponge suspension, and printing scaffolds using a customized bioprinter and software system with

resolution on the order of 500 µm [194]. In another method called freeform reversible embedding of suspended hydrogels (FRESH), a MakerBot Replicator was modified to use a syringe-based extruder to release the collagen hydrogel suspension into a HEPES and gelatin slurry bath; viscosity differences between solutions allowed for structural maintenance of the printed collagen while proper pH and temperature control promoted self-assembly of the collagen hydrogel in the shape of the printed structure, which had a resolution on the order of 200 µm [195]. Unlike many other methods, FRESH allows for 3D printing of collagen structures that are self-assembled rather than unnaturally crosslinked [195]. Though relatively low cost, FRESH has associated complexities with set-up, and issues with nozzle-based printing as previously mentioned, namely nozzle clogging with hydrogel suspension [186, 195].

While many of these 3D printing systems have decreased in cost and allow for printing with relatively high spatial resolution, the technologies still require significant modifications to work with type-I collagen. Herein, we present a method for simple free-form fabrication of collagen-based material – collagen methacrylamide (CMA) – with the goal of creating macroscale, customized scaffolds with good pattern fidelity. Collagen methacrylamide (CMA) is a methacrylate-derivatized type-I collagen that retains the ability to form D-banded fibrillar hydrogels [55, 107]. CMA has two unique properties that allow for free-form fabrication: 1) following fibrillogenesis, CMA can be photocrosslinked using a photoinitiator and UV light to stiffen the hydrogel where it is exposed to light, and 2) fibrillogenesis of CMA is thermoreversible – it can reversibly cycle

between liquid and fibrillar hydrogel states based on temperature [55, 107]. Lastly, photocrosslinking eliminates thermoreversibility. Together, these properties allow for simple free-form fabrication of CMA to construct fibrillar, customized, collagen-based scaffolds for regenerative medicine. This method is distinct from solid free-form fabrication, as it does not require the production of a negative mold for fabrication, reducing times for scaffold customization. Further, in comparison to many 3D printing or free-form fabrication techniques, this method is very easy to implement, merely requiring CMA, a UV light source, and laser-printed transparencies for photopatterning.

In this paper, we describe the method for free-form fabrication of CMA, the resolution of printing, the construction of photopatterned hydrogels and scaffolds, and the ease of creating cell-laden, printed hydrogels. The first *in vivo* biocompatibility study of CMA is also performed. The ease of implementation of this free-form fabrication strategy presents many opportunities for scaffold customization of a collagen-based material to further applications of collagen in regenerative medicine.

5.2 MATERIALS AND METHODS

5.2.1 CMA Hydrogel Preparation

Type-I collagen was purchased from Elastin Products Company (C857, Owensville, MO) and was reconstituted in 0.02 M acetic acid at 3.75 mg/mL. Collagen methacrylamide (CMA) was synthesized from the solubilized type-I collagen in the method outlined in Gaudet et al and was also reconstituted in

0.02 M acetic acid at 3.75 mg/mL [55]. For free-form fabrication unless otherwise stated, CMA was buffered on ice according to the following formula: 20 µL 1M HEPES (H3537, Sigma-Aldrich, St. Louis, MO), 134 µL 0.15N NaOH (S2770, Sigma-Aldrich), 100 µL 10X PBS (P5493, Sigma-Aldrich), 59 µL 1X PBS (860454, Thermo Fisher Scientific, Waltham, MA), 10 µL 10% Irgacure (I2959, a gift from Ciba Specialty Chemicals) solubilized in neat methanol, and 677 µL CMA at 3.75 mg/mL. Buffered CMA was plated in 14 mm glass-bottomed MatTek dishes (P35G-0-14-C, MatTek Corporation, Ashland, MA) and self-assembled for one hour at 37 °C to create CMA hydrogels. All samples exposed to UV were always plated in MatTek dishes.

5.2.2 Photomask Design

Two classes of photomasks were employed for the photolithographic approach to free-form fabrication. Photomasks of larger, defined shapes were designed in Microsoft PowerPoint and printed on transparencies using a laser-printer. These masks were used for free-form fabrication unless otherwise stated. Separate high resolution photomasks were designed as grids of defined line widths and line spacings ranging from 0.25 mm to 1 mm and 1 mm to 2.5 mm respectively. Photomasks were designed in AutoCad and printed by CAD/Art Services (Bandon, OR).

5.2.3 Free-form Fabrication of CMA

Self-assembled CMA hydrogels in MatTek dishes were photocrosslinked using UV light (365 nm, 50 mW/cm^2) for times ranging between 25 and 120 seconds depending on the batch of CMA and hydrogel volume. Exposure time

was determined through mechanical testing of CMA hydrogels during UV photocrosslinking (Figure 5.1). The UV photocrosslinking set-up included use of an X-Cite 120 PC light source (Excelitas Technologies Corp., Waltham, MA) and light guide (Figure 5.2). The light guide was held in a metal cylinder using a 3D printed set-screw. From bottom-up, the light passed through a UV bandpass filter and quartz glass plate before photocrosslinking the sample. To fully photocrosslink CMA hydrogels, the entire hydrogel was exposed to UV light with no photomask. To photopattern specific regions of the CMA hydrogel, a laser-printed transparency was placed between the MatTek dish and quartz glass bottom plate. While all UV photocrosslinking was performed using this set-up, it is also possible perform CMA free-form fabrication using a handheld UV lamp (Blak-Ray Lamp, Model UVL-21, UVP, San Gabriel, CA) for a longer periods of time (~15 minutes) (Figure 5.3). To obtain the photopatterned CMA hydrogel, photocrosslinked CMA samples were cold-melted on pre-cooled aluminum plates at 4 °C for 10 minutes. Unphotocrosslinked CMA disassembled, and was removed through dilution with cold PBS and gentle agitation. Following cold-melting, photopatterned hydrogels were imaged using an Aven Digital Handheld Microscope (26700-302, Aven Inc. Ann Arbor, MI).

CMA was buffered according to the method outlined in 5.2.1. The mechanical properties of the samples were measured as outlined in Gaudet et al [55]. The photocrosslinking time for each batch of CMA is determined as the amount of time needed to reach 95% of the maximum storage modulus measured. By reaching this storage modulus, thermoreversibility was prevented. This was measured for each batch of CMA due to lot-to-lot variability in the starting collagen and the CMA produced, and accounts for the ranges of photocrosslinking times used throughout this study.

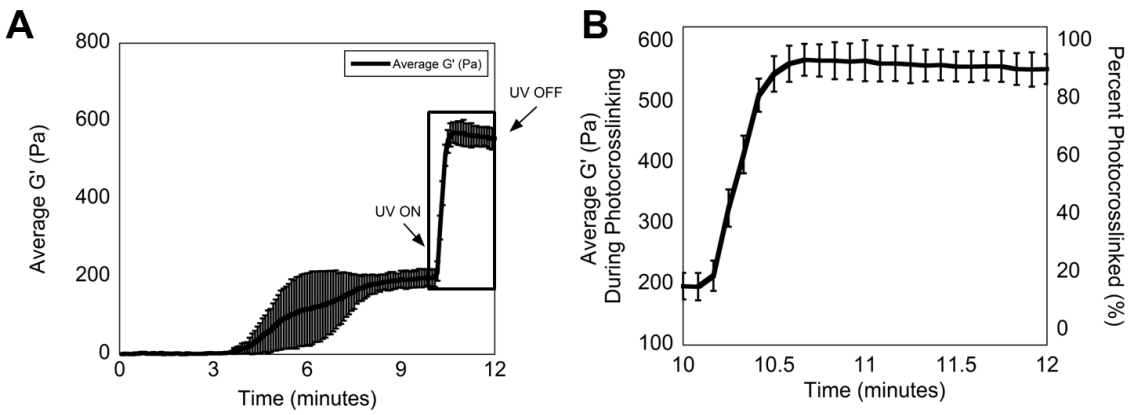

Figure 5.1 Rheological Analysis to Determine Photocrosslinking Time. A) A typical self-assembly and photocrosslinking curve obtained for CMA, averaged for 3 separately prepared samples of one lot of CMA. The sample began to self-assemble at the 4 minute timepoint where the storage modulus (G') increased. G' stabilized over time. The sample was photocrosslinked at the 10 minute timepoint, and G' further increased. **B)** The same self-assembly and photocrosslinking curve from 10 – 12 minutes demonstrated that this particular

batch of CMA needed to be photocrosslinked for approximately 25 seconds to reach 95% of the maximum storage modulus.

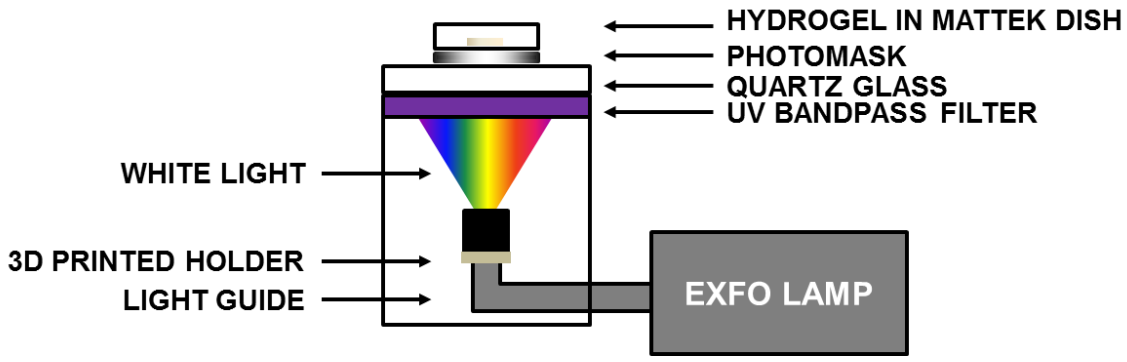

Figure 5.2 UV Photocrosslinking Set-up for CMA Free-Form Fabrication. Light filtered to allow UV to photocrosslink sample using a photomask. Without a photomask, samples will be fully exposed to UV light, which results in complete photocrosslinking of the entire hydrogel.

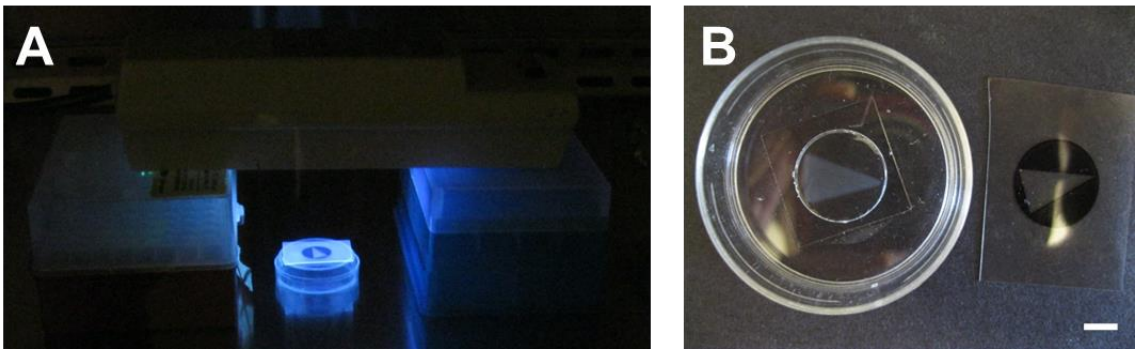

Figure 5.3 Photopatterning CMA Using an Alternate UV Light Source. A) Photocrosslinking set-up using Blak-Ray Lamp (Model UVL-21, UVP, San Gabriel, CA). Photocrosslinking times were drastically increased using this lamp, as the intensity is much weaker. This set-up is top-down, photocrosslinking the sample from above, whereas the set-up used throughout the majority of this study photocrosslinks from below. **B)** Despite the slower photocrosslinking times, macroscale, photopatterned hydrogels can still be produced with good pattern fidelity. Scale bar is 1 mm.

5.2.4 Spatial Resolution of Free-form Fabrication

CMA hydrogels were formulated as described above, and 100 µL of CMA suspension was plated in the MatTek dishes. Self-assembled hydrogels were photocrosslinked through the high resolution photomasks for 45 seconds. For measurements of spatial resolution, the area and shape of the voids or regions that cold-melted (because they were not exposed to UV light) were measured and compared to the grid pores in the photomask. Circularity measurements were performed to analyze the shape change from the square in the photomask to a circle, which was likely due to occur from the diffusion of free radicals from areas of light exposure. For circularity measurements (circularity = 4*pi*(area/perimeter^2)), a perfect circle would have a circularity of 1, whereas the square seen in the photomasks has a circularity of ~0.78. Images were processed in ImageJ software (ImageJ, NIH, Bethesda, MD) with no adjustments to contrast or brightness. The pores in the photopatterned hydrogels and photomasks were traced using the Polygon Selections Tool. Only pores that were entirely within the interior of the hydrogel (i.e. not at the edges of the hydrogel) were traced. A total of five hydrogels were photopattered per photomask, and the average pore area and circularity measurement obtained for the set of five was reported.

The width of patterned lines was measured via image analysis from changes in pixel intensity in a linear region taken across the sample. For line width measurements, the photopatterned CMA image was aligned to the photomask image using spatial referencing in MATLAB, and the transformed

CMA image was written to a new image file. The photomask and transformed CMA images were opened in ImageJ and contrast was adjusted without affecting the line widths of the sample. A line of constant length was drawn in both images in the exact plane, and the Plot Profile function in ImageJ was used to identify the intensity value as a function of position along the line. A moving average filter with a span of 0.03 was applied to smooth the pixel intensity value curves.

5.2.5 Spatial Resolution of CMA Sponges Created through Free-form Fabrication

Buffered CMA suspension (400 µL) was plated in MatTek dishes, self-assembled, and photocrosslinked through a photomask for two minutes due to the increase in gel volume. Following cold-melting to remove CMA that was not exposed to UV light, hydrogels were subsequently frozen at -80 °C for three hours and lyophilized overnight to create freeze-dried scaffolds. Then, scaffolds were hydrated with PBS for one hour. Scaffolds were imaged at each stage of the process using an Aven Digital Handheld Microscope. Images were loaded into ImageJ software, with no adjustments to contrast or brightness, and the area of each scaffold was measured in comparison to the photomask using the Polygon Selections Tool. The average area was reported for a set of five scaffolds in each state.

5.2.6 Free-form Fabrication of Cell-encapsulated Hydrogels

Adult human mesenchymal stem cells (hMSC) were acquired from the Institute for Regenerative Medicine at the Texas A&M College of Medicine (item# 8013L). Cells were expanded in tissue culture flasks until 70-80% confluency in MEM-alpha (12561-049, Thermo Fisher Scientific), 10% fetal bovine serum

(S11550, Atlanta Biologicals, Flowery Branch, GA), 1% Penicillin/Streptomycin (P/S) (P4458, Sigma-Aldrich), 1% L-glutamine (G7513, Sigma-Aldrich), and 1 ng/mL bFGF (100-18B, Peprotech, Rocky Hill, NJ). Following expansion, hMSC were detached using trypsin/EDTA (T4049, Sigma-Aldrich) and washed in culture media, and were encapsulated in buffered hydrogel suspensions at ~150,000 cells/mL.

Photopatterned, cell-laden CMA hydrogels were prepared by including cells in the buffered hydrogel solutions. Self-assembly entrapped the cells within the hydrogel. These cellular gels were then used for free-form fabrication. These CMA hydrogels were formulated as described, but 10X MEM (M0275, Sigma-Aldrich) and Medium 199 (M199) (12350-039, Thermo Fisher Scientific) were used instead of 10X PBS and 1X PBS, respectively. The amount of M199 was further reduced by 30 µL, and 10 µL of L-glutamine, 10 µL of P/S, 10 µL of 1M ascorbic acid (255564, Sigma-Aldrich) in M199 was added. Ascorbic acid was used to temper the effect of free radicals on cells, and its addition had no effect on pattern fidelity (Figure 5.4) [196-198]. Cell-encapsulated, buffered collagen and CMA suspensions were plated in MatTek dishes (200 µL). Free-form fabrication of the cell-laden hydrogels was performed as described above, except for hydrogels that were not exposed to UV. Photopatterned CMA hydrogels were exposed to UV through a photomask. UV exposure time varied between 25 and 30 seconds depending on the batch of CMA. All samples were cold-melted for 10 minutes. Cold-melted CMA in photopatterned, cell-laden hydrogels was removed using cold hMSC media. Samples were given warmed media (2 mL) for 15

minutes, and it was then replaced with fresh warmed media (2 mL), serving to remove any reaction byproducts from photocrosslinking. Cell-laden, photopatterned constructs were incubated at 37 °C, 5% CO_2 for 24 hours, and stained using calcein-AM from the LIVE/DEAD Viability/Cytotoxicity kit (L3224, Thermo Fisher Scientific), and imaged using the Aven Digital Handheld Microscope and Olympus IX81 fluorescence microscope.

In parallel, a cytotoxicity study was performed to evaluate cell viability following free-form fabrication. Cellular CMA gels were prepared with and without irgacure and were exposed to UV light. Also, cellular CMA gels were prepared with irgacure and were not exposed to UV light. Separate cellular collagen gels were similarly prepared and characterized (20 µL 1 M HEPES, 126 µL 0.15N NaOH, 100 µL 10X MEM, 37 µL M199, 10 µL L-glutamine, 10 µL P/S, 10 µL ascorbic acid, 10 µL 10% irgacure in neat methanol, 677 µL collagen at 3.75 mg/mL in 0.02 M acetic acid). Collagen and CMA hydrogels without irgacure were prepared as described, supplementing the final hydrogel volume with M199. Samples that were exposed to UV light were prepared as described and plated in MatTek dishes, whereas samples that were not exposed to UV light were plated in 48 well plates, and were given 2 mL or 200 µL media, respectively. Samples were self-assembled, fully photocrosslinked, and cold-melted for 10 minutes. If samples disassembled because they were not exposed to UV with irgacure, hydrogels were re-assembled at 37 °C for 15 minutes. Samples in MatTek dishes or 48 well plates were given warmed media (2 mL or 200 µL, respectively), and spent media was replaced after 15 minutes. Cell-laden constructs were

incubated at 37 °C, 5% CO_2 for 24 hours, and were evaluated for cell viability using a LIVE/DEAD Viability/Cytotoxicity kit. There were 3 constructs per condition, and 3 Z-stacks were taken of each sample at 100 µm increments for a total of 1000 µm using an Olympus IX81 fluorescence microscope. Z-stacks were pseudo-colored (live – green, dead – red), merged using ImageJ software, and the Z Project function (Max Intensity) was used to create a 2D image. Images were counted using the Cell Counter Plugin. Data reported was the average of three separate experiments.

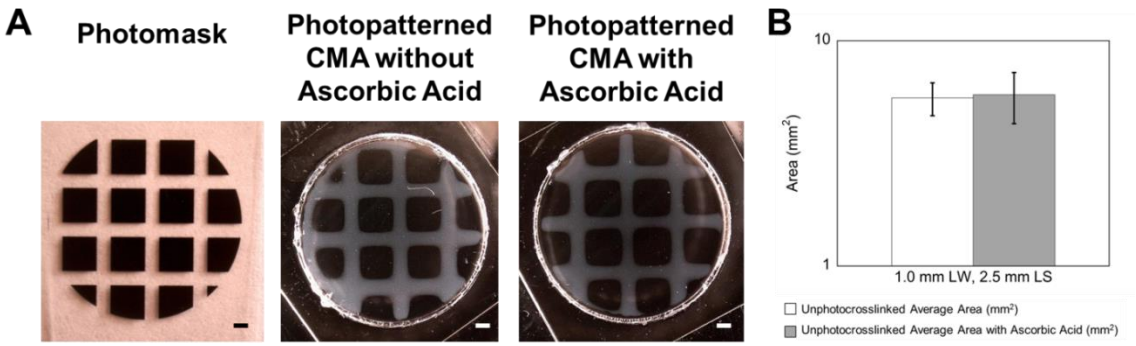

Figure 5.4 Spatial Resolution of Photopatterned CMA with and without Ascorbic Acid. A) CMA hydrogels photopatterned with and without ascorbic acid demonstrated good pattern fidelity in comparison to the photomask, and were not discernable from one another. **B)** Area measurements demonstrated no statistical difference between the cold-melted (unphotocrosslinked) regions of the hydrogels. Scale bar is 1 mm.

5.2.7 In Vivo Biocompatibility Studies

The biocompatibility of CMA and photocrosslinked CMA hydrogels was assessed in a subcutaneous implantation study in rats and compared to type-I collagen control hydrogels. Collagen and unphotocrosslinked CMA suspensions were prepared similar to cell-encapsulated hydrogels, but without irgacure or ascorbic acid, supplementing the remaining volume with M199. A 200 µL sample of buffered suspension was plated within polydimethylsiloxane (PDMS) rings in small Petri dishes to form hydrogels that were 9.5 mm diameter and 3 mm in height.

Photocrosslinked CMA hydrogels were prepared with irgacure, but without ascorbic acid, using the free-form fabrication method. These hydrogels were plated in MatTek dishes (432 µL), self-assembled, and photocrosslinked using a photomask of a circle with a diameter of 9.5 mm to create hydrogels of the same height and diameter of the collagen and unphotocrosslinked CMA plated in PDMS molds. These samples were photocrosslinked for 2 minutes due to the increase in gel thickness. Photocrosslinked CMA was cold-melted and rinsed with sterile PBS to remove cold-melted CMA to obtain the hydrogels for implantation.

All procedures were conducted in accordance with approved protocols from the Institutional Animal Care and Use Committee (IACUC). Male Sprague-Dawley rats (SD, Charles River Laboratories, Wilmington, MA, 300 g – 350 g) were housed on alpha dry bedding in plastic cages with wire lids in temperature-controlled rooms. Animals were fed lab chow (LabDiet 5012, Brentwood, MO)

and had ad libitum access to water. Prior to surgery, rats were anesthetized with 5% isoflurane gas. The backs of the rats were shaved and disinfected. During surgery, rats were maintained under 1 – 2% isoflurane gas. An incision was made vertically along the length of the rat. Pockets ~3 cm deep were created at two sites on each side of the midline approximately 5 cm apart for a total of four implantation sites per animal. Hydrogels were subcutaneously implanted in each pocket. The incision was closed with a single staple. A total of six rats were used – three were evaluated at one week and three were evaluated at six weeks. With four implant sites per animal and three types of gels (collagen, CMA, and photocrosslinked CMA), there were 12 samples total at each time point, or four for each gel type Hydrogels were randomly assigned to the implant sites, with each animal receiving at least one implant of each type. At one and six week timepoints, rats were euthanized via carbon dioxide asphyxiation. The back of the rats were shaved, disinfected, and an incision was made vertically along the length of the rat to find the pockets where the scaffold was implanted. This tissue was explanted, capturing the remaining scaffold when observable, and was fixed in 4% paraformaldehyde for one week.

Following fixation, explants were embedded in OCT compound, frozen, and sectioned transversely into 40 µm sections. Hematoxylin and eosin (H&E) staining was performed to assess the response to implantation. H&E stained sections were imaged using a VS120 Color Microscope at 40X. Sections were also stained immunohistochemically using a mouse anti-rat type-I collagen antibody (clone 1F10C2, 7043, Chondrex, Inc., Redmond, WA) at a 1:500

dilution and a rabbit anti-bovine type-I/type-III collagen antibody (2150-2305, Bio-Rad, Raleigh, NC) at a 1:100 dilution. Secondary antibodies of goat anti-mouse AlexaFluor647 (A-11008, Thermo Fisher Scientific) and goat anti-rabbit AlexaFluor488 were used (A-21235, Thermo Fisher Scientific) at 1:500 dilution. A DAPI stain was applied during mounting (D3571, Thermo Fisher Scientific). Immunohistochemically stained sections were imaged using an Olympus IX81 fluorescence microscope at 4X. ImageJ software was used to pseudo-color and overlay images taken in each channel.

5.2.8 Statistical Analysis

Photopatterned samples were compared to the photomask using a Student's t-test with the area and circularity of the photomask as the test statistic. Data from the sponge spatial resolution study were analyzed using a Student's t-test in comparison to the photomask, and a one-way ANOVA between the scaffold types followed by posthoc pairwise comparisons with Tukey's All Pairs Comparisons. Data from the cytotoxicity were analyzed using a one-way ANOVA followed by posthoc pairwise comparisons with Tukey's All Pairs Comparisons. In all statistical analysis, data were considered significant at $p < 0.05$.

5.3 RESULTS

5.3.1 Free-form fabrication of CMA hydrogels is accurate to ~250 μm

Spatial resolution was assessed following exposure through photomasks with a range of line widths (0.25 mm – 1.0 mm) and line spacing (1.0 mm to 2.5 mm). Spatial resolution of photopatterning decreased as function of line width

and line spacing (Figure 5.5). Hydrogels photopatterned with the 1 mm width and 2.5 mm spacing photomask had the closest pattern fidelity to the photomask pore measured via area and circularity (Figure 5.5 B and C). CMA hydrogels photopatterned with 0.25 mm width and 1 mm spacing had the lowest pattern fidelity, illustrated by on average 50% over-photocrosslinking in the photomask pore area (Figure 5.5 B). Despite the pattern fidelity of the resultant hydrogels compared to the photomask, the area of the cold-melted regions in the CMA hydrogels was always statistically lower than the corresponding area of the photomask. Circularity measurements demonstrated a slightly different trend – hydrogels patterned with 1.0 mm width and 1.0 mm spacing had the closest circularity to the ideal (~0.88 and ~0.78, respectively) (Figure 5.5 C). Spacing above 1.0 mm resulted in gels that were similar in circularity. However, as the line width decreased below 1.0 mm, the circularity increased. Circularities for all photopatterned hydrogels were statistically higher than the photomask circularity, suggesting that excess free radicals diffused away from areas of light exposure. Pixel intensity measurements in photopatterned CMA-photomask overlays demonstrated some specificity of photocrosslinking in the regions exposed to UV light, with excess photocrosslinking occurring (Figure 5.6). Consistent with the previous measurements, over-photocrosslinking increases as the line width decreases. Overall, there are significant differences between the photomask and photocrosslinked hydrogel, particularly at line widths and spacings below 1.0 mm, but the method demonstrated similar pattern fidelity to the photomask at 2.5 mm width and 1.0 mm spacing.

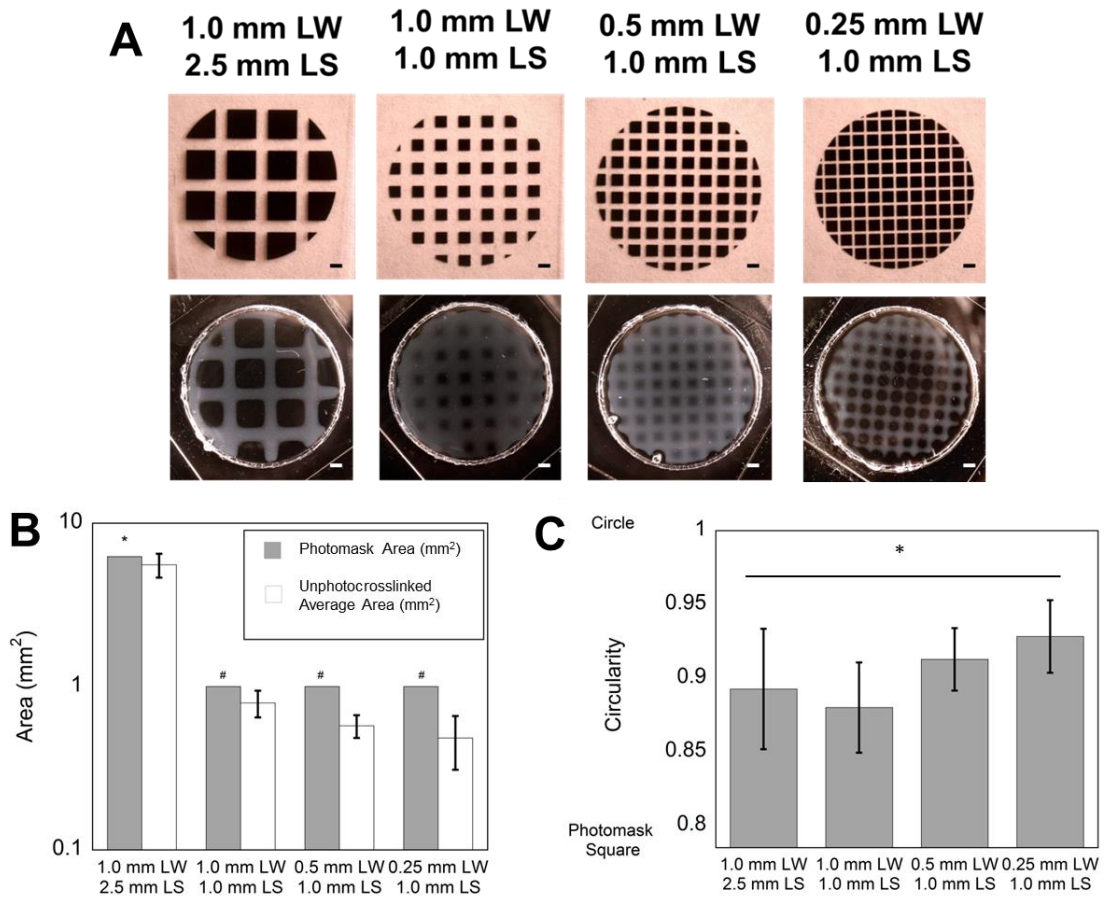

Figure 5.5 Free-Form Fabrication and Spatial Resolution of Photopatterned CMA Hydrogels to High Resolution Photomasks. A) Comparison of photomask and photopatterned hydrogel of various line widths and line spacings ranging from 0.25 mm to 1.0 mm and 1.0 mm to 2.5 mm, respectively. All hydrogels were successfully photopatterned, although the hydrogel with the maximum line spacing (2.5 mm) best reflected the photomask. Pattern fidelity decreased as a function of line width. **B)** Area of the cold-melted (unphotocrosslinked) region was always significantly smaller than the photomask

pore. Regardless, pattern fidelity was still quite accurate in the 1.0 mm width, 2.5 mm spacing sample, however, decreased as a function of line width. The 0.25 mm width, 1.0 mm spacing sample had the least pattern fidelity and was ~50% overphotocrosslinked. **C)** Circularity measurements ranged from ~0.78 (circularity of the photomask pore) to 1 (perfect circle). All photopatterned hydrogels were statistically more circular than the photomask pore, where the 0.25 mm width, 1.0 mm spacing had the largest circularity. Scale bar is 1 mm.

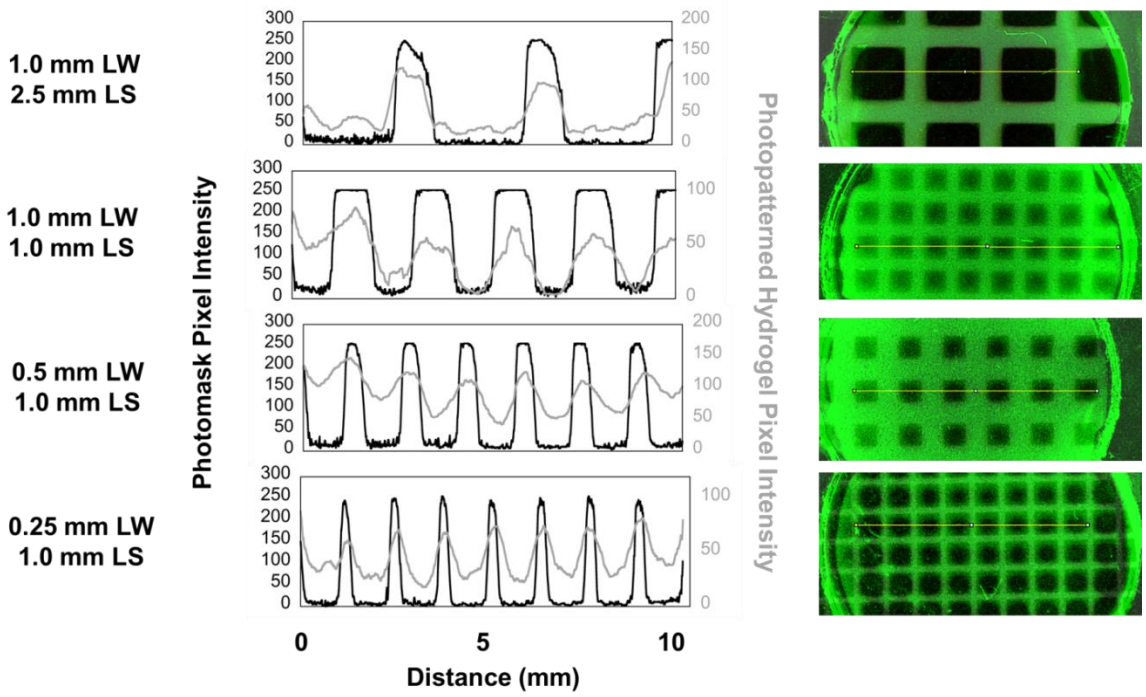

Figure 5.6 Change in Pixel Intensity Across the Photopatterned CMA Hydrogel and High Resolution Photomask. Pixel intensity measurements of photopatterned line widths across the photopatterned hydrogels were compared to respective intensity changes across the photomask. Overlaid images (right) show the tracing for the intensity measurement (left) in the photopatterned hydrogel (green, gray line) and the photomask (black and clear, black line). Evidence of excess free radical production causing overphotocrosslinking can be seen in these images as the rounded corners in the square pore areas of the photomask. All intensity peaks in the photopatterned hydrogels corresponded to the same peaks in the photomask, however, the slope of the change in intensity is lower in photopatterned hydrogels compared to the photomasks.

5.3.2 Free-form fabrication can be used to produce customized sponges

CMA hydrogels were subject to free-form fabrication to create customized CMA hydrogels (Figure 5.7 A and B). Samples were subsequently lyophilized and rehydrated to determine the spatial resolution of samples subject to post-processing steps, such as those involved in making a collagen “sponge” (Figure 5.7 C and D). Photocrosslinked hydrogels maintained very close pattern fidelity to the photomask, with no statistically significant differences in area (Figure 5.7 E). Edges in the photocrosslinked hydrogel were slightly more rounded when compared to the photomask (Figure 5.7 A and B). Lyophilized and rehydrated scaffolds were easily handled and maintained pattern fidelity, although decreased in area by approximately 20% following processing steps (Figure 5.7 C, D, and E).

These results echoed that this simple free-form fabrication method produces hydrogels with high pattern fidelity, and that hydrogels can be subject to post-processing steps to create collagen ‘sponges’ of customized shapes and sizes. Additionally, while this study used a high-intensity light source for photocrosslinking, it is also possible to use hand-held UV light sources for photocrosslinking larger scale (> 5 mm across) scaffolds, albeit with longer photocrosslinking times (Figure 5.3).

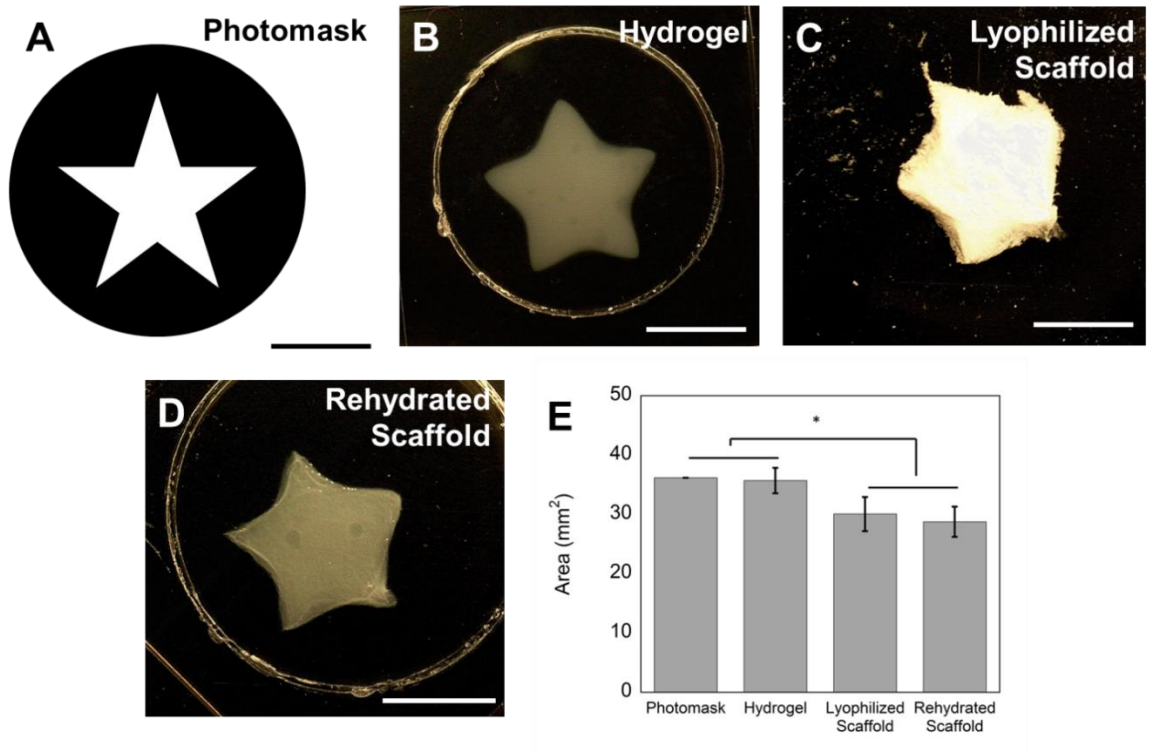

Figure 5.7 Free-Form Fabrication and Spatial Resolution of CMA Hydrogels, Lyophilized Scaffolds, and Rehydrated Scaffolds. A) Photomask used to photopattern macroscale, customized CMA hydrogels. **B)** Representative photopatterned hydrogel exhibited accurate pattern fidelity in comparison to the photomask. **C)** and **D)** CMA hydrogels can be further processed: hydrogels can be frozen and freeze-dried to create sponges and can be rehydrated as sponges and retain pattern fidelity. **E)** The CMA hydrogel had the most accurate pattern fidelity compared to the photomask, whereas the lyophilized and rehydrated scaffolds were statistically smaller in area than the photomask and hydrogel. Scale bar is 5 mm.

5.3.3 Cells remain viable when subject to CMA free-form fabrication

Cells were encapsulated in collagen and CMA scaffolds to evaluate the aspects of free-form fabrication that may affect cell viability. The effects of the photoinitiator, UV treatment, and free radicals on cell viability were each examined. All hydrogels were exposed to cold-temperatures for “cold-melting.” Additionally, all hydrogels contained ascorbic acid, which was added to temper the effect of free radicals on cell viability [196-198]. Reducing free radical concentration with ascorbic acid did not affect pattern fidelity (Figure 5.4).

Cells demonstrated good viability in all collagen and CMA hydrogels after 24 hours in culture (Figure 5.8 A). Collagen hydrogels containing irgacure that were not exposed to UV had the highest viability (~88%) whereas collagen hydrogels containing irgacure and that were exposed to UV had the lowest viability (~75%). Collagen hydrogels containing irgacure had a statistically significant higher proportion of viable cells compared to CMA. This was also seen in collagen and CMA hydrogels without irgacure that were exposed to UV (~81% and ~75% cell viability, respectively) indicating that UV exposure alone induces some cell death. In contrast, collagen and CMA hydrogels containing irgacure that were exposed to UV light were not statistically different, and had the lowest viability overall (~75%). Despite some cell death, a large portion of the cells were viable following all steps of free-form fabrication.

The cell-encapsulated, photopatterned hydrogel experienced some cell-mediated compaction due to the high cell density seen in the corners of the hydrogel after 24 hours compared to initial fabrication (Figure 5.8 B, C, and D).

Overall, cell-encapsulated CMA hydrogels were photopatterned with good resolution, similar to the previous set of photopatterned CMA hydrogels from the sponge spatial resolution study (Figure 5.7 B and 5 B). These data suggest that cells can be subject to free-form fabrication of CMA and maintain viability, and allow for the production of cell-laden, customized hydrogels.

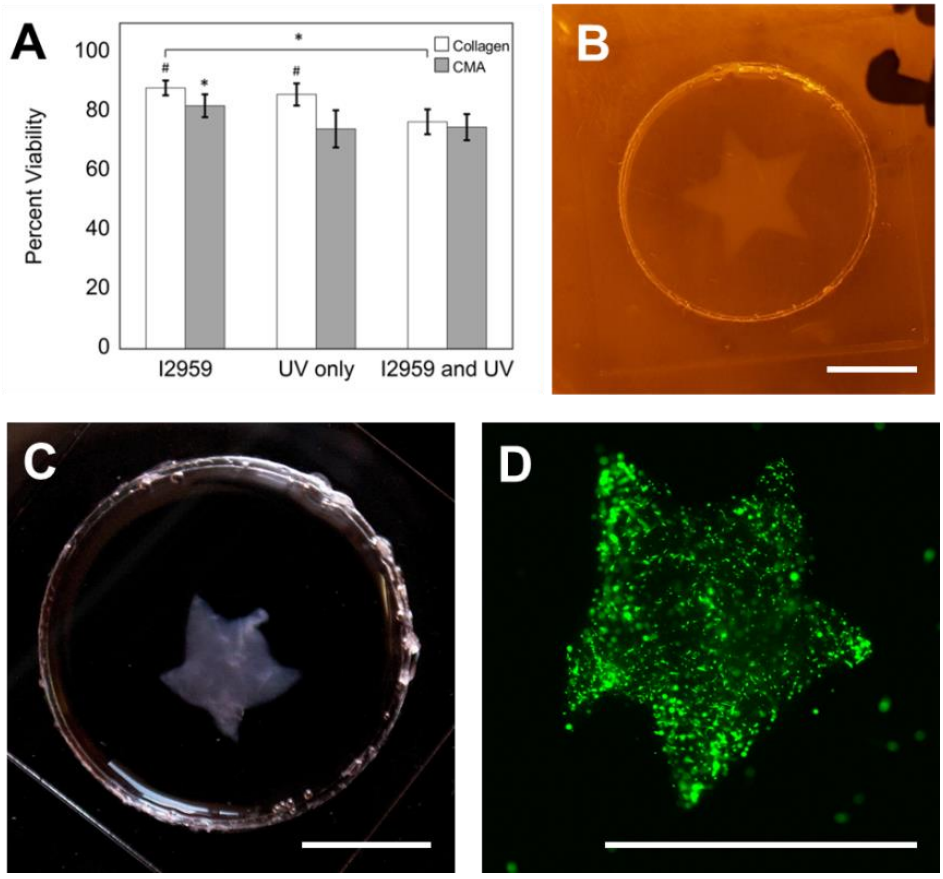

Figure 5.8 Cytotoxicity and Free-Form Fabrication of MSC-Encapsulated Hydrogels. A) Cell viability was maximum in collagen hydrogels containing I2959 (~88%), and lowest in CMA hydrogels with irgacure and exposed to UV (~75%). Percent cell viability decreased in each condition; hydrogels containing irgacure had the highest percent viability, and hydrogels containing irgacure and exposed to UV had the lowest percent viability. These differences were significant when comparing each condition between collagen hydrogels (*); however, CMA hydrogels containing irgacure had a statistically higher percent viability compared to the other CMA conditions (*). Cell viability in collagen hydrogels was statistically higher compared to CMA hydrogels, except for

conditions that contained irgacure and were exposed to UV. **B)** Photopatterned, cell-laden hydrogel immediately after cold-melting. **C)** Photopatterned, cell-laden hydrogel 24 hours after cell culture. **D)** Calcein-AM stained hMSC in photopatterned CMA hydrogel. All photopatterned, cell-laden hydrogels demonstrated good pattern fidelity as seen in the previous figure (Figure 5. 7). Scale bar is 5 mm.

5.3.4 CMA and photocrosslinked CMA are biocompatible

The biological response to CMA hydrogels compared to the response to type-I collagen, which has been used *in vivo* for wound healing for the past 30 years [45]. Macroscopically, no implant sites at either timepoint demonstrated signs of inflammation (data not shown). Sectioning proved difficult for such soft tissue and mechanically week hydrogels even after fixation. In images seen herein, hydrogels are clearly visible for the collagen and photocrosslinked CMA samples, but only a portion of the hydrogel is present for the unphotocrosslinked CMA hydrogel. Histological analysis showed that all implanted hydrogels at the one week timepoint caused an inflammatory response (Figure 5.9). A dense layer of cells can be seen surrounding the scaffold with some signs of infiltration. The inflammatory response at one week was greater in both CMA and photocrosslinked CMA compared to collagen, consistent with a mild reaction to a foreign implant [199]. At six weeks, the hydrogels were almost fully degraded (data not shown). Although sections at this timepoint did not contain the hydrogel, some regions of high cell density were still evident, particularly in the CMA hydrogel conditions. When compared to the one week timepoint, the cell density had subsided some, suggesting a decreased immune response.

Sections were also immunostained at the one week timepoint where scaffolds were more intact and far less degraded. The mouse anti-rat type-I collagen antibody demonstrated non-specificity, and dual-stained both the rat and bovine type-I collagen. Therefore, in the overlaid images, bovine collagen is seen as yellow instead of green. The scaffolds are the farthest layer away from

the epidermis (Figure 5.10). Again, the CMA hydrogel was the smallest due to damage during sectioning. All other regions stained for rat type-I collagen. DAPI staining clearly demonstrated a layer of cells surrounding the scaffold. In all samples, a high concentration of DAPI labeling was also seen in the tissue surrounding the hydrogels, suggestive of the immune response seen in H&E staining. Overall, our study indicates the biocompatibility of unphotocrosslinked and photocrosslinked CMA.

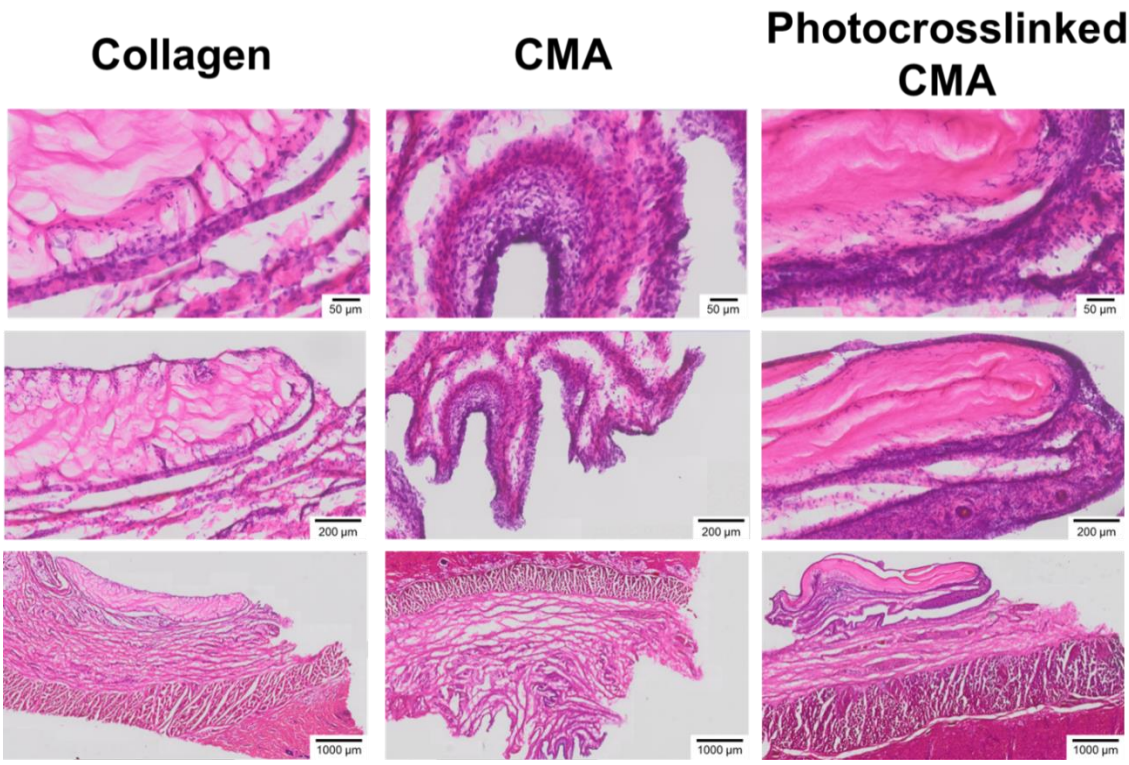

Figure 5.9 Histology of Collagen, CMA, and Photocrosslinked CMA Implants One Week After Subcutaneous Implantation. H&E stained sections at one week of collagen, CMA, and photocrosslinked CMA scaffolds and tissue surrounding the implant site. All samples showed signs of an inflammatory response; the response in the tissue surrounding the collagen implant was more acute compared to that elicited by the CMA and photocrosslinked CMA samples. Cell densities in the CMA and photocrosslinked CMA sections were much higher. Signs of an inflammatory response are seen as cell immigration to the area surrounding the scaffold, with some signs of cell infiltration into the scaffold.

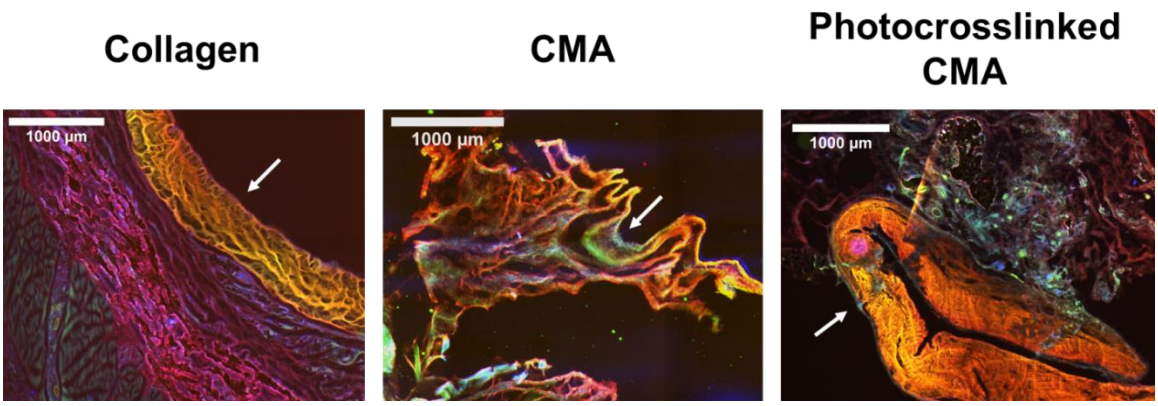

Figure 5.10 Immunostaining of Collagen, CMA, and Photocrosslinked CMA Implants One Week After Subcutaneous Implantation. Immunostaining for rat collagen (red), bovine collagen (yellow), and cell nuclei via DAPI labeling (blue). The rat collagen antibody stained collagen non-specifically; therefore, while bovine collagen should have been labeled green, it is seen as yellow in the overlay. Portions of the collagen and CMA scaffolds were clearly evident in each of the sections (white arrows). DAPI labeling was significant, labeling the immediate area around the scaffold. There was also a high cell density evident in the area surrounding the scaffold, emulating the cell densities seen in H&E staining.

5.4 DISCUSSION

Unlike many other materials used in 3D printing applications that utilize UV photocrosslinking, photocrosslinking is not required for hydrogel formation [28, 29, 65, 200]. Instead, neutralized collagen suspension will form a fibrillar hydrogel at temperatures above ~20 °C that naturally presents the collagen structure and epitopes .Collagen self-assembly introduces problems with many 3D printing approaches, specifically those utilizing nozzle-based 3D printing methods, as collagen can clog the nozzle due to fibril formation when temperature is not properly controlled [186, 195]. The unique properties of CMA allowed for the development of a free-form fabrication method with good pattern fidelity through 1) self-assembly of the CMA hydrogel, 2) photocrosslinking the hydrogel through a photomask, and 3) cooling the hydrogel to cold-melt regions not exposed to UV light. Following wash steps, the customized hydrogel of interest is easily obtained. This entire process can be completed in less than an hour. Cell-laden, photopatterned hydrogels maintain viability through free-form fabrication, or, hydrogels can be further processed into collagen sponges, which are strategies often employed for a variety of applications in tissue engineering.

Although additional steps could be taken to optimize the method to obtain hydrogels or scaffolds with better spatial resolution, it was our goal to demonstrate the potential of CMA for rapid production of macroscale, customized collagen-based scaffolds for tissue engineering rather than micron-feature sized hydrogels. Photopatterned CMA hydrogels could be patterned on the order of ~250 µm; smaller line widths and spacings (0.25 mm and 1.0 mm respectively)

had lower pattern fidelity compared to the largest spacing (2.5 mm). Overphotocrosslinking was observed across most of the conditions, as evidenced by the circularity measurements; this was likely due to excess free radicals diffusing away from areas of light exposure. Larger-scale, photopatterned CMA scaffolds in customized shapes had excellent pattern fidelity when compared to the photomasks. Because we aimed to design an easy method to adapt in any lab for free-form fabrication of a collagen-based material, we optimized our method for speed and simplicity. Photopatterning can be improved a number of ways to potentially generate CMA hydrogels with micron-sized features. For example, in our current set-up, the photoinitiator concentration, light intensity, and exposure time can be further optimized for pattern fidelity rather than speed. Other methods for improving pattern fidelity used in other 3D printing techniques include using a collimated light source, free-radical quenchers, or nitrogen purging [201, 202].

MSC demonstrated good viability following free-form fabrication, and photopatterned cellular hydrogels retained pattern fidelity after 24 hours in culture. Some cell-mediated compaction occurred in these hydrogels, as can be expected with cell populated collagen gels [203-208]. Other cells may not be as tolerable to the free-form fabrication process, particularly due to the UV photocrosslinking, which generates free radicals that can be toxic to cells. While MSC are naturally robust, ascorbic acid was used in this study as a free radical quencher to further prevent cytotoxicity [196-198]. Future research will focus on viability studies following free-form fabrication with alternative cell types. If cell

types are far too susceptible to the toxic environment, it is possible to rinse hydrogels of free radicals following free-form fabrication, and seed cells in 2D. While this study focuses on photocrosslinking methacrylates on CMA to stiffen and prevent thermoreversibility of the hydrogel, it is also possible to couple acrylated bioactive ligands to CMA. Hydrogels can be partially photocrosslinked to prevent thermoreversibility while adding bioactivity, which could be used to promote desired cell infiltration in scenarios where cells are seeded on top of the hydrogel following free-form fabrication.

In a subcutaneous implant model, we demonstrated that CMA, like collagen, is biocompatible. At one week, photocrosslinked and unphotocrosslinked CMA hydrogels elicited a more severe immune response in comparison to collagen; however, the hydrogels were not toxic to the host, which would have caused an extremely severe immune response with much higher cell densities and localized cell death [209]. This was not seen in any of our sections. Further, at six weeks, the immune response was subdued in all cases when comparing the surrounding tissue to that harvested from the one week timepoints.

Customized collagen-based scaffolds have a range of uses throughout tissue engineering, including made-to-order scaffolds for facial implants or the design of scaffolds for wound healing with pre-patterned internal vasculature. This method can produce customized hydrogels within an hour and freeze-dried scaffolds within 24 hours. While this paper has focused on free-form fabrication, the properties of CMA should also allow for modified, layer-by-layer 3D printing,

which has been accomplished with other materials [28, 210]. 3D printing of CMA could be achieved through self-assembly and photocrosslinking the desired structure of interest layer-by-layer. Upon completion, the entire photopatterned hydrogel could be cooled to cold-melt unphotocrosslinked CMA in each layer. Further development of 3D printing methods for CMA could allow for organ printing or complex tissue engineered scaffolds with layer-specific properties.

The free-form fabrication method presented herein is quite simple, and is easy for academic/government institutions, start-ups, or large biotechnology companies to implement. Many other studies of free-form fabrication or 3D printing utilize 3D printers, lasers, or digital projection systems [28, 29, 195, 210]. While the cost of these respective systems has decreased over the years, printing systems often require modifications for use with specific materials [181]. This method requires only CMA, a UV light source, photomasks that can be easily printed using a laser-printer, and incubators and refrigerators. UV light sources or fairly powerful white light sources that usually contain UV are widely available in many laboratories, and are typically used with any imaging technology. The advantages for this method, including its ease of implementation and accurate pattern fidelity, along with its high similarity to type-I collagen are very compelling for further development of CMA in tissue engineering and regenerative medicine.

5.5 CONCLUSION

CMA has unique properties in comparison to type-I collagen that allow for the development of free-form fabrication of 3D printing methodologies to easily

customize scaffolds for regenerative medicine. CMA is photocrosslinkable: in the presence of UV light and a photoinitator, methacrylates present on CMA will photocrosslink, stiffening the material where it is exposed to light. CMA is also thermoreversible, and can reversibly form a fibrillar hydrogel at 37 °C and a liquid suspension at temperatures below 10 °C. Further, photocrosslinking eliminates thermoreversibility. Free-form fabrication of CMA hydrogels is simply conducted as follows: self-assembly of a hydrogel, UV photocrosslinking of the desired geometry of interest, and cold-melting to remove CMA that was not exposed to UV light. This free-form fabrication method allows for the rapid production of macroscale, customized, collagen-based scaffolds for tissue engineering. Hydrogels can be photopatterned with good pattern fidelity on the order of hundreds of microns, and can be further freeze-dried and or rehydrated to create collagen ‘sponges,’ which are widely used throughout tissue engineering. MSC encapsulated hydrogels maintained high viability through free-form fabrication, and were able to be successfully photopatterned with high spatial resolution. Implanted CMA hydrogels were biocompatible in a subcutaneous implant study, however, the immune response to type-I collagen hydrogels was more acute when compared to CMA or photocrosslinked CMA. Overall, the method of free-form fabrication of CMA hydrogels is quite simplistic, merely requiring CMA, a UV light source, and laser-printed photomasks for photopatterning, and can be easily implemented in academic/government institutions and industry alike.

CHAPTER 6. CONCLUSIONS AND FUTURE WORK

6.1 THESIS SUMMARY

Type-I collagen was one of the first materials used for wound healing applications over 20 years ago, and continues to be developed for skin regeneration [40, 45]. Unfortunately, collagen materials are rarely developed for other applications in tissue engineering, as it is often criticized for weak mechanical properties and lack of control over other hydrogel properties. Our lab functionalized the lysines of type-I collagen with methacrylic acid to render collagen photoreactive. This photoreactive collagen, collagen methacrylamide (CMA), had similar properties to type-I collagen including fibril diameter, kinetics of self-assembly, and degradation properties; however, following fibrillogenesis, CMA hydrogels could be photocrosslinked in the presence of UV light to control the spatiotemporal bioactive and mechanical properties [55]. Interestingly, further research and development with CMA also elucidated an additional, unintended property – CMA is themoreversible: it can reversibly self-assemble into a hydrogel and disassembles into a liquid suspension based on temperature. This newly discovered property prompted further research and development in CMA to further understand the extent of thermoreversibility, the aspects of CMA synthesis that promote this temperature-dependent behavior, and the unique applications of thermoreversible, photocrosslinkable collagen in tissue engineering. We also discovered new insights into the process of collagen fibrillogenesis and disassembly.

In Chapter 2, we studied the degree of CMA thermoreversibility, learning that self-assembled CMA hydrogels rapidly disassembled at temperatures below 10 °C and reassembled at 37 °C. This process is repeatedly reversible, resembling a hysteresis of self-assembly and disassembly when CMA hydrogels are subject to heating and cooling temperature cycles. If hydrogels are properly hydrated, CMA can be disassembled even following incubation at 37 °C for 24 hours. Light scattering results demonstrated that self-assembled fibrils did not disassemble into triple helical monomers, which was the initial size of the suspension; although, rheology measurements demonstrated that the disassembled fibrils were small enough that a fibrillar hydrogel was not maintained. This disparity may be of further interest in thermoreversibility studies regarding the disassembly mechanism or its utility. Circular dichroism (CD) spectra through temperature cycling echoed the results obtained through other modalities. Interestingly, the initial positive triple-helical CD spectra of both collagen and CMA transitioned to a strong negative signal at conditions coincident with fibrillogenesis, and disappeared following heat denaturation. This signal was further investigated in a later chapter as a new modality to measure collagen fibrillogenesis. Characterization of this behavior ultimately supported the remaining chapters in understanding aspects of CMA synthesis that contribute to thermoreversible behavior and the development of a method for free-form fabrication of CMA for tissue engineering.

In Chapter 3, we further investigated how methacrylation causes collagen to become thermoreversible. Specific aspects of CMA synthesis were varied,

including the volumetric ratio of crosslinkers/methacrylic acid to collagen, the crosslinkers, and the source of collagen, telo- or atelocollagen. CMA was reversible regardless of the volumetric ratio between the reaction mixture and collagen, although lower ratios did lower the amount of methacrylation and extent of photocrosslinking. The use of two crosslinkers, EDC and NHS, were required to make CMA thermoreversible; using solely EDC to conjugate methacrylic acid to type-I collagen promoted photoreactive properties, but not thermoreversibility. Additionally, organic compounds characterized by low molecular weight and pKa in the range of $4.2 < pKa \leq 4.88$ successfully grafted and made collagen thermoreversible; however, other larger molecules with pKa out of this range did not. Atelocollagen, unlike telocollagen, was naturally thermoreversible; further, methacrylation of atelocollagen resulted in significant modification of the triple-helix (~60%) and atelo-CMA produced similar fold-increases in stiffness following photocrosslinking when compared to CMA produced from telocollagen. Together, these results suggest that the location of coupling to collagen is of utmost importance, and is in part dictated by the properties of the molecule grafted. While this set of studies does not offer a complete story of collagen thermoreversibility, it offers a significant starting point for future areas to explore. For example, experimental studies contributed to the creation of a classifier that can predict if a modified collagen will be thermoreversible based on properties of the molecule to be coupled, namely, molecular weight and/or pKa.

In Chapter 4, the unique CD signal that appeared at conditions consistent with collagen and CMA fibrillogenesis was further explored in comparison to

widely-accepted methodologies used to monitor fibril formation. The collagen triple-helix signal is measured in CD spectroscopy as a positive peak at ~222 nm and a negative peak at ~195 nm. In monitoring the positive mean residue ellipticity (MRE) at 222 nm during a temperature sweep from 4 °C to 60 °C, the MRE of collagen transitioned to a strong, negative signal at temperatures coincident for fibrillogenesis, which disappeared as the proteins denatured through heating. This transition in CD occurred in all conditions that promoted self-assembly, regardless of species and in the presence or absence of telopeptides, and was highly specific to ordered, type-I collagen fibrils. The signal of the collagen fibril is a spectrum with a strong negative peak at ~204 nm. Computational analysis of the three states of collagen – triple-helix, fibril, and denatured – validated that the temperature-dependent CD of collagen fibrillogenesis was comprised of these three signals. While the exact cause of the negative MRE signal is unknown, it is likely due to exciton interactions between collagen triple-helices when fibrils are formed. Regardless, this unique transition indicative of collagen fibrillogenesis allows for CD spectroscopy to be utilized in monitoring multiple states of collagen structure, and as proof-of-concept, it was successfully used to monitor the digestion of collagen fibrils.

In Chapter 5, one application of a photocrosslinkable, thermoreversible collagen was investigated. Because photocrosslinking eliminates thermoreversibility, we were able to devise a method that allowed for a unique, rapid method of free-form fabrication of collagen hydrogels; such hydrogels could be fabricated to create customized geometries with proper fibrillar structure that

previously required the production of customized molds for each personalized use, or, 3D printing methods that usually alter the ordered fibril structure. Free-form fabrication of CMA hydrogels proceeded as 1) fibrillogenesis, 2) photocrosslinking of the desired shape of interest, and 3) cold-melting of the hydrogel to disassemble regions unexposed to light to obtain the final customized geometry. This method printed hydrogels on the order of 250 µm in resolution, and resulted in some overphotocrosslinking seen as sharp edges becoming round likely due to free radical diffusion into areas that were not exposed to light. Photopatterned hydrogels can be subsequently frozen and lyophilized and/or rehydrated while retaining pattern fidelity, which allows for the creation of customized collagen-based sponges, often used in wound healing applications. Cells can be encapsulated in CMA hydrogels, and cells and hydrogels maintain high viability and pattern fidelity, respectively, through free-form fabrication. CMA and photocrosslinked CMA hydrogels were found to be biocompatible in a subcutaneous implant study in comparison to collagen hydrogels. Many methods exist that allow for 3D printing on the order of hundreds of microns in resolution, however, with the cost burden of purchasing 3D printers and subsequent modification to 3D print the material of interest. Free-form fabrication of CMA is quite simple for academic and government research laboratories and/or biotechnology companies to implement. Hydrogels and/or scaffolds for tissue engineering can be photopatterned on the order of ~250 µm, and the materials required, which include, CMA, UV light, and laser-printed photomasks, are easily purchased and/or are likely already available in the lab.

6.2 AREAS OF FUTURE IMPACT AND RESEARCH

The characterization and continued development of CMA will have major impacts on both basic research on type-I collagen structure and fibrillogenesis as well as in translational research. Studies on the basic structure and higher order self-assembly of modified collagens and CMA also contribute to an improved understanding of misfolding and/or possible disordered fibrillogenesis of type-I collagen in diseases such as Osteogenesis imperfecta. Additionally, the applications of collagen in tissue engineering are broad and continue to expand, especially with the added properties of modified collagens discussed herein. A few areas of immediate and future research are discussed in the context of basic research on type-I collagen structure and reversible self-assembly, and translational research utilizing CMA for tissue engineering.

6.2.1 Basic research: Collagen structure and thermoreversibility

6.2.1.1 Studies of the interactions in collagen fibrils through circular dichroism

Collagen mimetic peptides could be used to further investigate sequence-specific interactions that cause the collagen fibril signal in CD measurements. These peptides must not only self-assemble into the collagen triple-helix, but into higher-order fibrils or aggregates of triple-helices. Even if the peptides do not form proper D-banded fibrils, interactions that promote both higher order structure formation in peptide systems and collagen fibrils may elicit similar CD

profiles. Research in a few labs has focused on studying a few collagen mimetic peptide systems with different mechanisms of self-assembly [211, 212].

The Brodsky group has found that triple-helical $(Pro\text{-}Hyp\text{-}Gly)_{10}$ self-assembles into branched, filamentous aggregates at neutral pH and warm temperatures ~50 °C [211]. Self-assembly proceeded similar to type-I collagen in terms of nucleation or lag phase, followed by rapid fibril growth and stabilization [211]. The group hypothesized that self-association proceeds as follows: the hydrated $(Pro\text{-}Hyp\text{-}Gly)_{10}$ triple-helix forms a loosened intermediate in response to the temperature increase [211]. This intermediate can either unfold, or self-associate, where self-association would reorder the hydration structure and assist in fibril formation [211].

The Xu team expressed a portion of collagen sequence in *E. coli,* dubbed Col108; this is a recombinant collagen is comprised of a non-interrupted Gly-X-Y repeating sequence of a total of 378 residues [212]. Col108 forms a triple-helix, and further self-associates at physiological conditions to form fibrils, with dark bands ~ 25 nm in width and light bands of ~ 10 nm in width [212]. Self-association occurs via one-sequence unit staggering between triple-helices, which optimally arrange due to hydrophobic and charged interactions between adjacent chains [212].

These two collagen peptide systems are capable of higher order structure formation and may provide useful insight to the types of interactions that promote self-assembly, and therefore the unique collagen fibril CD profile. It is also

possible that these systems could be modified and may retain the ability to form triple-helices and fibrils, where collagen structures can be monitored using CD to measure specific changes in molecular associations. If existing systems do not contribute to studying this phenomenon, it may be a starting point for designing a library of collagen mimetic peptides for which the mechanism of self-association can be specified in the peptide design. These peptide systems are of great use in understanding collagen triple-helix folding, with the potential for further investigation in studying the interactions that dictate higher order structure formation.

6.2.1.2 Studying the molecular basis of collagen thermoreversibility

Work conducted in this thesis has demonstrated thermoreversibility is not specific to CMA, and that multiple molecules with properties similar to methacrylic acid can evoke the same property when conjugated to type-I collagen. Atelocollagen, methacrylated or not, was also thermoreversible, potentially supporting that modifications may affect the non-triple-helical telopeptide region. Investigation of the specifics of CMA synthesis showed that CMA was thermoreversible only when methacrylic acid was coupled with EDC and NHS at many of the volumetric ratios (reaction mixture: collagen) tested and not EDC alone. There are a variety of avenues to explore in this area to further study collagen thermoreversibility.

Mass spectrometry can be used to determine the exact amount of collagen that is modified in producing CMA or other modified collagens, and

where those modifications occur. Specifically, we believe that mass spectrometry of collagen, CMA (EDC/NHS), and CMA (EDC) samples would elucidate if the fluorescamine assay is a reliable estimate of functionalization. It would also provide specific information regarding methacrylation site differences between CMA prepared with EDC or EDC/NHS that may contribute to the cause of thermoreversibility. Once a protocol for mass spectrometry is identified, future studies could focus on other modifications, such as a subset of those that did or did not evoke collagen thermoreversibility, or differences in methacrylation between CMA and atelo-CMA to evaluate similarities in modification site locations. Preliminary studies are ongoing in performing mass spectrometry on collagen and CMA samples, however, the high sequence similarity in collagen and number of post-translational modifications complicate efforts [213].

The collective data from both the biochemical properties of molecules and/or experimental data obtained from the modified collagens were used to create a decision tree for further predictions of modifications that could make collagen thermoreversible. With an initial dataset, it is possible to conduct computational studies of fibril destabilization. A coarse-grain model would be less computationally heavy for this analysis, where a modified collagen fibril could be subject to temperature changes as local perturbations in the fibril structure were analyzed. Some coarse-grain models, where many amino acids are represented as ‘one’ particle, retain information specific to the amino acid sidechains, which has been produced for collagen molecules [214, 215]. If modification sites are unknown, multiple simulations could help to determine the most likely

modification sites that dictate thermoreversibility. Information from mass spectrometry could give insight into areas of the collagen fibril to modify. Once initial studies of fibril destabilization of CMA or other modified thermoreversible collagens are mapped, it would be possible to modify the collagen fibril with new molecules that have not been tested to build the library, followed by experimental validation. Overall, both experimental and computational approaches outlined would contribute to the discovery of other modified collagens that are thermoreversible or with additional properties for applications in tissue engineering.

6.2.2 Translational research: Applications of CMA

6.2.2.1 CMA as a thermoreversible hydrogel for temporary cell encapsulation

One application of thermoreversible polymers is its use as a temporary substrate for cell culture prior to transplantation. These polymers could offer mechanical properties similar to the native tissue of the cell-type, and because it is thermoreversible, cells could be recovered without the use of enzymes for cellular detachment. A caveat of most previously identified polymers is that cells can easily be recovered because cells do not attach to the polymer and maintain a rounded morphology in culture [129]. In comparison, CMA offers a unique advantage as a thermoreversible hydrogel because it is collagen-based and supports cell attachment. However, preliminary studies have shown that CMA hydrogels are no longer reversible one day following cell encapsulation, likely due to the high density of the cells (> 10^5/mL) and/or the cells' tendency to compact the hydrogel. While the CMA concentration can be increased to

circumvent compaction, it is possible that higher concentration hydrogels would disassemble quite slowly. Future studies varying cell concentration, cell type, and CMA concentration will be needed to develop a protocol for encapsulation and recovery of cells.

6.2.2.2 3D printing CMA

This thesis focused on devising a method for free-form fabrication of CMA for macroscale, customized scaffolds to demonstrate the ease of implementation and as proof-of-concept that CMA is amenable to rapid prototyping strategies. There are, however, numerous strategies that can be adopted for 3D printing CMA, such as droplet-based bioprinting, two-photon polymerization, or digital light projection techniques that have specific advantages for different applications in tissue engineering and regenerative medicine.

Droplet-based bioprinting has roots in inkjet printing, invented in the 1950s [216]. It was first thought to be used to print biologic tissues when the inkjet printer was modified to print a solution of collagen and fibronectin in the late 1980s [217]. There are many modes of use for inkjet bioprinting, but simply put, an inkjet printer can physically manipulate a bioink solution to form droplets in a specific location on a substrate [186]. Further manipulation of the instrument and set-up would be required to print CMA. For example, the instrument would be highly controlled for temperature with the nozzle held at 4 °C and the substrate at 37 °C to prevent and promote fibrillogenesis, respectively. In this approach, photocrosslinking may not be necessary except to increase the stiffness of the

final construct. Resolution of droplet-based bioprinting may be on the order of hundreds of microns, but is highly dependent on the nozzle size and bioink because the ink can spread across the substrate [65, 218]. A high concentration of CMA is likely necessary in order to increase bioink viscosity to prevent spreading of the CMA on the substrate. While tissues can be printed through this mechanism layer-by-layer, there are also applications in high-throughput drug screening and/or cell microenvironment design, such as mimicking the tumor microenvironment [186].

Two-photon polymerization microfabrication (TPPM) is the most developed method of 3D printing using two-photon absorption (TPA) [219]. Briefly, the method of TPA relies on a high intensity laser that causes one molecule to simultaneously absorb two photons and reach the excited state from the ground state [219]. In the presence of a photoinitiator specific to the lasers used, TPA has been used to photocrosslink acrylated bioactive ligands to photoreactive polymers, such as poly(ethylene) glycol diacrylate (PEGDA) [29]. This method has the highest resolution of any other method described herein, with resolution below 1 μm due to the high focus of the laser beam [219]. For CMA, self-assembled hydrogels could be subject to TPA for photocrosslinking to photopattern durotactic or haptotactic cues in 2D or 3D with high pattern fidelity. Due to the tight focus of the beam and therefore highly localized changes in hydrogel properties, this method is of great use in high-throughput design of cell microenvironments for drug screening. When tissue engineering advances to the point of restoring organs with fully man-made tissue equivalents, TPPM will be of

great use to create vasculature in tissue or define neural pathways, which require micron-level resolution.

Digital light projection (DLP) strategies utilize a light source and a digital micromirror device (DMD). In this case, a DMD is utilized as an “unlimited” source of photomasks. The DMD is composed of thousands of mirrors that are rotated electronically to reflect light toward the sample or away from it [28]. This results in light exposure that will react with the photointiator to generate free radicals, which mediates photocrosslinking of a sample in a particular pattern. These patterns can be programmed using software and loaded onto the DMD. Collimated light would project from the light source onto the DMD, and only light reflected due to the uploaded pattern will be focused onto the sample. This method can be implemented in 3D if biomaterials are photocrosslinked layer-by-layer, where an adjustable stage is lowered each layer to maintain the focus in the plane to be photocrosslinked. This method is not very difficult to implement, though is somewhat costly (~$5,000 for DMD and high intensity UV light source). Materials such as PEGDA and methacrylated gelatin been used recently in DLP strategies to produce photopatterned, customized tissue equivalents; hydrogels have been printed on the order of hundreds of microns in resolution [28, 220]. This set-up, very similar to free-form fabrication, is currently being evaluated to 3D print CMA through layer-by-layer self-assembly and photocrosslinking in the shape of interest. After the entire 3D structure is created, the hydrogel can be cold-melted to disassemble CMA that was not exposed to light. Currently, hydrogels of approximately ~5 mm in size can be photocrosslinked in 5 seconds

with a high intensity UV light source. Future studies will focus on optimizing resolution of photocrosslinking and layer-by-layer scaffold fabrication.

Though these strategies hold promise for rapid prototyping of CMA in a broad range of applications, there are potential difficulties in using CMA for each of these approaches that need to be taken into consideration. In droplet-based bioprinting, it is common that bioinks will clog the nozzle [186]. This is likely to occur with CMA, a collagen-based material that would require a very high concentration and therefore viscosity to result in biomaterials with mechanical properties on the order of tissue stiffness. TPA may be difficult to implement, as it is likely that the density of collagen fibers could interfere with photocrosslinking, especially with thick samples. Bovine corneas, composed primarily of type-I collagen have been UV photocrosslinked successfully using UV light, but sections had a thickness of approximately 50 μm [221]. It would be easy to create photopatterned CMA coated plates for drug screening, but improvements would be required to rapidly crosslink thicker hydrogels with accuracy. The main limitation of 3D printing via DLP is that layer-by-layer self-assembly of CMA hydrogels can be quite slow, on the order of 30 minutes per layer. Pre-warming the hydrogel solution or increasing CMA concentration may improve the speed of self-assembly to decrease printing times.

6.2.2.3 Functionalization of CMA for tissue engineering

Many of the studies in our lab have utilized the photoreactive properties of CMA to control the mechanical properties of hydrogels or scaffolds. Free-form

fabrication of customized hydrogels requires photocrosslinking of CMA to eliminate thermoreversibility. Sponges were fabricated from CMA and further examined for their ability to be photocrosslinked post-lyophilization to increase mechanical properties [68]. This would circumvent a common issue with sponges, which is that sponges are easily damaged when sutured to a patient; this could be addressed using CMA because the sponge could be photocrosslinked in regions to be sutured for additional mechanical strength.

However, it is also possible to couple methacrylated bioactive ligands to CMA through photocrosslinking [55]. Some studies have aimed to promote sensory neuron outgrowth or neurite count in areas where neurogenic bioactive ligands were conjugated to CMA [67]. Studies had limited success in this area, mostly due to solubility issues with peptides, especially when peptides were methacrylated.

Ongoing studies in our lab have shown that similar to fully photocrosslinked CMA, which is not reversible, photocrosslinking of acrylated molecules to CMA also prevents thermoreversibility. Therefore, in free-form fabrication applications, customized hydrogels or scaffolds can be photopatterned with bioactive and mechanical cues while maintaining pattern fidelity. This has a number of applications in customized scaffold development for regenerative medicine. For example, tissue engineered scaffolds for wound healing are not often pre-vascularized, and even if vascularization was successful, scaffolds are often limited in their ability to promote angiogenesis once implanted [222]. CMA can be photopatterned to be devoid of a vasculature

tree, mimicking the tissue structure; area lining the trees can be further functionalized to contain angiogenic factors to promote vascularization [181].

Peripheral nerve regeneration and the haptotactic and durotactic cues that promote and/or guide neurite outgrowth have been major areas of research in our lab [56, 57, 83, 108]. These studies have shown that sensory neurite outgrowth is biased down a gradient of stiffness rather than up in gradients of mechanical stiffness generated by genipin-mediated crosslinking of type-I collagen [57]. Similar studies showed increased neurite outgrowth up steep gradients of YIGSR and up shallow gradients of IKVAV, which are two bioactive fragments of the laminin sequence that were conjugated to collagen [83]. In these approaches, bioactive or mechanical properties were patterned one-dimensionally, whereas CMA offers the ability to combine these approaches to photopattern haptotactic and/or durotactic cues in 2D or 3D [57, 83]. Photopatterned CMA hydrogels can be used as nerve guidance conduit fillers or as customized biomaterial implants. In addition to the examples discussed herein, there are many avenues that warrant exploration for continued development and functionalization of CMA hydrogels.

There are some limitations that need to be addressed in continued development of CMA for tissue engineering. As previously mentioned, there have been issues in solubilizing methacrylated molecules and/or peptides [67]. While studies in the lab continue to use methacrylated peptides, these attempts resulted in partial solubility of the peptide, which decreases the likelihood that the

bioactivity will have any effect in cell culture. Further studies should focus on peptide solubility for continued work in biomaterials.

Free-form fabrication studies were conducted at low CMA hydrogel concentrations (2.5 mg/mL) for proof-of-concept. Collagen concentrations for wound healing applications are often rather high, reaching concentrations as high as 20 mg/mL. Additionally, the initial subcutaneous implant study demonstrated preliminary biocompatibility of CMA. Future studies that focus on a particular indication should further evaluate CMA concentration and biocompatibility for continued use of CMA in tissue engineering.

Overall, CMA is a novel collagen-based biomaterial that has been utilized in this dissertation to evaluate collagen self-assembly and disassembly, collagen higher order structure, methods for free-form fabrication in tissue engineering. Its interesting properties and utility throughout medicine are obvious, and future research on CMA and collagen modifications will contribute to a variety of fields across biomedical research including biochemistry, bioinformatics, materials science, and tissue engineering.

BIBLIOGRAPHY

1. America, D.L. Organ, Eye and Tissue Donation Statistics. 2016; Available from: https://www.donatelife.net/statistics/.
2. Zhu, J. and R.E. Marchant, Design properties of hydrogel tissue-engineering scaffolds. Expert Rev Med Devices, 2011. 8(5): p. 607-26.
3. Guvendiren, M., et al., Designing Biomaterials for 3D Printing. ACS Biomaterials Science & Engineering, 2016.
4. Bajaj, P., et al., 3D biofabrication strategies for tissue engineering and regenerative medicine. Annu Rev Biomed Eng, 2014. 16: p. 247-76.
5. Yang, S., et al., The Design of Scaffolds for Use in Tissue Engineering. Part I. Traditional Factors. Tissue Engineering, 2001. 7(6): p. 679-689.
6. Drury, J.L. and D.J. Mooney, Hydrogels for tissue engineering: scaffold design variables and applications. Biomaterials, 2003. 24(24): p. 4337-4351.
7. Ahmed, E.M., Hydrogel: Preparation, characterization, and applications: A review. J Adv Res, 2015. 6(2): p. 105-21.
8. Ullah, F., et al., Classification, processing and application of hydrogels: A review. Mater Sci Eng C Mater Biol Appl, 2015. 57: p. 414-33.
9. Zhu, J., Bioactive modification of poly(ethylene glycol) hydrogels for tissue engineering. Biomaterials, 2010. 31(17): p. 4639-56.
10. Galperin, A., T.J. Long, and B.D. Ratner, Degradable, Thermo-Sensitive Poly(N-isopropylacrylamide)-Based Scaffolds with Controlled Porosity for Tissue Engineering Applications. Biomacromolecules, 2010. 11: p. 2583-2592.
11. Contreras-Caceres, R., et al., Effect of the cross-linking density on the thermoresponsive behavior of hollow PNIPAM microgels. Langmuir, 2015. 31(3): p. 1142-9.
12. Nash, M.E., et al., Cell and cell sheet recovery from pNIPAm coatings; motivation and history to present day approaches. Journal of Materials Chemistry, 2012. 22(37): p. 19376.
13. Kumashiro, Y., et al., Modulatory Factors on Temperature-Synchronized Degradation of Dextran Grafted with Thermoresponsive Polymers and Their Hydrogels. Biomacromolecules, 2001. 2: p. 874-879.
14. Kim, S., et al., Synthetic MMP-13 degradable ECMs based on poly(N-isopropylacrylamide-co-acrylic acid) semi-interpenetrating polymer networks. I. Degradation and cell migration. J Biomed Mater Res A, 2005. 75(1): p. 73-88.
15. Mura, S., J. Nicolas, and P. Couvreur, Stimuli-responsive nanocarriers for drug delivery. Nature Materials, 2013. 12: p. 991-1003.
16. Pitto-Barry, A. and N.P.E. Barry, Pluronic® block-copolymers in medicine: from chemical and biological versatility to rationalisation and clinical advances. Polym. Chem., 2014. 5(10): p. 3291-3297.
17. Batrakova, E.V. and A.V. Kabanov, Pluronic block copolymers: evolution of drug delivery concept from inert nanocarriers to biological response modifiers. J Control Release, 2008. 130(2): p. 98-106.

18. Zhu, W., et al., Preparation of a thermosensitive and biodegradable microgel via polymerization of macromonomers based on diacrylated Pluronic/oligoester copolymers. European Polymer Journal, 2005. 41(9): p. 2161-2170.
19. Mata, J.P., et al., Concentration, temperature, and salt-induced micellization of a triblock copolymer Pluronic L64 in aqueous media. J Colloid Interface Sci, 2005. 292(2): p. 548-56.
20. Li, L., et al., Thermoreversible micellization and gelation of a blend of pluronic polymers. Polymer, 2008. 49(7): p. 1952-1960.
21. Al Khateb, K., et al., In situ gelling systems based on Pluronic F127/Pluronic F68 formulations for ocular drug delivery. Int J Pharm, 2016. 502(1-2): p. 70-9.
22. Peppas, N.A., et al., Poly(ethylene glycol)-containing hydrogels in drug delivery. Journal of Controlled Release, 1999. 62: p. 81-87.
23. Metters, A. and J. Hubbell, Network Formation and Degradation Behavior of Hydrogels Formed by Michael-Type Addition Reactions. Biomacromolecules, 2005. 6: p. 290-301.
24. Elisseeff, J., et al., Transdermal photopolymerization for minimally invasive implantation. PNAS, 1999. 86: p. 3104-3107.
25. Beamish, J.A., et al., The effects of monoacrylated poly(ethylene glycol) on the properties of poly(ethylene glycol) diacrylate hydrogels used for tissue engineering. J Biomed Mater Res A, 2010. 92(2): p. 441-50.
26. Bakaic, E., N.M.B. Smeets, and T. Hoare, Injectable hydrogels based on poly(ethylene glycol) and derivatives as functional biomaterials. RSC Advances, 2015. 5: p. 35469-35486.
27. Ye, Z.Y. and J. Elisseeff, Engineering Peptides in Hydrogels for Cartilage Tissue Regeneration, in Biologically-Responsive Hybrid Biomaterials, E. Jabbari and A. Khademhosseini, Editors. 2010, World Scientific. p. 311-345.
28. Han, L.H., et al., Fabrication of three-dimensional scaffolds for heterogeneous tissue engineering. Biomed Microdevices, 2010. 12(4): p. 721-5.
29. Hahn, M.S., J.S. Miller, and J.L. West, Three-Dimensional Biochemical and Biomechanical Patterning of Hydrogels for Guiding Cell Behavior. Advanced Materials, 2006. 18(20): p. 2679-2684.
30. Varghese, S. and J.H. Elisseeff, Hydrogels for Musculoskeletal Tissue Engineering. 2006. 203: p. 95-144.
31. Chia, H.N. and B.M. Wu, High-resolution direct 3D printed PLGA scaffolds: print and shrink. Biofabrication, 2015. 7(1): p. 015002.
32. Chu, C., et al., Articular cartilage repair using allogeneic perichondrocyte seeded biodegradable porous polylactic acid (PLA): A tissue-engineering study*. J Biomed Mater Res, 1995. 29: p. 1147-1154.
33. Xu, H., et al., Rapid prototyped PGA/PLA scaffolds in the reconstruction of mandibular condyle bone defects. Int J Med Robot, 2010. 6(1): p. 66-72.

34. Salerno, A., et al., Bio-safe fabrication of PLA scaffolds for bone tissue engineering by combining phase separation, porogen leaching and scCO2 drying. The Journal of Supercritical Fluids, 2015. 97: p. 238-246.
35. Elisseeff, J., et al., Controlled-release of IGF-I and TGF-P 1 in a photopolymerizing hydrogel for cartilage tissue engineering. Journal of Orthapedic Research, 2001. 19: p. 1098-1104.
36. Clapper, J.D., et al., Development and characterization of photopolymerizable biodegradable materials from PEG–PLA–PEG block macromonomers. Polymer, 2007. 48(22): p. 6554-6564.
37. Kim, J., M.J. Yaszemski, and L. Lu, Development of biodegradable and injectable macromers based on poly(ethylene glycol) and diacid monomers. J Biomed Mater Res A, 2009. 90(4): p. 1010-20.
38. Bostmon, O., Current Concepts Review: Absorbable Implants for the Fixation of Fractures. JBJS, 1990. 73A(1): p. 148-153.
39. Ricard-Blum, S., The collagen family. Cold Spring Harb Perspect Biol, 2011. 3(1): p. a004978.
40. Abou Neel, E.A., et al., Collagen--emerging collagen based therapies hit the patient. Adv Drug Deliv Rev, 2013. 65(4): p. 429-56.
41. Christiansen, D.L., E.K. Huang, and F.H. Silver, Assembly of type I collagen: fusion of fibril subunits and the influence of fibril diameter on mechanical properties. Matrix Biology, 2000. 19: p. 409-420.
42. Harris, J.R., A. Soliakov, and R.J. Lewis, In vitro fibrillogenesis of collagen type I in varying ionic and pH conditions. Micron, 2013. 49: p. 60-8.
43. Gross, J. and D. Kirk, The Heat Precipitation of Collagen from Neutral Salt Solutions: Some Rate-Regulating Factors*. Journal of Biological Chemistry, 1958. 233(2): p. 355-360.
44. Sundararaghavan, H.G., et al., Genipin-induced changes in collagen gels: correlation of mechanical properties to fluorescence. J Biomed Mater Res A, 2008. 87(2): p. 308-20.
45. Burke, J.F., et al., Successful Use of a Physiologically Acceptable Artificial Skin in the Treatment of Extensive Burn Injury. Annals of Surgery, 1981. 194(4): p. 413-428.
46. Caruso, A.B. and M.G. Dunn, Changes in mechanical properties and cellularity during long-term culture of collagen fiber ACL reconstruction scaffolds. J Biomed Mater Res A, 2005. 73(4): p. 388-97.
47. Nam, K., T. Kimura, and A. Kishida, Controlling coupling reaction of EDC and NHS for preparation of collagen gels using ethanol/water co-solvents. Macromol Biosci, 2008. 8(1): p. 32-7.
48. Cornwell, K.G., et al., Crosslinking of discrete self-assembled collagen threads: Effects on mechanical strength and cell-matrix interactions. J Biomed Mater Res A, 2007. 80(2): p. 362-71.
49. Buttafoco, L., et al., Electrospinning of collagen and elastin for tissue engineering applications. Biomaterials, 2006. 27(5): p. 724-34.
50. Davidenko, N., et al., Optimisation of UV irradiation as a binding site conserving method for crosslinking collagen-based scaffolds. J Mater Sci Mater Med, 2016. 27(1): p. 14.

51. Weadock, K.S., et al., Physical crosslinking of collagen fibers: Comparison of ultraviolet irradiation and dehydrothermal treatment. J. Biomed. Mater. Res., 1995. 29: p. 1373-1379.
52. Vyas, K.S. and H.C. Vasconez, Wound Healing: Biologics, Skin Substitutes, Biomembranes and Scaffolds. Healthcare (Basel), 2014. 2(3): p. 356-400.
53. Cheung, H.-Y., et al., A critical review on polymer-based bio-engineered materials for scaffold development. Composites Part B: Engineering, 2007. 38(3): p. 291-300.
54. Parenteau-Bareil, R., R. Gauvin, and F. Berthod, Collagen-Based Biomaterials for Tissue Engineering Applications. Materials, 2010. 3(3): p. 1863-1887.
55. Gaudet, I.D. and D.I. Shreiber, Characterization of methacrylated type-I collagen as a dynamic, photoactive hydrogel. Biointerphases, 2012. 7(1-4): p. 25.
56. Masand, S.N., et al., Neural cell type-specific responses to glycomimetic functionalized collagen. Biomaterials, 2012. 33(3): p. 790-7.
57. Sundararaghavan, H.G., et al., Neurite growth in 3D collagen gels with gradients of mechanical properties. Biotechnol Bioeng, 2009. 102(2): p. 632-43.
58. Monteiro, G.A., et al., Positively and Negatively Modulating Cell Adhesion to Type I Collagen Via Peptide Grafting. Tissue Eng Part A, 2011. 17(13 and 14): p. 1663-1673.
59. Hoque, M.E., et al., Gelatin Based Scaffolds for Tissue Engineering - A Review. Polymers Research Journal, 2015. 9(1): p. 15-32.
60. Glowacki, J. and S. Mizuno, Collagen scaffolds for tissue engineering. Biopolymers, 2008. 89(5): p. 338-44.
61. Tan, H. and K.G. Marra, Injectable, Biodegradable Hydrogels for Tissue Engineering Applications. Materials, 2010. 3(3): p. 1746-1767.
62. Gorgieva, S. and V. Kokol, Collagen- vs. Gelatine-Based Biomaterials and Their Biocompatibility: Review and Perspectives, in Biomaterials Applications for Nanomedicine, R. Pignatello, Editor 2011, InTech.
63. Hayashi, A. and S. Oh, Gelation of Gelatin Solution. Agric. Biol. Chem., 1983. 47(8): p. 1711-1716.
64. Yue, K., et al., Synthesis, properties, and biomedical applications of gelatin methacryloyl (GelMA) hydrogels. Biomaterials, 2015. 73: p. 254-71.
65. Bertassoni, L.E., et al., Direct-write bioprinting of cell-laden methacrylated gelatin hydrogels. Biofabrication, 2014. 6(2): p. 024105.
66. Brinkman, W.T., et al., Photo-Cross-Linking of Type I Collagen Gels in the Presence of Smooth Muscle Cells: Mechanical Properties, Cell Viability, and Function. Biomacromolecules, 2003. 4: p. 890-895.
67. Gaudet, I.D., DEVELOPMENT, CHARACTERIZATION, AND APPLICATIONS OF SELF-ASSEMBLING, PHOTOCROSSLINKABLE COLLAGEN-BASED HYDROGELS, in Biomedical Engineering2012, Rutgers, The State University of New Jersey: New Brunswick, NJ. p. 310.

68. Branch, J.R., SYNTHESIS AND CHARACTERIZATION OF COLLAGEN METHACRYLAMIDE SPONGES FOR USE AS A BIOLOGICAL SCAFFOLD, in Biomedical Engineering2012, Rutgers, The State University of New Jersey: New Brunswick, NJ. p. 120.
69. Klouda, L. and A.G. Mikos, Thermoresponsive hydrogels in biomedical applications. Eur J Pharm Biopharm, 2008. 68(1): p. 34-45.
70. Billiet, T., et al., A review of trends and limitations in hydrogel-rapid prototyping for tissue engineering. Biomaterials, 2012. 33(26): p. 6020-41.
71. Jeong, B., S.W. Kim, and Y.H. Bae, Thermosensitive sol–gel reversible hydrogels. Adv Drug Deliv Rev, 2002. 54: p. 37-51.
72. Shoulders, M.D. and R.T. Raines, Collagen structure and stability. Annu Rev Biochem, 2009. 78: p. 929-58.
73. Silver, F.H., J.W. Freeman, and G.P. Seehra, Collagen self-assembly and the development of tendon mechanical properties. J Biomech, 2003. 36(10): p. 1529-1553.
74. Lee, C.H., A. Singla, and Y. Lee, Biomedical applications of collagen. International Journal of Pharmaceutics, 2001. 221: p. 1-22.
75. Kadler, K.E., et al., Collagen Fibril Formation. Biochem. J., 1996. 316: p. 1-11.
76. Danielsen, C., Mechanical Properties of Reconstituted Collagen Fibrils. Connective Tissue Research, 1981. 9: p. 51-57.
77. Engler, A.J., et al., Matrix elasticity directs stem cell lineage specification. Cell, 2006. 126(4): p. 677-89.
78. Burdick, J.A. and G. Vunjak-Novakovic, Engineered Microenvironments for Controlled Stem Cell Differentiation. Tissue Eng Part A, 2009. 15(2): p. 205-219.
79. Schoof, H., et al., Control of Pore structure and size in freeze-dried collagen sponges. J Biomed Mater Res. , 2001. 58(4): p. 352-357.
80. Chvapil, M., Collagen Sponges: Theory and Practice of Medical Applications. J. Biomed. Mater. Res., 1977. 11: p. 721-741.
81. Leikina, E., et al., Type I collagen is thermally unstable at body temperature. Proc Natl Acad Sci U S A, 2002. 99(3): p. 1314-8.
82. Persikov, A.V., et al., Electrostatic Interactions Involving Lysine Make Major Contributions to Collagen Triple-Helix Stability. Biochemistry, 2005. 44: p. 1414-1422.
83. Sundararaghavan, H.G., S.N. Masand, and D.I. Shreiber, Microfluidic generation of haptotactic gradients through 3D collagen gels for enhanced neurite growth. J Neurotrauma, 2011. 28(11): p. 2377-87.
84. Monteiro, G.A., et al., Positively and Negatively Modulation Cell Adhesion to Type I Collagen Via Peptide Grafting. Tissue Eng Part A, 2011. 17(13 and 14): p. 1663-1673.
85. Tronci, G., S.J. Russell, and D.J. Wood, Photo-active collagen systems with controlled triple helix architecture. Journal of Materials Chemistry B, 2013. 1(30): p. 3705.

86. Gathercole, L.J. and A. Keller, X-ray Diffraction Effects Related to Superstructure in Rat Tail Tendon Collagen. Biochimica et Biophysica Acta (BBA) - Protein Structure, 1978. 535(2): p. 253-271.
87. Brodsky B, et al., Low Angle X-ray Diffraction Studies on Stained Rat Tail Tendons. Biochim Biophys Acta, 1978. 535(1): p. 25-32.
88. Woody, R.W., Aromatic side-chain contributions to the far ultraviolet circular dichroism of peptides and proteins. Biopolymers, 1978. 17(6): p. 1451-1467.
89. Kar, K., et al., Aromatic interactions promote self-association of collagen triple-helical peptides to higher-order structures. Biochemistry, 2009. 48(33): p. 7959-68.
90. Cejas, M.A., et al., Thrombogenic collagen-mimetic peptides: Self-assembly of triple helix-based fibrils driven by hydrophobic interactions. Proc Natl Acad Sci U S A, 2008. 105(25): p. 8513-8.
91. Kar, K., et al., Self-association of Collagen Triple Helic Peptides into Higher Order Structures. Journal of Biological Chemistry, 2006. 281(44): p. 33283 - 33290.
92. Kuznetsova, N. and S. Leikin, Does the Triple Helical Domain of Type I Collagen Encode Molecular Recognition and Fiber Assembly while Telopeptides Serve as Catalytic Domains?. EFFECT OF PROTEOLYTIC CLEAVAGE ON FIBRILLOGENESIS AND ON COLLAGEN-COLLAGEN INTERACTION IN FIBERS. Journal of Biological Chemistry, 1999. 274(51): p. 36083-36088.
93. Eyre, D.R., Cross-linking in Collagen and Elastin. Ann. Rev. Biochem., 1984. 53: p. 717-748.
94. Pratoomsoot, C., et al., A thermoreversible hydrogel as a biosynthetic bandage for corneal wound repair. Biomaterials, 2008. 29(3): p. 272-81.
95. Landers, R., et al., Rapid prototyping of scaffolds derived from thermoreversible hydrogels and tailored for applications in tissue engineering. Biomaterials, 2002. 23: p. 4437–4447.
96. Yan, H., et al., Thermoreversible Protein Hydrogel as Cell Scaffold. Biomacromolecules, 2006. 7: p. 2776-2782.
97. Park, J.S., et al., Multi-lineage differentiation of hMSCs encapsulated in thermo-reversible hydrogel using a co-culture system with differentiated cells. Biomaterials, 2010. 31(28): p. 7275-87.
98. Bhattarai, N., et al., PEG-grafted chitosan as an injectable thermosensitive hydrogel for sustained protein release. J Control Release, 2005. 103(3): p. 609-24.
99. Orgel, J.P., J.D. San Antonio, and O. Antipova, Molecular and structural mapping of collagen fibril interactions. Connect Tissue Res, 2011. 52(1): p. 2-17.
100. Kadler, K.E., Y. Hojima, and D.J. Prockop, Assembly of Type I Collagen Fibrils de Novo: Between 37 and 41 the Process is Limited by Micro-unfolding of Monomers*. Journal of Biological Chemistry, 1988. 253(21): p. 10517-10523.

101. Nikolaeva, T.I., S.M. Kuznetsova, and V.V. Rogachevsky, Collagen fibril formation in vitro at nearly physiological temperatures. Biophysics, 2013. 57(6): p. 757-763.
102. Comper, W. and A. Veis, The mechanism of nucleation for in vitro collagen fibril formation. Biopolymers, 1977. 16(10): p. 2113-2131.
103. Helseth, D. and A. Veis, Collagen self-assembly in vitro. Journal of Biological Chemistry, 1980. 256(14): p. 7118-7128.
104. Yamauchi, M. and G.L. Mechanic, Cross-linking of collagen. Collagen, ed. M.E. Nimni1988, Boca Raton, FL: CRC Press.
105. Antipova, O. and J.P. Orgel, In situ D-periodic molecular structure of type II collagen. J Biol Chem, 2010. 285(10): p. 7087-96.
106. Kuznetsova, N. and S. Leikin, Does the Triple Helical Domain of Type I Collagen Encode Molecular Recognition and Fiber Assembly while Telopeptides Serve as Catalytic Domains?: EFFECT OF PROTEOLYTIC CLEAVAGE ON FIBRILLOGENESIS AND ON COLLAGEN-COLLAGEN INTERACTION IN FIBERS. Journal of Biological Chemistry, 1999. 274(51): p. 36083-36088.
107. Drzewiecki, K.E., et al., Methacrylation induces rapid, temperature-dependent, reversible self-assembly of type-I collagen. Langmuir, 2014. 30(37): p. 11204-11.
108. Masand, S.N., et al., The effect of glycomimetic functionalized collagen on peripheral nerve repair. Biomaterials, 2012. 33(33): p. 8353-62.
109. Hermanson, G.T., Zero-Length Crosslinkers, in Bioconjugate Techniques, J. Audet, Editor 2013, Elsevier: Waltham, MA, USA and London, UK. p. 263-265.
110. Prockop, D.J., et al., The Biosynthesis of Collagen and Its Disorders. The New England Journal of Medicine, 1979. 301: p. 13-23.
111. Prockop, D.J., et al., The Biosynthesis of Collagen and Its Disorders. The New England Journal of Medicine, 1979. 301: p. 77-85.
112. Landers, R., et al., Rapid prototyping of scaffolds derived from thermoreversible hydrogels and tailored for applications in tissue engineering. Biomaterials, 2002. 23: p. 4437-4447.
113. Kim, S., et al., PubChem Substance and Compound databases. Nucleic Acids Res., 2016. 44(D1): p. D1202-D1213.
114. Wishart, D.S., et al., HMDB: the Human Metabolome Database. Nucleic Acids Res, 2007. 35(Database issue): p. D521-6.
115. Wishart, D.S., et al., HMDB: a knowledgebase for the human metabolome. Nucleic Acids Res, 2009. 37(Database issue): p. D603-10.
116. Wishart, D.S., et al., HMDB 3.0--The Human Metabolome Database in 2013. Nucleic Acids Res, 2013. 41(Database issue): p. D801-7.
117. Ulrich, E.L., et al., BioMagResBank. Nucleic Acids Res, 2008. 36(Database issue): p. D402-8.
118. Hssina, B., et al., A comparative study of decision tree ID3 and C4.5. International Journal of Advanced Computer Science and Applications, 2014(Special Issue on Advances in Vehicular Ad Hoc Networking and Applications).

119. Khoonsari, P.E. and A. Motie, A Comparison of Efficiency and Robustness of ID3 and C4.5 Algorithms Using Dynamic Test and Training Data Sets. International Journal of Machine Learning and Computing, 2011: p. 540-543.
120. Blockheel, H. and J. Struyf, Efficient Algorithms for Decision Tree Cross-validation. Journal of Machine Learning Research, 2002. 3: p. 621-650.
121. Rokach, L. and O. Mainmon, Decision Trees, in Data Mining and Knowledge Discovery Handbook, O. Maimon and L. Rokach, Editors. 2005, Springer US. p. 165-192.
122. Viera, A. and J. Garret, Understanding Interobserver Agreement: The Kappa Statistic. Family Medicine, 2005. 37(5): p. 360-363.
123. Gelman, R.A., D.C. Poppke, and K.A. Piez, Collagen Fibril Formation in Vitro: THE ROLE OF THE NONHELICAL TERMINAL REGIONS*. Journal of Biological Chemistry, 1979. 254(22): p. 11741-11745.
124. Gelman, R.A., B.R. Williams, and K.A. Piez, Collagen Fibril Formation: EVIDENCE FOR A MULTISTEP PROCESS*. Journal of Biological Chemistry, 1979. 254(1): p. 180-186.
125. Nimptsch, A., et al., Quantitative analysis of denatured collagen by collagenase digestion and subsequent MALDI-TOF mass spectrometry. Cell Tissue Res, 2011. 343(3): p. 605-17.
126. Zhang, G., et al., Mass spectrometric analysis of enzymatic digestion of denatured collagen for identification of collagen type. J Chromatogr A, 2006. 1114(2): p. 274-7.
127. Pataridis, S., et al., Identification of collagen types in tissues using HPLC-MS/MS. J Sep Sci, 2008. 31(20): p. 3483-8.
128. Brodsky, B., et al., Triple-helical peptides: an approach to collagen conformation, stability, and self-association. Biopolymers, 2008. 89(5): p. 345-53.
129. Katoaka, K. and N. Huh, Application of a Thermo-reversible Gelation Polymer, Melbiol Gel, for Stem Cell Cuture and Regenerative Medicine. Journal of Stem Cells and Regenerative Medicine, 2010. 6(1): p. 10-14.
130. Chevallay, B. and D. Herbage, Collagen-based biomaterials as 3D scaffold for cell cultures: applications for tissue engineering and gene therapy. Cellular Engineering: Tissue Engineering and Biomaterials, 2000. 38: p. 211-218.
131. Clayman, M.A., S.M. Clayman, and D.W. Mozingo, The use of collagen-glycosaminoglycan copolymer (Integra) for the repair of hypertrophic scars and keloids. J Burn Care Res, 2006. 27(3): p. 404-9.
132. Dantzer, E., et al., Dermal regeneration template for deep hand burns: clinical utility for both early grafting and reconstructive surgery. British Journal of Plastic Surgery, 2003. 56(8): p. 764-774.
133. Helfrich, Y.R., D.L. Sachs, and J.J. Voorhees, Overview of Skin Aging and Photoaging. Dermatology Nursing, 2008. 20(3): p. 177-183.
134. Muiznieks, L.D. and F.W. Keeley, Molecular assembly and mechanical properties of the extracellular matrix: A fibrous protein perspective. Biochim Biophys Acta, 2013. 1832(7): p. 866-75.

135. Green, H. and B. Goldberg, Collagen and Cell Protein Synthesis by an Established Mammalian Fibroblast Line. Nature, 1964. 204: p. 347-349.
136. Green, H., B. Goldberg, and G.J. Todaro, Differentiated Cell Types and the Regulation of Collagen Synthesis. Nature, 1966. 212: p. 631 - 633.
137. Li, J. and G. Li, The thermal behavior of collagen in solution: effect of glycerol and 2-propanol. Int J Biol Macromol, 2011. 48(2): p. 364-8.
138. Hayashi, T., S. Curran-Patel, and D.J. Prockop, Thermal stability of the triple helix of type I procollagen and collagen. Precautions for minimizing ultraviolet damage to proteins during circular dichroism studies. Biochemistry, 1979. 18(19): p. 4182-4187.
139. Li, Y. and E.P. Douglas, Effects of various salts on structural polymorphism of reconstituted type I collagen fibrils. Colloids Surf B Biointerfaces, 2013. 112: p. 42-50.
140. Greenfield, N.J., Using circular dichroism spectra to estimate protein secondary structure. Nat Protoc, 2006. 1(6): p. 2876-90.
141. Brodsky, B. and J.A.M. Ramshaw, The Collagen Triple-Helix Structure. Matrix Biology, 1997. 15: p. 545-554.
142. Silver, F.H. and D.E. Birk, Kinetic analysis of collagen fibrillogenesis: I. Use of turbidity--time data. Collagen Related Research, 1983. 3(5): p. 393-405.
143. Li, Y., et al., pH effects on collagen fibrillogenesis in vitro: Electrostatic interactions and phosphate binding. Materials Science and Engineering: C, 2009. 29(5): p. 1643-1649.
144. Williams, B.R., et al., Collagen Fibril Formation Optimal In Vitro Conditions and Preliminary Kinetic Results. Journal of Biological Chemistry, 1978. 253(18): p. 6578-6585.
145. Stoller, P., et al., Quantitative second-harmonic generation microscopy in collagen. Applied Optics, 2003. 42(25): p. 5209-5219.
146. Theodossiou, T.A., et al., Second harmonic generation confocal microscopy of collagen type I from rat tendon cryosections. Biophys J, 2006. 91(12): p. 4665-77.
147. Chen, X., et al., Second harmonic generation microscopy for quantitative analysis of collagen fibrillar structure. Nat Protoc, 2012. 7(4): p. 654-69.
148. Boldon, L., F. Laliberte, and L. Liu, Review of the fundamental theories behind small angle X-ray scattering, molecular dynamics simulations, and relevant integrated application. Nano Rev, 2015. 6: p. 25661.
149. Bentz, H., et al., Physical Evidence for the Assembly of A and B Chains of Human Placental Collagen in a Single Triple Helix. Eur. J. Biochem., 1978. 92: p. 563-567.
150. Gayatri, R., et al., Chromium(III)-induced structural changes and self-assembly of collagen. Biochem Biophys Res Commun, 2001. 283(1): p. 229-35.
151. Ikoma, T., et al., Physical properties of type I collagen extracted from fish scales of Pagrus major and Oreochromis niloticas. Int J Biol Macromol, 2003. 32(3-5): p. 199-204.

152. Madhan, B., et al., Stabilization of collagen using plant polyphenol: role of catechin. Int J Biol Macromol, 2005. 37(1-2): p. 47-53.
153. Peltonen, L., et al., Thermal Stability of Type-I and Type-III Procollagens from Normal Human Fibroblasts and from a Patient with Osteogenesis Imperfecta. PNAS, 1980. 77(1): p. 162-166.
154. Schmid, T.M. and T.F. Linsenmayer, Denaturation-renaturation properties of two molecular forms of short-chain cartilage collagen. Biochemistry, 1984. 23(3): p. 553-558.
155. Scott, P.G., Spectroscopic study of environment-dependent changes in the conformation of the isolated carboxy-terminal telopeptide of type I collagen. Biochemistry, 1986. 25(5): p. 974-980.
156. Zhang, Z., G. Li, and B. Shi, Physicochemical Properties of Collagen, Gelatin and Collagen Hydrolysate Derived from Bovine Limed Split Washes. Journal of the Society of Leather Technologists and Chemists, 2005. 90: p. 23-28.
157. Persikov, A.V., Y. Xu, and B. Brodsky, Equilibrium thermal transitions of collagen model peptides. Protein Sci, 2004. 13(4): p. 893-902.
158. Biomatrix Inc., A. TeloCol. 2014; Available from: https://www.advancedbiomatrix.com/wp-content/uploads/2015/11/DFU-TeloCol-Solution-5026-Rev-04.pdf.
159. Biomatrix Inc., A. PureCol. 2015; Available from: https://www.advancedbiomatrix.com/wp-content/uploads/2015/11/DFU-PureCol-Solution-5005-Rev-07.pdf.
160. Hennessey, J. and W. Johnson Jr., Information Content in the Circular Dichroism of Proteins. Biochemistry, 1981. 20: p. 1085-1094.
161. Hyvarinen, A. and E. Oja, Independent Component Analysis: Algorithms and Applications. Neural Networks, 2000. 13(4-5): p. 411-430.
162. Hyvarinen, A., Fast and Robust Fixed-Point Algorithms for Independent Component Analysis. IEEE Transactions on Neural Networks, 1999. 10(3): p. 626-634.
163. Fleischmajer, R., et al., Dermal collagen fibrils are hybrids of type I and type III collagen molecules. Journal of Structural Biology, 1990. 105(1-3): p. 162-169.
164. Wood, G.C. and M.K. Keech, The formation of fibrils from collagen solutions 1. The effect of experimental conditions: kinetic and electron-microscope studies. Biochem. J., 1960. 75(3): p. 588-598.
165. Birkedal-Hansen, H., et al., Matrix Metalloproteinases: A Review. Critical Reviews in Oral Biology and Medicine, 1993. 4(2): p. 197-250.
166. Paige, M., A. Lin, and C. Goh, Real-time enzymatic biodegradation of collagen fibrils monitored by atomic force microscopy. International Biodeterioration and Biodegradation, 2002. 20: p. 1-10.
167. Barrett, A.J., N.D. Rawlings, and J.F. Woessner, Handbook of Proteolytic Enzymes1998, London: Elsevier Academic Press.
168. Lopes, J.L., et al., Distinct circular dichroism spectroscopic signatures of polyproline II and unordered secondary structures: applications in secondary structure analyses. Protein Sci, 2014. 23(12): p. 1765-72.

169. Wallace, B. and R. Janes. Protein Circular Dichroism Data Bank 2016; Available from: http://pcddb.cryst.bbk.ac.uk/home.php.
170. Lobley, A., L. Whitmore, and B.A. Wallace, DICHROWEB: an interactive website for the analysis of protein secondary structure from circular dichroism spectra. Bioinformatics Application Note, 2002. 18(1): p. 211-212.
171. Whitmore, L. and B.A. Wallace, DICHROWEB, an online server for protein secondary structure analyses from circular dichroism spectroscopic data. Nucleic Acids Res, 2004. 32(Web Server issue): p. W668-73.
172. Whitmore, L. and B.A. Wallace, Protein secondary structure analyses from circular dichroism spectroscopy: methods and reference databases. Biopolymers, 2008. 89(5): p. 392-400.
173. Wallace, B. and R. Janes. Protein Circular Dichroism Data Bank 2016.
174. Benjwal, S., et al., Monitoring protein aggregation during thermal unfolding in circular dichroism experiments. Protein Sci, 2006. 15(3): p. 635-9.
175. Ioannidis, E.I. and H.J. Kulik, Towards quantifying the role of exact exchange in predictions of transition metal complex properties. J Chem Phys, 2015. 143(3): p. 034104.
176. Chia, H.N. and B.M. Wu, Recent advances in 3D printing of biomaterials. J Biol Eng, 2015. 9: p. 4.
177. Leong, K.F., C.M. Cheah, and C.K. Chua, Solid freeform fabrication of three-dimensional scaffolds for engineering replacement tissues and organs. Biomaterials, 2003. 24(13): p. 2363-2378.
178. Seol, Y.-J., T.-Y. Kang, and D.-W. Cho, Solid freeform fabrication technology applied to tissue engineering with various biomaterials. Soft Matter, 2012. 8(6): p. 1730-1735.
179. Collins, S.F., Bioprinting is changing regenerative medicine forever. Stem Cells Dev, 2014. 23 Suppl 1: p. 79-82.
180. Zhu, W., et al., 3D printing of functional biomaterials for tissue engineering. Curr Opin Biotechnol, 2016. 40: p. 103-12.
181. Murphy, S.V. and A. Atala, 3D bioprinting of tissues and organs. Nat Biotechnol, 2014. 32(8): p. 773-85.
182. Do, A.V., et al., 3D Printing of Scaffolds for Tissue Regeneration Applications. Adv Healthc Mater, 2015. 4(12): p. 1742-62.
183. Tibbitt, M.W., et al., Progress in material design for biomedical applications. Proc Natl Acad Sci U S A, 2015. 112(47): p. 14444-51.
184. Chvapil, M., Collagen Sponge: Theory and Practice of Medical Applications. J. Biomed. Mater. Res., 1977. 11: p. 721-741.
185. Dong, C. and Y. Lv, Application of Collagen Scaffold in Tissue Engineering: Recent Advances and New Perspectives. Polymers, 2016. 8(2): p. 42.
186. Gudapati, H., M. Dey, and I. Ozbolat, A comprehensive review on droplet-based bioprinting: Past, present and future. Biomaterials, 2016. 102: p. 20-42.

187. Sachlos, E., et al., Novel collagen scaffolds with predefined internal morphology made by solid freeform fabrication. Biomaterials, 2003. 24: p. 1487–1497.
188. Bell, A., M. Kofron, and V. Nistor, Multiphoton crosslinking for biocompatible 3D printing of type I collagen. Biofabrication, 2015. 7(3): p. 035007.
189. Yoon, H., et al., Development of cell-laden 3D scaffolds for efficient engineered skin substitutes by collagen gelation. RSC Advances, 2016. 6: p. 21439-21447.
190. Kim, Y. and G. Kim, Collagen/alginate scaffolds comprising core (PCL)–shell (collagen/alginate) struts for hard tissue regeneration: fabrication, characterisation, and cellular activities. Journal of Materials Chemistry B, 2013. 1(25): p. 3185.
191. Xu, T., et al., Complex heterogeneous tissue constructs containing multiple cell types prepared by inkjet printing technology. Biomaterials, 2013. 34(1): p. 130-9.
192. Pataky, K., et al., Microdrop printing of hydrogel bioinks into 3D tissue-like geometries. Adv Mater, 2012. 24(3): p. 391-6.
193. Weng, B., et al., Inkjet printed polypyrrole/collagen scaffold: A combination of spatial control and electrical stimulation of PC12 cells. Synthetic Metals, 2012. 162(15-16): p. 1375-1380.
194. Nocera, A.D., N.A. Salvatierra, and M.P. Cid, Printing Collagen 3D Structures. 2015. 49: p. 136-139.
195. Hinton, T.J., et al., Three-dimensional printing of complex biological structures by freeform reversible embedding of suspended hydrogels. Sci Adv, 2015. 1(9): p. e1500758.
196. Fang, Y.Z., S. Yang, and W. G, Free Radicals, Antioxidants, and Nutrition. Nutrition, 2002. 18(10): p. 872-879.
197. Williams, C.G., et al., Variable cytocompatibility of six cell lines with photoinitiators used for polymerizing hydrogels and cell encapsulation. Biomaterials, 2005. 26(11): p. 1211-1218.
198. Sabnis, A., et al., Cytocompatibility studies of an in situ photopolymerized thermoresponsive hydrogel nanoparticle system using human aortic smooth muscle cells. J Biomed Mater Res A, 2009. 91(1): p. 52-9.
199. Anderson, J.M., A. Rodriguez, and D.T. Chang, FOREIGN BODY REACTION TO BIOMATERIALS. Semin Immunol, 2008. 20(2): p. 86-100.
200. Nichol, J.W., et al., Cell-laden microengineered gelatin methacrylate hydrogels. Biomaterials, 2010. 31(21): p. 5536-44.
201. Park, S.H., et al., Improvement of spatial resolution in nano-stereolithography using radical quencher. Macromolecular Research, 2006. 14(5): p. 559-564.
202. Stansbury, J.W. and M.J. Idacavage, 3D printing with polymers: Challenges among expanding options and opportunities. Dent Mater, 2016. 32(1): p. 54-64.
203. Fernandez, P. and A.R. Bausch, The compaction of gels by cells: a case of collective mechanical activity. Integr Biol (Camb), 2009. 1(3): p. 252-9.

204. Andujar, M., et al., Cell migration influences collagen gel contraction. Journal of Submicroscopic Cytology and Pathology, 1992. 24(2): p. 145-154.
205. Arora, P., N. Narani, and C. McCollough, The Compliance of Collagen Gels Regulates Transforming Growth Factor-Beta Induction of Alpha-Smooth Muscle Actin in Fibroblasts. American Journal of Pathology, 1999. 154(3): p. 871-882.
206. Shreiber, D.I., P.A. Enever, and R.T. Tranquillo, Effects of pdgf-bb on rat dermal fibroblast behavior in mechanically stressed and unstressed collagen and fibrin gels. Exp Cell Res, 2001. 266(1): p. 155-66.
207. Shreiber, D., V. Barocas, and R. Tranquillo, Temporal Variations in Cell Migration and Traction during Fibroblast-Mediated Gel Compaction. Biophysical Journal, 2003. 84: p. 4102–4114.
208. Stevenson, M.D., et al., Pericellular conditions regulate extent of cell-mediated compaction of collagen gels. Biophys J, 2010. 99(1): p. 19-28.
209. Anderson, J.M., Soft tissue response, in Handbook of Biomaterial Properties, J. Black and G. Hastings, Editors. 1998, Springer US. p. 490-499.
210. Cha, C., et al., Structural Reinforcement of Cell-Laden Hydrogels with Microfabricated Three Dimensional Scaffolds. Biomater Sci, 2014. 2(5): p. 703-709.
211. Kar, K., et al., Self-association of collagen triple helic peptides into higher order structures. J Biol Chem, 2006. 281(44): p. 33283-90.
212. Kaur, P.J., et al., The self-assembly of a mini-fibril with axial periodicity from a designed collagen-mimetic triple helix. J Biol Chem, 2015. 290(14): p. 9251-61.
213. Simon, H.J., et al., Uncoiling collagen: a multidimensional mass spectrometry study. Analyst, 2016. 141(1): p. 157-65.
214. Vesentini, S., A. Redaelli, and A. Gautieri, Nanomechanics of collagen microfibrils. Muscles, Ligaments and Tendons Journal, 2013. 3(1): p. 23-34.
215. Gautieri, A., et al., Coarse-Grained Model of Collagen Molecules Using an Extended MARTINI Force Field. Journal of Chemical Theory and Computation, 2010. 6: p. 1210–1218.
216. Le, H., Progress and Trends in Ink-jet Printing Technology. Journal of Imaging Science and Technology, 1998. 42: p. 49-62.
217. Klebe, R., Cytoscribing: a method for micropositioning cells and the construction of two- and three-dimensional synthetic tissues. Exp Cell Res., 1988. 179(2): p. 362-373.
218. Kolesky, D.B., et al., 3D bioprinting of vascularized, heterogeneous cell-laden tissue constructs. Adv Mater, 2014. 26(19): p. 3124-30.
219. Xing, J., M. Zheng, and X. Duan, Two-photon polymerization microfabrication of hydrogels: an advanced 3D printing technology for tissue engineering and drug delivery. Chem Soc Rev, 2015. 44: p. 5031-5039.

220. Gauvin, R., et al., Microfabrication of complex porous tissue engineering scaffolds using 3D projection stereolithography. Biomaterials, 2012. 33(15): p. 3824-34.
221. Kwok, S.J.J., et al., Selective two-photon collagen crosslinking in situ measured by Brillouin microscopy. Optica, 2016. 3(5): p. 469.
222. Naderi, H., M.M. Matin, and A.R. Bahrami, Review paper: critical issues in tissue engineering: biomaterials, cell sources, angiogenesis, and drug delivery systems. J Biomater Appl, 2011. 26(4): p. 383-417.